

ISTANBUL TECHNICAL UNIVERSITY ★ GRADUATE SCHOOL OF SCIENCE
ENGINEERING AND TECHNOLOGY

**THE INVESTIGATION OF STABILITY OF TUNNELS AND SETTLEMENTS
WITH CENTRIFUGE MODELLING**

M.Sc. THESIS

Tuğçe ERTAN

Department of Civil Engineering

Soil Mechanics and Geotechnical Engineering Programme

Thesis Advisor: Prof. Dr. Ayfer ERKEN

Thesis Advisor: Prof. Dr. Eng-WEI WU

JUNE 2012

ISTANBUL TECHNICAL UNIVERSITY ★ GRADUATE SCHOOL OF SCIENCE
ENGINEERING AND TECHNOLOGY

**THE INVESTIGATION OF STABILITY OF TUNNELS AND SETTLEMENTS
WITH CENTRIFUGE MODELLING**

M.Sc. THESIS

Tuğçe ERTAN
(501091331)

Department of Civil Engineering

Soil Mechanics and Geotechnical Engineering Programme

Thesis Advisor: Prof. Dr. Ayfer ERKEN

Thesis Advisor: Prof. Dr. Eng-Wei WU

JUNE 2012

İSTANBUL TEKNİK ÜNİVERSİTESİ ★ FEN BİLİMLERİ ENSTİTÜSÜ

**SANTRİFÜJ MODELLEME İLE TÜNEL STABİLİTESİ VE OTURMALARIN
ARAŞTIRILMASI**

YÜKSEK LİSANS TEZİ

**Tuğçe ERTAN
(501091331)**

İnşaat Mühendisliği Anabilim Dalı

Zemin Mekaniği Ve Geoteknik Mühendisliği Programı

Tez Danışmanı: Prof. Dr. Ayfer ERKEN

Tez Danışmanı: Prof. Dr. Wei WU

HAZİRAN 2012

Tuğçe ERTAN, a **M.Sc.** student of **ITU Graduate School of Science Engineering** student ID **501091331**, successfully defended the **thesis** entitled “The Investigation Of Stability Of Tunnels And Settlements With Centrifuge Modelling” which she prepared after full filling the requirements specified in the associated legislations, before the jury whose signatures are below.

Thesis Advisor : **Prof. Dr. Ayfer ERKEN**

Istanbul Technical University

Co-advisor : **Prof.Dr. Eng- Wei WU**

Bodunkultur University, Vienna

Jury Members :

Prof. Dr. Kutay ÖZAYDIN

Yıldız Technichal University

Yard. Doç. Dr. Berrak TEYMUR

Istanbul Technical University

Date of Submission : 04 May 2012

Date of Defense : 04 June 2012

To my family and good friends,

FOREWORD

I would like to start expressing my gratitude to my Supervisor Prof. Dr. Eng- Ayfer Erken, who supported me whole heartedly and never avoided her confidence in me during my master's education at the processes of preparing my experiments and writing my thesis at Istanbul Technical University. This dissertation is a product of her confidence.

All the experiments of my thesis have been completed at the Bodunkultur University, Vienna. I also would like to extend my special thanks to Prof. Dr. Eng- Wei Wu, who, at this very selective university of Austria, provided all support for me, made me feel as one of the students of the department although I was a term-student and who provided very valuable advices for me. My greatest thanks go to Dipl.Eng- Gregor Idinger, who has the greatest share in this thesis by permitting me to use the tunnel model prepared for his studies and who supported me with great patience during all my studies.

And there is one person, whose contributions I will never be able to forget, Mikail Yıldız. If it were not with you, this dissertation could not have been completed in such a short time. You almost generated everything that I needed in a city, which was mostly unfamiliar for me. You have a share in all my experiments, thank you very much.

My final word is for my immediate family, who has a share in all parts of my life. It is not possible for me to find any sufficient words to thank for the never-ending support. Without you it would not have been possible for me to arrive at this stage. Thank you very much for giving this chance to me. Also, I have special thanks for the great women of my family, both my super grandmothers. Dear Grandfather Ayhan Araslı, whom I lost on this journey of my dissertation, I laid the foundation for the engineering mathematics with you, you made me love mathematics, I will never forget your support and your being with me all the time.

January 2012

Tuğçe ERTAN
(Civil Engineer)

TABLE OF CONTENTS

	<u>Page</u>
FOREWORD	ix
TABLE OF CONTENTS	xi
ABBREVIATIONS	xiii
LIST OF TABLES	xv
LIST OF FIGURES	xvii
SUMMARY	xxiii
ÖZET	xxv
1. INTRODUCTION	29
1.1 Scope of Thesis	29
1.2 Sections Of The Thesis	30
1.3 Literature Review	30
1.1.1 The History of Tunnel.....	30
1.1.2 The Technical History of Tunnel	33
1.1.3 Tunneling in Soft Ground and Shallow Zones.....	35
1.1.4 Induced Ground Movements –Because of Tunneling.....	37
1.1.4.1 Face Stability.....	38
1.1.4.2 Propagation Of Movements Towards The Surface.....	39
1.1.5 Causes For Construction Induced Settlements.....	44
2. GEOTECHNICAL CENTRIFUGE	49
2.1 Past – Present - Future.....	49
2.2 Centrifuges In Modelling Principles And Scale Effects	50
2.2.1 Scaling Laws For Models	51
2.2.2 Scale Effects.....	53
2.2.3 Rotational Acceleration Field	54
3. PARTICLE IMAGE VELOCIMETRY (PIV)	55
3.1 Step by Step how PIV works.....	56
3.2 Close Range Photogrammetry.....	59
3.3 GEOPIV8	61
4. EXPERIMENTAL SET UP	63
4.1 Description Of IGT Beam Centrifuge	63
4.2 Design Of The Model.....	67
4.3 Tunnel Model	69
4.3.1 Instrumentation	71
4.4 Illumination	74
4.5 Soil	75
4.5.1 Soil 1 (S1)	75
4.5.2 Soil 2 (S2)	75
4.6 Typical Test Procedure.....	77
4.6.1 Assembling Of The Model Box	77
4.6.2 Mounting The Model Box To The Centrifuge Swinging Basket.....	77
5. RESULTS	81
5.1 Experimental Results.....	82
5.1.1 Experiment 1	82
5.1.2 Experiment 2	86
5.1.3 Experiment 3	90

5.1.4 Experiment 4	94
5.1.5 Experiment 5	98
5.1.6 Experiment 6	102
5.1.7 Experiment 7	106
5.2 Comparison Of Experiments	110
5.2.1 Experiment 1- Experiment 2 S1, C/D=0.5	110
5.2.2 Experiment 3- Experiment 4 S2, C/D=0.5	112
5.2.3 Experiment 1- Experiment 3, C/D=0.5, no surcharge.....	114
5.2.4 Experiment 2- Experiment 4, C/D=0.5, with surcharge.....	117
5.2.5 Experiment 1- Experiment 5, C/D=0.5, S1	119
5.2.6 Experiment 6- Experiment 7, C/D=1.0, S1	121
5.2.7 Experiment 1- Experiment 6, S1, no surcharge load.....	123
6. ANALYSIS OF THE RESULTS	125
6.1 Interpretation Of The Results	125
6.2 Conclusions	131
REFERENCES	135
APPENDICES	139
CURRICULUM VITAE	141

ABBREVIATIONS

ASCII	: American Standard Code for Information Interchange (data file type)
C	: Layer thickness of the ground
CCD	: Charge Coupled Device (photosensitive elements of digital camera)
D	: Diameter of the tunnel
EPV	: Earth Pressure Balance (shield heading)
FOV	: Field Of View
G	: Earth Gravity (9.81m/sec ²)
H	: Tunnel overburden
LVDT	: Linear Variable Differential Transformer
MP	: Mega Pixel
N	: Gravity scale factor
PIV	: Particle Image Velocimetry
TBM	: Tunnel Boring Machines

LIST OF TABLES

Table 1.1 : Classification of visible damage that may affect standard structures (Leca, 2007)	46
Table 2.1 : Scaling factors for centrifuge modelling (Ferstl, 1998).....	52
Table 4.1 : Technical specifications of IGT centrifuge (TRIO-TECH, 1988).....	63
Table 4.2 : RPM at certain model factors g for $r=1.42\text{m}$ (radius to tunnel axis)	67
Table 4.3 : Parameters of Soil S1	75
Table 5.1 : Conditions Of Experiments.....	81
Table 5.2 : The conditions of experiment 1	82
Table 5.3 : The conditions of experiment 2	86
Table 5.4 : The conditions of experiment 3	90
Table 5.5 : The conditions of experiment 4	94
Table 5.6 : The conditions of experiment 5	98
Table 5.7 : The conditions of experiment 6	102
Table 5.8 : The conditions of experiment 7	106
Table 5.9 : The comparing conditions of experiment 1 and experiment 2.....	110
Table 5.10 : The comparing conditions of experiment 3 and experiment 4.....	112
Table 5.11 : The comparing conditions of experiment 1 and experiment 3.....	115
Table 5.12 : The comparing conditions of experiment 2 and experiment 4.....	117
Table 5.13 : The comparing conditions of experiment 1 and experiment 5.....	119
Table 5.14 : The comparing conditions of experiment 6 and experiment 7.....	121
Table 5.15 : The comparing conditions of experiment 1 and experiment 6.....	123
Table 6.1 : Summary of experiment results	127
Table 6.2 : The Soil Conditions of the resarch of Lee et., al. (2006).....	129
Table 6.3 : Supporting pressure p_c of the investigation of Lee et., al. (2006).....	129
Table 6.4 : Basic propertios of the soil bed Lee et., al. (2006)	130
Table 6.5 : The supporting of the twin and single tunnels at clayey soil	130

LIST OF FIGURES

Figure 1.1 : The First Immersed Tube under Shirley Gut in Boston (Lotysz,2010).	33
Figure 1.2 : Displacement of the excavation profiles (Leca, 2007).....	38
Figure 1.3 : a) Yielded zone rear of the face. b) Yielded zone ahead of the face. (Leca, 2007)	38
Figure 1.4 : Face Collapse- Basic Diagram in Cohesive Ground Soils (Leca, 2007	39
Figure 1.5 : Face Collapse: Basic Diagram in Dry Granular Soils (Leca, 2007).....	39
Figure 1.6 : Primary mode: basic transverse cross–section (Leca, 2007).....	40
Figure 1.7 : Secondary mode: basic transverse cross-section (Leca,2007)	40
Figure 1.8 : Failure Bulb for Fully Lined Tunnel (Chambon et al., 1991)	41
Figure 1.9 : Failure Bulbs For Different C/D Ratios (Chambon et al., 1991)	41
Figure 1.10 : Influence of Tunnel Diameter on Collapse Pressure pf (Chambon et al.,1991)	41
Figure 1.11 : Three-dimesional transverse settlement trough (Attewell et al.,1986)	42
Figure 1.12 : Transverse settlement trough (Sugiyama et. al., 1999)	42
Figure 1.13 : Variation in surface settlement trough width parameter with tunnel depth for tunnels in sands and gravel (Sugiyama et. al., 1999)	43
Figure 1.14 : Variation in surface settlement trough width parameter with tunnel depth for tunnels in clays (Sugiyama et. al., 1999).....	43
Figure 1.15 : Typical idealized building response (Attewell et al., 1986).....	45
Figure 2.1 : Comparison of stress variations on depth in a centrifuge model and its corresponding prototype (Taylor, 1995).....	53
Figure 3.1 : Typical strain ranges experienced in geotechnical engineering (Mair, 1993)	55
Figure 3.2 : Principles of PIV analysis (White and Take, 2002)	57
Figure 3.3 : Flowchart of the GeoPIV analysis procedure (White and Take, 2002)	58
Figure 3.4 : Calibration of different coordinate systems (Thusyanthan, 2008)	59
Figure 3.5 : Centroiding of window markers (Thusyanthan, 2008).....	61
Figure 3.6 : GeoPIV software usage (White and Take, 2002).....	62
Figure 4.1 : Schematic sketch of Trio-Tech 1231 Geotechnical Centrifuge (Ferstl, 1998).....	64
Figure 4.2 : Centrifuge equipment: (1.) video camera, (2.) halogen light, (3.) balance fixing and (4.) DB15 plug bar (Idinger,2010)	65
Figure 4.3 : IGT Beam Centrifuge: (1.) slip ring tower, (2.) high strength steel enclosure, (3.) rotating arm, (4.) DC motor (Idinger,2010).....	66
Figure 4.4 : Rotating beam - model at the back and box with counterweights at front (Idinger,2010)	66
Figure 4.5 : Model box mounted on swing basket before the start of test (C/D=1.0), 1. Model box, 2. tunnel, 3. LED lights, 4. camera, 5.engine, 6. engine driver, 7. Batteries (Idinger,2010)	68
Figure 4.6 : Sketch of PIV-model assembly, top view (Idinger, 2010)	68

Figure 4.7 : Sketches of tunnel model, frontal view and cross-section(Idinger,2010)	70
Figure 4.8 : Grain size curve of S1 and S2 Soils	76
Figure 5.1 : The first Picture (when the experiment started)	82
Figure 5.2 : The picture, after 5 mm of Tunnel Face Displacement	83
Figure 5.3 : C/D=0.5 S1 loose: vector field of resultant ground movement at 0.5mm face	83
Figure 5.4 : C/D=0.5 S1 loose: vector field of resultant ground movement at 5mm	84
Figure 5.5 : C/D=0.5 S1 loose: a)contours of resultant max. shear strain after 0.5mm face b)contours of resultant max. shear strain after 5mm face	84
Figure 5.6 : C/D=0.5 S1 loose: surface settlement after $\Delta s=0.5$ mm face displacement total face displacement $d_s=5$ mm;max. settlement: 5 mm	85
Figure 5.7 : C/D=0.5 S1 loose: support pressure over face displacement; five millimetres;mean pressure after failure: $p_f=10.0$ kN/m ²	85
Figure 5.8 : The first picture (when the experiment started)	86
Figure 5.9 : The picture, after 5 mm of Tunnel Face Displacement	87
Figure 5.10 : C/D=0.5 S1 loose, with surcharge: vector field of resultant ground movement at 0,5mm face	87
Figure 5.11 : C/D=0.5 S1 loose, with surcharge: vector field of resultant ground movement at 5 mm face	88
Figure 5.12 : C/D=0.5 S1 loose(with surcharge): a)contours of resultant max. shear strain after 0,5mm face b)contours of resultant max. shear strain after 5mm face	88
Figure 5.13 : C/D=0.5 S1 loose(with surcharge): surface settlement after $\Delta s=0.5$ mm face displacement, total face displacement $d_s=5$ mm; max. settlement: 10.2 mm	89
Figure 5.14 : C/D=0.5S1 loose (with surcharge): support pressure over face displacement five millimetres;mean pressure after failure: $p_f=5.0$ kN/m ²	89
Figure 5.15 : The first Picture (when the experiment started)	90
Figure 5.16 : The picture, after 5 mm of Tunnel Face Displacement	91
Figure 5.17 : C/D=0.5 S2 loose: vector field of resultant ground movement at 0.5 mm face	91
Figure 5.18 : C/D=0.5 S2 loose: vector field of resultant ground movement at 5mm face	92
Figure 5.19 : C/D=0.5 S2 loose: a)contours of resultant max. shear strain after 0.5mm face b)contours of resultant max. shear strain after 5 mm face	92
Figure 5.20 : C/D=0.5 S2 loose: surface settlement after $\Delta s=0.5$ mm face displacement, total face displacement $d_s=5$ mm; max. settlement: 7.3 mm	93
Figure 5.21 : C/D=0.5 S2 loose: support pressure over face displacement; five millimetres;mean pressure after failure: $p_f=0.0$ kN/m ²	93
Figure 5.22 : The first Picture (when the experiment started)	94
Figure 5.23 : The picture, after 5 mm of Tunnel Face Displacement	95
Figure 5.24 : C/D=0.5 S2 loose, with surcharge: vector field of resultant ground movement	95
Figure 5.25 : C/D=0.5 S2 loose, with surcharge: vector field of resultant ground movement at 5mm face	96

Figure 5.26 : C/D=0.5 S2 loose(with surcharge): a)contours of resultant max. shear strain after 0.5mm face b)contours of resultant max. shear strain after 5mm face.....	96
Figure 5.27 : C/D=0.5 S2 loose(with surcharge): surface settlement after $\Delta s=0.5\text{mm}$ face displacement, total face displacement $d_s=5\text{mm}$; max. settlement: 10,2 mm.....	97
Figure 5.28 : C/D=0.5 S2 loose (with surcharge): support pressure over face displacement; five millimetres;mean pressure after failure: $p_f=0.0\text{kN/m}^2$	97
Figure 5.29 : The first Picture (when the experiment started)	98
Figure 5.30 : The picture, after 5 mm of Tunnel Face Displacement.....	99
Figure 5.31 : C/D=0.5 S1 loose, with textile: vector field of resultant ground movement at 0,5mm face.....	99
Figure 5.32 : C/D=0.5 S1 loose, (with textile) vector field of resultant ground movement at 5mm face.....	100
Figure 5.33 : C/D=0.5 S1 loose(with textile): a)contours of resultant max. shear strain after 0.5mm face b)contours of resultant max. shear strain after 5mm face.....	100
Figure 5.35 : C/D=0.5 S1 loose(with textile): support pressure over face displacement; five millimetres;mean pressure after failure: $p_f= 10.0\text{kN/m}^2$	101
Figure 5.34 : C/D=0.5 S1 loose(with textile): surface settlement after $\Delta s=0.5\text{mm}$ face displacement, total face displacement $d_s=5\text{mm}$; max. settlement: 4.5 mm	101
Figure 5.36 : The first Picture (when the experiment started)	102
Figure 5.37 : The picture, after 5 mm of Tunnel Face Displacement.....	103
Figure 5.38 : C/D=1.0 S1 loose: vector field of resultant ground movement at 0,5mm face.....	103
Figure 5.39 : C/D=1.0 S1 loose: vector field of resultant ground movement at 5mm face.....	104
Figure 5.40 : C/D=1.0 S1 loose a)contours of resultant max. shear strain after 0.5mm face b)contours of resultant max. shear strain after 5mm face.....	104
Figure 5.42 : C/D=1.0 S1 loose: support pressure over face displacement; five millimetres;mean pressure after failure: $p_f=0.0\text{kN/m}^2$	105
Figure 5.41 : C/D=1.0 S1 loose: surface settlement after $\Delta s=0.5\text{mm}$ face displacement, total face displacement $d_s=5\text{mm}$; max. settlement: 1.4 mm	105
Figure 5.43 : The first Picture (when the experiment started)	106
Figure 5.44 : The picture, after 5 mm of Tunnel Face Displacement.....	107
Figure 5.45 : C/D=1.0 S1 loose, with textile: vector field of resultant ground movement at 0.5mm face.....	107
Figure 5.46 : C/D=0.5 S1 loose, (with textile) vector field of resultant ground movement at 5mm face.....	108
Figure 5.47 : C/D=1.0 S1 loose(with textile): a)contours of resultant max. shear strain after 0.5mm face b)contours of resultant max. shear strain after 5mm face.....	108
Figure 5.48 : C/D=1.0 S1 loose(with textile): surface settlement after $\Delta s=0.5\text{mm}$ face displacement, total face displacement $d_s=5\text{mm}$; max. settlement: 1,1 mm	109

Figure 5.49 : C/D=1.0 S2 loose(with textile): support pressure over face displacement; five millimetres;mean pressure after failure: pf= 5.0kN/m ²	109
Figure 5.50 : C/D=0.5 S1 loose contours of resultant max. shear strain after 5mm face a)with no surcharge b)with 2 kg surcharge	110
Figure 5.51 : C/D=0.5 S1 loose: surface settlement after total face displacement ds=5mm;a) with no surcharge load max. settlement: 5.0 mm b) a)with surcharge load max. settlement: 5.5 mm	111
Figure 5.52 : C/D=0.5 S1 loose: support pressure over face displacement; five millimetres;mean pressure after failure:a) with no surcharge pf=10.0kN/m ² b) with surcharge pf=5.0kN/m ²	112
Figure 5.53 : C/D=0.5 S2 loose contours of resultant max. shear strain after 5mm face a)with no surcharge b)with 2 kg surcharge	113
Figure 5.54 : C/D=0.5 S2 loose: surface settlement after total face displacement ds=5mm;a) with no surcharge load max. settlement: 7.3 mm b) a)with surcharge load max. settlement: 10.2 mm	114
Figure 5.55 : C/D=0.5 S2 loose: support pressure over face displacement; five millimetres;mean pressure after failure:a) with no surcharge pf=0.0kN/m ² b) with surcharge pf=0.0kN/m ²	114
Figure 5.56 : C/D=0.5 loose contours of resultant max. shear strain after 5mm face a)with S1 soil b)with S2 Soil	115
Figure 5.57 : C/D=0.5 loose: surface settlement after total face displacement ds=5mm;a)with S1 Soil max. settlement: 5.0 mm b)with S2 Soil max. settlement: 7.3mm.....	116
Figure 5.58 : C/D=0.5 loose: support pressure over face displacement; five millimetres;mean pressure after failure:a) with S1 soil pf=10.0kN/m ² b) with S2 soil pf=0.0kN/m ²	116
Figure 5.59 : C/D=0.5 loose (with surcharge load) contours of resultant max. shear strain after 5mm face a)with S1 soil b)with S2 Soil	117
Figure 5.60 : C/D=0.5 loose: surface settlement after total face displacement ds=5mm; a) with S1 Soil max. settlement: 5.5 mm b) a)with S2 Soil max. settlement: 10,2 mm	118
Figure 5.61 : C/D=0.5 (with surcharge)loose: support pressure over face displacement; five millimetres;mean pressure after failure:a) with S1 soil pf=5.0kN/m ² b)with S2 soil pf=0.0kN/m ²	118
Figure 5.62 : C/D=0.5 S1 loose contours of resultant max. shear strain after 5mm face a)with no textile b)with textile	119
Figure 5.63 : C/D=0.5 S1 loose: surface settlement after total face displacement ds=5mm;a) with no textile max. settlement: 5.0 mm b) a)with textile max. settlement: 4.5 mm	120
Figure 5.64 : C/D=0.5 S1 loose: support pressure over face displacement; five millimetres;mean pressure after failure:a) with no textile pf=10.0kN/m ² b) with textile pf= 10.0kN/m ²	120
Figure 5.65 : C/D=1.0 S1 loose contours of resultant max. shear strain after 5mm face a)with no textile b)with textile	121
Figure 5.66 : C/D=1.0 S1 loose: surface settlement after total face displacement ds=5mm;a) with no textile max. settlement: 1.4 mm b) a)with textile max. settlement: 1.1 mm	122

Figure 5.67 : C/D=1.0 S1 loose: support pressure over face displacement; five millimetres;mean pressure after failure:a) with no textile $p_f=0.0\text{kN/m}^2$ b) with textile $p_f= 5.0\text{kN/m}^2$	122
Figure 5.68 : S1 loose contours of resultant max. shear strain after 5mm face a)C/D=0.5 b)C/D=1.0	123
Figure 5.69 : S1 loose: surface settlement after total face displacement $d_s=5\text{mm}$;a) C/D=0.5 max. settlement: 5.0 mm b) a)C/D=1.0 max. settlement: 1.4 mm	124
Figure 5.70 : S1 loose: support pressure over face displacement; five millimetres;mean pressure after failure:a) C/D=0.5 $p_f=10.0\text{kN/m}^2$ b) C/D=1.0 $p_f=0.0\text{kN/m}^2$	124
Figure 6.1 : Failure bulbs depends on overburden ratio (Chambon et al., 1991)	126
Figure 6.2 : Influence of Tunnel Diameter on Collapse Pressure	129
Figure 6.3 : Variation in surface settlement trough width parameter with tunnel depth for tunnels in sands and gravels	131
Figure 6.4 : S1 loose C/D= 0.5: surface settlement after total face displacement $d_s=5\text{mm}$;a) with no surcharge max. settlement: 5.0 mm b) With surcharge load max. settlement: 5.5 mm c) with textile max. settlement 4.5 mm	132
Figure 6.5 : Failure process: internal pressure versus face displacement in prototype dimensions (König, 1991).....	133
Figure 6.6 : Idealised stresses acting on tunnel face (Franzius,2003).....	134

THE INVESTIGATION OF STABILITY OF TUNNELS AND SETTLEMENTS WITH CENTRIFUGE MODELLING

SUMMARY

In most of the larger cities underground transportation systems are preferred. Such systems are constructed in urban areas and involve a tunnel, especially in soft ground and in shallow zones. Underground structures are most well-known challenge for civil engineers in respect to planning of the measurements and performing of underground structure.

One of major concerns for tunneling operations in urban area is the effect on neighbouring buildings, because the tunneling operation and near structures highly interact with each other. Whatever the used construction method is, the excavation of a tunnel causes displacement around the opening and may expand towards the ground surface. The dislocations of the buildings interact with the ground movement, and the rigidity of existing structures will promote reduction of the magnitude of displacements induced by tunnelling.

The lateral displacements of heavily strengthened buildings will be smaller than the foundation ground. When compared to ground distortions, the flexural stiffness of these structures causes distortions to be reduced, especially if continuous foundation supports are used (long strip footing or raft). Stiff structures show a tendency to be exposed to tilt rather than distortion and exhibit a great resistance against shear stress. This reaction form is related to the building height (floor number), the number of openings and type of structure (concrete walls, beams and pillars, etc.).

In this thesis, to determine displacements, centrifuge modelling is used. The small scale centrifuge model, which is newly designed, provided dependable information about the face collapse of a shallow tunnel. A required support pressure for shield driven tunnels in soft materials, and the ground deformations along the longitudinal section of the tunnel model, can be identified by simulating a loss of tunnel face stability.

In soft ground and shallow zones, formation of deformations which are taking place according to the different soil grain size, different line thickness and whether there is a structure on the surface or not is discussed in this thesis.

SANTRİFÜJ MODELLEME İLE TÜNEL STABİLİTESİ VE OTURMALARIN ARAŞTIRILMASI

ÖZET

Dünya üzerindeki şehirlerin gelişimi sürdürdükçe yaşanan yer problemleri yer altı sistemlerinin kullanımını zorunlu hale getirmektedir. Genellikle ulaşım problemlerine çözüm sağlayan tünellerin artık yaygın olarak kullanılmaya başlanmasına rağmen, büyük şehirlerde tünel inşaatı beraberinde önemli problemleride açığa çıkarmaktadır.

Bilindiği gibi inşaat metodu ne olursa olsun, tünel açımı sırasında deformasyonların oluşumu kaçınılmazdır. Spt değeri 50'den düşük olan zeminlerde, genellikle tünel açma makineleri (TBM) kullanılmaktadır. Bu makineler, tünel yüzeyinin kazılması esnasında, yüzeylere basınç uygular. Teoride, aktif toprak basıncı ile tünel kazım esnasında uygulanan basınç birbirine eşit olur ise, tünel açma esnasında herhangi bir deformasyon oluşmaz. Ancak, tünel yüzeylerine uygulanan basınçların artması, inşaat sürelerinin ve maliyetlerinin artmasına neden olduğu için, genellikle inşaat aşamasında basınçlar doğru ayarlanamamakta ve zeminde deformasyonlar gözlenmektedir. Aynı şekilde sığ tünellerin imalatı esnasında deformasyon problemi ile karşılaşabilmektedir. Eğer tünel çapı D , tünel merkezinden zemin yüzeyine mesafe C olarak tanımlanırsa, C/D oranının 0.5 olması halinde tünel çeperindeki deformasyon, zemin yüzeyine ulaşacaktır. Bu deformasyonlar çevre yapılarında büyük hasarlar meydana getirebileceğinden, inşaat öncesinde ne kadar deformasyonun oluşabileceği hesaplanmalı ve gerekli önlemler alınmalıdır.

Günümüzde birçok numerik analiz programı yardımıyla bilgisayar ortamında deformasyonlar rahatlıkla hesaplanabilmektedir. Ancak, zemin parametrelerinde küçük alanlarda oluşabilen büyük değişiklikler kesin deformasyonların bulunmasını engellemekte, yalnızca yaklaşık sonuçlar elde edilmesine olanak sağlanmaktadır. Bu durum büyük projelerde ve özellikle spt değeri elliden küçük olan zeminlerde, sığ tünellerin inşaatı sırasında belirsizlikler yaşanmasına neden olabilmektedir. Belirsizliklerin giderilebilmesi ise ancak gerçek bir modelleme ile mümkündür.

Santrifüj modelleme, gerçekte varolan bir durumun N kere küçültülerek modellenmesidir. Aynı koşullar yer çekimi ivmesinin N kere büyütülmesi ile sağlanır. Örneğin gerilme formülünü, $\sigma_{vm} = \rho Ng h_m$ olarak yazarsak, modelde oluşacak gerilme $\sigma_{vp} = \rho g h_p$ formülündeki kadardır. Zemine ait parametre olan özgül ağırlık ve yerçekimi ivmeleri değişmediğinden $h_m = h_p N^{-1}$, $\sigma_{vm} = \sigma_{vp}$. Buradan da çıkarılabileceği gibi aynı gerilme uygulanmasına rağmen model, doğal koşullarından

N kat küçük olarak modellenilebilmektedir. Bu yöntem kullanılarak tüm büyüklükler N'in katları olarak küçültülebilir.

Bu araştırmada kullanılan Santrifüj makinesi Bodunkultur Üniversitesi, Viyana' daki geoteknik laboratuvarlarında bulunan, Trio- Tech tarafından 1989 yılında üretilmiş bir giriş santrifüj makinesidir. 3.0 m çapında olan giriş santrifüj makinesi, 10 ton yük kapasitesine, 56 adet kontak bileziğine sahiptir, 15 HP DC motor yardımı ile 0 ile 200 g arasında radial ivmeye ulaşabilmektedir.

Merkezine sabit, dönebilen kollardan dolayı bu ismi almış olan makinede, motor, sistemdeki kolları dönmeye zorlar. Her bir dönen kolun sonunda sallanan bir sepet bulunur, bu sepetlerden birine model, diğerine ise simetriyi bozmamak için modele eş büyüklükte ağırlık yerleştirilir. Yer çekimi ivmesinin (g), N kere büyütülmesi kolun dönme hızını artırarak gerçekleştirilir.

N kere küçültülmüş model santrifüj makinesine yerleştirildikten sonra, N kadar büyütülmüş yer çekimi ivmesi (g)' ye ulaşana kadar, dönen kolun hızı artırılır. Bu işlem bir kontrol odasından yapılır. Deney sırasında bir fotoğraf makinesi, sürekli olarak (yaklaşık olarak 6 sn'de bir) fotoğraf çeker, bu sayede modelde deney sırasında oluşan göçmeler, oturmalar vs.deney başlangıcında çekilen fotoğraf ile PIV programı yardımı ile karşılaştırılır. PIV (Particle Image Velocimetry), matlab içinde çalışan bir programdır ve iki ya da daha fazla resmi üst üste koyarak, model içindeki zeminin hareketini verir.

Bu çalışmada, Gregor Idinger tarafından hazırlanan deney düzeneği yardımı ile, değişik parametrelerin (zemin yüzeyine yük olup olmaması, farklı zemin koşulları, tünel yapımı sırasında yapılan destekler, son olarak da tünel üzerindeki tabaka kalınlığının değişimi) tünel yüzey basıncı, oturmalar üzerindeki etkisi incelendi.

Deney düzeneğini oluşturmak için üç adet alüminyum plaka ve bir adet 10 cm kalınlığında cam kullanılarak 441x 155 cm iç ebatlarında bir kutu hazırlandı, kutunun iç kısmına maksimum deformasyonların olduğu bölgeyi görebilmek için, tünel ekseninden dik kesilmiş olarak modellenen deney düzeneği yerleştirildi, tünel modeli deney düzeneği lineer tetikleyici, yük hücresi, deformasyon ölçer, CCD kamera ve aydınlatma birimlerinden oluşmaktadır. Düzeneğin üzeri kum tabakaları ile doldurularak zemin profili oluşturuldu, kumun yerleştirilmesi esnasında relatif sıklığın her yerde aynı değeri alması için, kumun yerleştirilmesi işlemi bir huni yardımı ile aynı yükseklikten yapıldı, yerleştirme işlemi tamamlandıktan sonra, tabaka yüzeyinin düzeltilmesi dışında herhangi bir işlem yapılmadı. Aydınlatma işlemi, hazırlanan kutunun sol ve sağ tarafına led ışıklar monte edilerek sağlandı.

Deney esnasında, düzenek büyük hızlara ulaştığı için, santrifüj makinesinin içine yerleştirilen bir kameradan alınan görüntüler kontrol odasından takip edilmektedir, çalışma esnasında bir problemle karşılaşmaması esnasında, daha önce belirlenen yer çekimi ivmesi değerine (N_{xg}) ulaşana kadar düzenek kontrollü olarak hızlandırılır. İstenilen değere ulaşıldıktan sonra, bilgisayar komutları ile tünel basıncı azaltılır. Tünelin yatay hareketi, lineer tetikleyici ile kontrol edilir, tünel basıncının azaltılması ise, tünel içindeki pistonun lineer tetikleyici yardımı ile, tünel yüzeyinin 500 adımda 5 mm geri çekilmesi ile elde edilir.

Tünel yüzeyindeki hareketin, oturmalar üzerindeki etkisini inceleyebilmek amacı ile daha önce pistonun arkasına yerleştirilmiş olan bir yük hücresi ve deformasyon ölçerin kayıtları tutulur. Bu yöntem, tünel yüzeyinde oluşan hareket ile

yüzey basıncının ve oturmaların değişimini incelemeye olanak sağlamaktadır. Deney esnasında aynı açıdan 6 saniyede bir alınan fotoğraflar kullanılarak, matlab içinde çalışan GeoPIV programı ile yüzey hareketleri kesin olarak belirlenebilmektedir.

Çalışma esnasında, iki farklı kuru temiz kum kullanıldı, farklı dane çapı dağılımına sahip kum zeminlerde, sürsarj yükü ya da tekstil kullanarak, yer çekimi ivmesinin 75g olduğu durumda yedi adet deney yapıldı. Deney düzeneğinin 75 g değerine ulaşabilmesi için, giriş santrifüj makinesinin merkezine sabit kollar, dakikada 237 tur yapacak şekilde 136 km/sa hız ile dönmektedir.

Sürsarj yükü olarak, 5 katlı bir binanın zemin yüzeyinde bulunduğu kabulüne göre iki adet deney yapıldı. 12mx14m oturma alanına sahip 5 katlı bir binanın ağırlığı, Kat sayısı*oturma alanı*1.1 (ton/m²) formülüne göre yaklaşık 924 ton olarak hesaplanır, ancak modelleme esnasında ağırlık 1/N³ ile orantılı olarak küçültülmektedir. Modelleme esnasında sürsarj yükü 924/ 75³ formülünden yaklaşık 2 kg olarak hesaplandı.

Yedi deneyden, 5 adedi C/D oranı 0.5 olarak sabit iken, diğer iki adedi C/D oranı 1.0 değerinde sabit olarak tutuldu, böylece yüzeye oluşan deformasyonların tabaka kalınlığına bağlı olarak inşaatın yüzey oturmaları üzerindeki etkisinde incelendi.

Deneylein değerlendirilmesi sonucu zemin yüzeyinde oluşan oturmalar için elde edilen veriler;

- 1) Zemin yüzeyinde, ekstra yapı ya da yükün var olması durumunda yüzey oturmaları yükün artışı ile doğru orantılı olarak artış gösterir,
- 2) Zemin özelliklerinin değişmesi durumunda, yüzey oturmaları, yüzeyde sürsarj yükünün olduğu durumdan daha fazla değişim gösterebilir,
- 3) Tünel çeperlerinde yapılan iyileştirme çalışmaları, yüzey oturmalarının önlenmesinde etkili olabilmektedir,
- 4) Tünel üzerinde ki tabaka kalınlığının arttırılabilmesi halinde, tünel yüzeyine etki eden oturmalar minimize edilebilir.

Tünel yüzey basıncının değişimi ile ilgili elde edilen veriler;

- 1) Zemin yüzeyinde ekstra yapı ya da yükün olması durumunda, maksimum yüzey basıncı yükün büyüklüğüne bağlı olarak değişir,
- 2) İki farklı zemin kullanılması durumunda, yüzey basınçlarında büyük değişiklikler görülebilir,
- 3) Tekstil kullanımı yüzey basınçlarını azaltır.

Tünel yüzey basıncı, tünel merkezinin yukarısındaki gerilme değerlerine, sürsarj yüküne, tabaka kalınlığının artmasına bağlı olarak artar. Ancak, tekstil kullanımı ile, oluşan maksimum yüzey basıncı değerleri azaltılabildiği gibi, herhangi bir göçme olması engellenebilir.

1. INTRODUCTION

The experiments explained to this thesis was conducted at Geotechnical laboratory of Bodunkultur University, Vienna. . The model box was designed to be used in the experiment explained thesis, but also considering realization of prospective projects, particularly those using the PIV (Particle Image Velocimetry) method. All equipments was designed by Dipl.-Eng. Gregor Idinger.

1.1 Scope of Thesis

The major purpose of this resarch is, to investigate the ground movements which take place due to tunnel face stability, and which depend on the different soil grain size, different line thickness and whether there is a structure on the ground surface or not. Tunneling effects on deformations and surface settlements is very important. As is known to all, provided the deformations extend beyond the highest values, extend of the ground movements reaches such a degree that the neighbouring buildings may be highly damaged.

Tunneling operation in soft ground is generally performed with mechanized tunnel boring machines (TBM). Working principle of these machines hinges on the fact that ground deformations can notably be brought down if tunnel face is excavated while a pressure is applied. Theoretically, if the active earth pressure acting on the excavating face colud be perfectly balanced by the TBM, there would be no deformations. Yet, if the face pressure increases, the construction gets slower and more expensive. As a result of practices it has been observed that tunnels in soft ground can be succesfully constructed using reduced face pressures without causing excessive ground deformations.

Related to the supplied face support, accurate predictions of ground movements caused by tunneling in soft ground are necessary for an efficient construction process which prevents nearby structures from any damage.

Purpose of the research is to model face stability problems, mostly with small scale models. Besides being economically challenging, full scale models, also called prototypes, are not appropriate for parameter studies. Moreover, tunnels which are about to collapse are not accessible due to safety issues.

1.2 Sections Of The Thesis

This thesis consists of 6 sections. Part one is based on the general information and literature researches. In part two, besides the information about the history of geotechnical centrifuge machine and its usage, information about the principles of the usage is given. In part three, PIV programme used in the analysis of the results is explained. Part four consists of the information about the experiment equipment. Part five is the section where the results of the experiment are explained. Part six includes the assessments regarding to the experiments.

1.3 Literature Review

1.1.1 The History of Tunnel

Humans dug tunnels and formed caves with the purpose of protecting themselves from dangerous enemies and storing foods that had been collected by hunting or fishing in the ancient times. It is proved that in the Stone Age, people sank shaft and drove tunnels to find flint which they used for bladed tools. Afterwards metal tools were invented and used for excavation of underground. People in Caucasia, near Black Sea, performed the early excavations on metal-bearing ores, which was about 3,500 BC . Most of the great civilizations like Aztec, Inca, Egyptian, Persian and Babylonian had built tunnels. While the tunneling tools were the primitive tools such as bone, antler, flint and wood in the early ages, more advanced tools such as bronze, iron, and steel are used as the civilization made progress. For hundreds of years, tunnels had driven in rocks by heating, which would cause expansion, and then to accelerate the process, wetting the rock face. Remaining was removing the fractured rock with picks and wedges. Mines of Egypt and Rome were reaching to a depth of about 200 m. Before the 6th century B.C. a hand-worked tunnel was possibly expected to be constructed with an advance rate of about 9 m per year.

In the initial phase of mining, rare minerals such as gold and jewels could be found on the ground surface or in the riverbed and collecting was not so difficult. Along

with the development of mankind, amount of rare mineral supplied to the market reduced and mining enterprise had to find new ways to obtain rare minerals from new and rich mines with their own financial capabilities.

Mineral ore often lies in deep in the underground and is difficult to dig out. Underground excavation, which is a challenging work, should be performed. With the developing mining engineering, tunnel excavation technology has made progress as well.

The main reason of tunnel excavation in mining is to obtain or explore minerals and is used temporarily until reaching the minerals. In order to transport the mineral to the surface safely, the “main tunnel” has to be kept stabilised. Mine tunnels are mainly excavated with no support in rocks, but if undesirable conditions are encountered, some types of support installed to prevent the rock collapse. In the early years of tunneling, timber support was installed by the skilled labor, and then steel rib and lag method is used.

In the 1760's when tunnels were constructed for transportation purpose, first modern tunnel construction started in England. When hills were encountered, the problem was solved by modifying the top in platforms and building of locks, thus ships reached the next level. The locks were used each time the water descended through the system, accordingly this method depended on a good alimentation with water to the top. Because of that the first channels were likely to eschew hills, making the travelling time very long and as a result the technique of constructing tunnels through the versants found.

In 1825, the opening of the Stockton railway in Darlington, England, opened a new period in transportation. The knowledge obtained by building the channel tunnels was then applied in constructing railway tunnels. By then, most of the work was done manually, and the excavated material was carried out by horses. In order to build long tunnels, wells were made along the route, therefore the work could be started in several points, and required time to finish the project was reduced.

One of the first tunnels passing under a river was the Rotherhithe Tunnel, connecting Rotherhithe and Wapping which was constructed beneath the Thames River (London). The work started in 1825, but the ending of it was delayed until 1843 because of a great flow of water and mud.

In 1802 the idea of a tunnel under the English Channel was suggested by the French engineer Albert Mathieu, but the work was started at the end of 1870's, using a machine for excavation. Because the British feared a French invasion through the tunnel, the work was stopped in 1882. After that, it was restarted in 1973, but stopped again in 1975 because of a rapid increase of the costs. For the last time the work was resumed by the end of 1980's and finished in 1994. Nowadays the EuroTunnel is connecting France and England in both directions through railway and vehicles.

Before starting construction of a tunnel, detailed ground analyses and probe drills are performed. Past displacements of the ground could have disturbed and crushed rocks even in regulated formations. Rock crevices can make the excavation more challenging, and also sudden and uncontrollable infusions of water may take place during the construction, especially if it's deep or the construction is under water.

In some cases, to check and investigate the rock layers, small exploration tunnels are constructed near the main route of the tunnel, but for testing the resultant signs of possible problems, the builders generally use to drill just a little further from the main front of the tunnel.

Smaller tunnels are often excavated by use of digging machines with a simple rotative head. On the other hand larger tunnels are excavated using a road header, having a rotative cutting head on a hydraulically driven spire, which makes it possible for it to reach all parts of the tunnel's forepart.

Tunnels in rock are excavated by perforation and dynamiting. The tunnel roof can be left unsustained for a limited time, but the tension amongst small rocks may change and cause stone collapses, so supporting is provided soon after excavation. Using steel vaults sheathed with wood is one of the common methods. As an alternative, concrete can be pulverized on the rocks, or reinforced concrete can be used. Some rocks have such a strong formation that bolstering is not required. In soft ground, tunnels have to be supported as close as possible to their front, to prevent any collapse. One of the methods is to go 60 cm forward with the front, and then install a sustentation ring made of cast iron or concrete. Instead, moisturized concrete can be used, and until the hardening occurs, temporary steel bolsters can be fixed.

If undersea tunnel are constructed, the immersed tube method is particularly used. Tunnel portions are made on the surface and then sunk into a dredge groove. So as to make them resistant to water, articulations between the sections are then tightened and the construction is covered by sand. Then, in order to start the works inside water is pumped out of the tunnel. For example, for the tunnel connecting Hong Kong to Kowloon (mainland China), this method was used. But The first immersed tunnel is under the Shirley Gut in Boston, and the construction began in June 1893 (Figure 1.1).

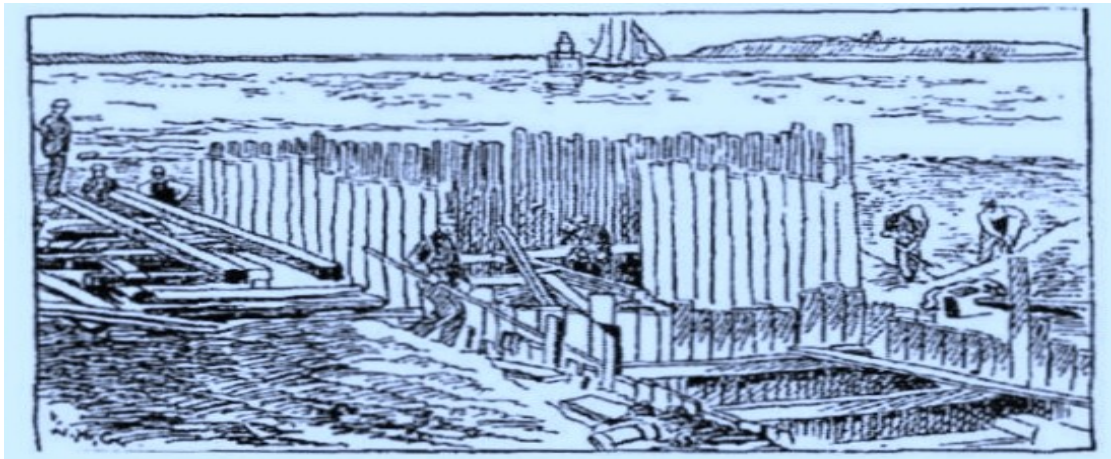


Figure 1.1 : The first immersed tube under Shirley Gut in Boston (Lotysz,2010)

The longest tunnel of the world (54 km) is between the Japanese islands Honshu and Hokkaido, under the Tsugaru Strait. It involves a large railway tunnel and two smaller road tunnels, it is also used for maintenance, draining and ventilation.

Length of the EuroTunnel (under the English Channel) is 50 km and width of each of its twin tunnels are 7.6 m. Its average construction speed was 12 cm per minute.

1.1.2 The Technical History of Tunnel

Peck (1969) presented a first state-of-the-art report based on many studies, stating three important requirements to construct a sufficient tunnel. The first one is about stability, because in order to build the tunnel safely the construction method used must be selected with paying attention especially to stability of the tunnel face, before placing the tunnel lining. Secondly, excavation and construction of the tunnel should not cause any ground displacements which may lead unwanted damages to neighbouring structures, utilities, and roadways. Thirdly, during the design lifetime

of the tunnel the lining should be serviceable in the case of exposing any subsequent influence.

Many research has been conducted regarding ground displacements related to tunneling in clay. Some of the initial centrifuge tests on this subject were performed by Mair (1979), who worked on centrifuge modelling research to examine collapse of tunnels in soft clay.

Upper and lower bound theorem solutions of plasticity for tunneling in soft clay was suggested by Davis et al. (1980). To obtain stability solutions for ground collapse under undrained conditions three different shapes of shallow underground opening were taken into consideration. Moreover, blow-out failure risk caused by excessively high support pressure, was examined.

Up to date, research on the centrifuge modelling of tunnels in sandy soils has been limited. The initial centrifuge studies about the relationship between face pressure and face stability was conducted by Chambon And Corte (1989, 1991, 1994). They performed centrifuge tests on tunnel models in dry sand. Examination of the pressures at which face stability was lost and observation of the post-instability ground deformations related to tunnel failures at various depths was also investigated by them. In order to examine the face stability of tunnels in sand and offer charts for evaluating the required face support pressure, Léca And Dormieux (1990) applied limit analysis techniques. Analysis of safety against both collapse and blow-out were performed. According to these upper and lower bound solutions a range of pressures for which tunnel face instability might occur, were predicted.

Face stability conditions in cohesionless soil under drained conditions, on slurry shield and earth-pressure-balanced (EPB) shield driven tunnels were examined by Anagnostou and Kovári (1994, 1996). Recently, these two machine tunneling methods have been successfully used throughout the world.

Using the elastic-plastic Mohr-Coulomb constitutive model, Vermeer et al. (2001, 2002) conducted a three-dimensional finite element analysis for drained soft ground conditions.

At 2011, the centrifuge model tests about the problem of tunneling beneath end-bearing piles in sand, presented by Marshall et. al. (2011). In that investigation, soil

and pile displacement measured using particle image velocimetry and close-range photogrammetry techniques. A soil zone displaced from around the piles towards the sides of the tunnel, the displacing soil indicates a roughly rigid body motion.

1.1.3 Tunneling in Soft Ground and Shallow Zones

While the population in urban areas increases, to keep space at the surface, essential services such as transportation and other utilities must be carried to under ground. Because tunneling causes less disruption and destruction than the cut-and-cover method and in most cities depth of tunneling remain within the soft ground zone at top, soft ground tunnels will be required more. Researches of special interest conducted in soft ground tunneling are mostly about distinctive stability properties of the material faced with at the tunnel face and conditions of the groundwater along the alignment. The first person who define the expected ground behaviour in soft ground tunnels was the author of the Tunnelman's Ground Classification (firm, raveling, squeezing, running, flowing, swelling), Terzaghi (1950). From the following equation (1.1), Peck (1969) makes an approximation of ground behaviour in soft ground tunneling:

$$N_t = (P_z - P_a) / S_u \quad (1.1)$$

Here, N_t is the stability factor, P_z is the overburden pressure at tunnel centerline, P_a is the pressure applied to the interior face and S_u is the undrained shear strength. Concerning the preponderant ground material, one can approximately estimate tunnel stability using this stability factor. Tables for cohesive soil, silty sand above water table, sand and gravel was published by Monsees (1996). Because of the destabilising effect of pore water pressure on the ground stability, groundwater control is of a great significance in soft ground tunneling. While a small amount of water contained in granular soils above the water table may offer more stand-up time benefiting of an apparent cohesion, water existing below the water table causes a severe reduction of the effective soil strength. A seepage pressure generated in noncohesive soils would cause a rapid failure. For that reason, in order to avoid ground failure when driving a shield tunnel under the ground-water table and drained conditions apply, the effective interior face pressure must be increased naturally by the pore water pressure. Furthermore, the weight under the water surface has to be used in all calculations. If open face tunnels are driven under the ground-water table

and drained conditions apply, the water shows an extra destabilising effect because groundwater flows towards the tunnel heading (Vermeer, 2002). However, due to technical and economical restrictions, the increasing of the interior support pressure is limited. If despite an increase, support at tunnel face can not afford to hold out the percolation of the water toward the tunnel, other kinds of acts required to be implemented. There is four main methods available: dewatering, compressed air, grouting and freezing. More detailed descriptions of these methods as well as the applicability for grain size, and thereby permeability, of the soil is done by Monsees (1996).

As described above, tunneling in urban areas is problematic because of soft ground conditions. In addition to this, depth of the installation of these tunnels is often shallow, in other words they are close to existing structures (if the cover is in a range of 3-5 times tunnel diameter or less, it is classified as shallow). Underground excavations are altering the stress field in the ground around the tunnel and deformations will occur. Throughout the construction process, control of these deformations has to be done strictly. Any other way, excessive ground movements would propagate upwards and cause an important damage to settlements on the surface or at structures (e.g. other buried infrastructure, footings) placed over the tunnel. Hence, it has the uttermost significance to reduce the degree and impact of ground deformations while constructing a tunnel in shallow depth. It should be noted that the control of the arising subsidence through the choice of the tunneling method and equipment is mostly in the contractor. Water table depression and/or lost ground can cause a subsidence. If external dewatering is applied, or the tunnel itself is working as a groundwater drain, water table depression will develop. In both cases the water table depression raises the effective stresses which is assessable by the soil mechanics theories. Tunnels in sand and gravel settlements, which are usually small, are approximated by elastic theory. On the other hand, tunnels in clay, silt or peats settlements are reasonably higher in magnitude and approximated by consolidation theory. In the 1970s, initial measurements on a resulting surface settlement had been made, in view of subsidence due to ground loss. The following equation (1.2) had been defined by these studies:

$$VS = VL - \Delta V \quad (1.2)$$

Here VS is the volume of the settlement on the ground surface, VL is the volume of ground movements happening around the tunnel, and ΔV is the volume change within the soil (+ expansion/ bulking, - compression). The complex relation among these quantities is defined insufficiently, but it is practicable to assume that ΔV is zero. This estimate is effective, on the condition that bulking or consolidation processes are not generated. Tunnel face, the shield and the tail are the points of ground loss reasons (Monsees, 1996). The maximum settlement and the extension in and perpendicular to the driving axis are of capital importance. For an individual tunnel the form of the perpendicular settlement trough on the surface is similar to that of the bell-shaped probability curve (Peck, 1969).

The evaluation of blowout or upheaval of the overlying ground is an additional feature of face stability analysis for shallow tunnels. This safety reveals economic consequences, because when earth pressure is of a larger design, necessary overburden increases. Related to the ground conditions for tunneling, a ground with and without a macro structure (stratification, schistosity, jointing) is differentiated. Urban areas founded in soft quaternary materials with no important macro structures are the focal point in this thesis. Grounds with macro structures ground are more common in deep tunneling. For soils and weathered rock, shear strength parameters which are measurable in laboratory tests determine the stability. Tunnels driven in ground with little (effective) cohesion are dependent on a shield to secure the stability of a tunnel face. If the cohesion is greater in the ground, an open face tunneling method such as the New Austrian Tunneling Method may possibly be used.

1.1.4 Induced Ground Movements –Because of Tunneling

Surface settlement and tunnel depth is interrelated, but not simply and linearly according to the ITA/ AITES REPORT 2006. In fact, factors such as 1) hydro-geological, geological and geotechnical conditions, 2) geometry of tunnel and depths, 3) excavations method and 4) the workmanship and management quality affect ground movement. But undoubtedly, a shallow tunnel has usually more tendency to affect the surface structures than a deep one.

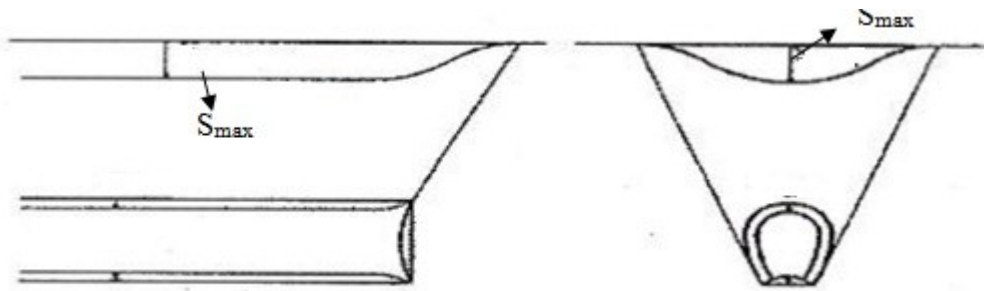


Figure 1.2 : Displacement of the excavation profiles (Leca, 2007)

S_{max} : Maximum ground surface settlement

Existing ground stresses and hydro-geological conditions are unavoidably affected by the construction of a tunnel. If the natural stress conditions are changed, typically the face rapidly displaces inward and the tunnel walls converge (Figure 1.2). Extra long term deformations may be seen in soft cohesive soil as a result of tunneling work induced changes in the pore pressure.

The magnitude orientation and ground movement locations close to the opening rely on several factors such as the geotechnical conditions encountered, existing geostatic stresses and surface loads, hydro-geological conditions, and the methods used for tunnel excavations and ground support. If the ground mass strength is exceeded, important displacements may happen in respect of both magnitude and acceleration.

1.1.4.1 Face Stability

At the ITA/ AITES Report 2006 , the failure mechanism of an unsupported tunnel is described. In soft ground the construction of an unsupported tunnel opening would cause ground displacements in a large scale, and then it could lead to a failure zone(Figure 1.3) to be formed behind the face. If the ground is weaker, the failure zone may involve the ground ahead of the tunnel face.

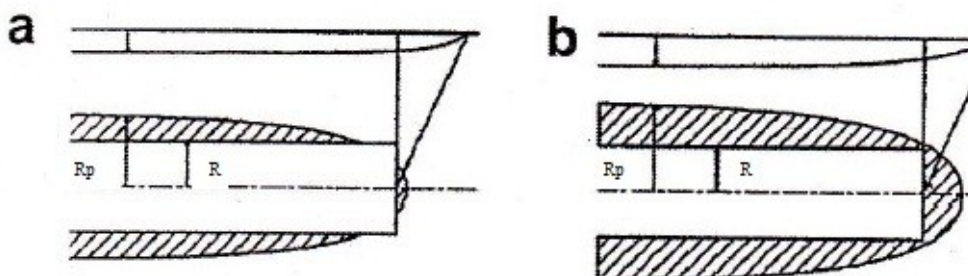


Figure 1.3 : a) Yielded zone rear of the face. b) Yielded zone ahead of the face. (Leca, 2007)

Two kinds of failure mechanisms may be observed depending on the structure of the ground encountered.

For cohesive soils, failure of the face propagates towards the ground ahead of the working front. This action causes a sinkhole which has a width larger than one tunnel diameter to be formed at the ground surface (Figure 1.4).

For cohesionless soils, failure typically propagates along a chimney like mechanism above the tunnel face (Figure 1.5).

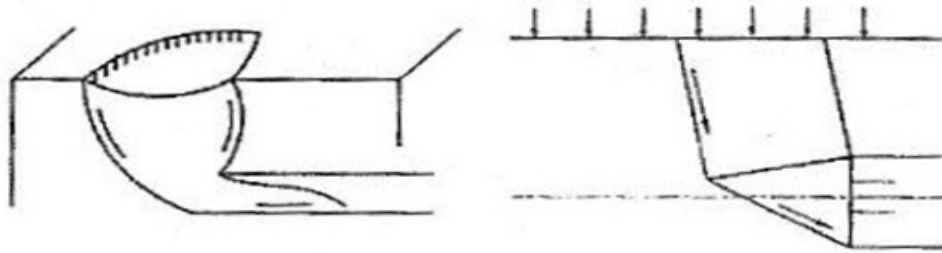


Figure 1.4 : Face Collapse- Basic Diagram in Cohesive Ground Soils (Leca, 2007)

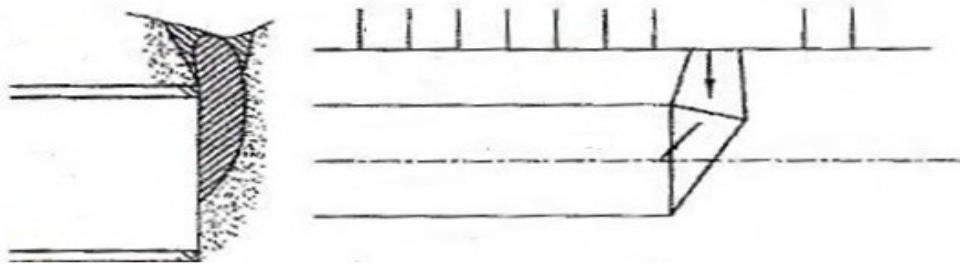


Figure 1.5 : Face Collapse: Basic Diagram in Dry Granular Soils (Leca, 2007)

1.1.4.2 Propagation Of Movements Towards The Surface

Initial ground movements at the opening of the tunnel will trigger propagation towards the ground surface. The range and time scale of this occurrence will generally be dependent upon the geotechnical and geometrical conditions, and construction methods used.

Relying on the measurements and observations performed in situ, two propagation modes have been determined. In a transverse plane, level of propagation of displacements initiated at the tunnel opening can be evaluated using these modes. As seen in the following, they will be entitled as primary mode and secondary mode (Pantent,1993).

The primary mode: occurs when the ground stresses are freed at the face. A zone formed by loosened ground above the excavations characterize it. This zone generally has a height of 1-1.5 times the tunnel diameter and width of about one diameter. Along the vertical direction two compression zones are formed laterally. For deeper tunnels ($c/d > 2.5$), most of the time the observed tunneling impact at the surface is limited (Cording and Hansmire, 1975; Leblais and Bacon 1991, Pantet 1991) (Figure 1.6).

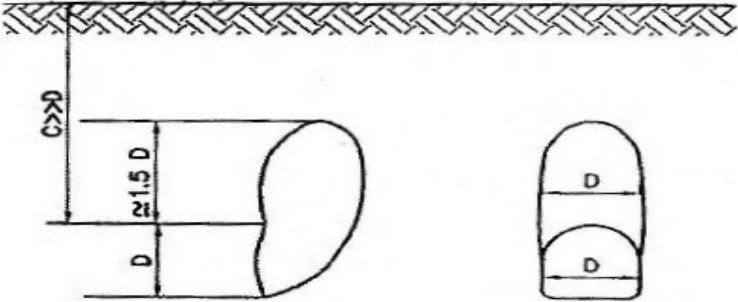


Figure 1.6 : Primary mode : basic transverse cross-section (Leca, 2007)

C : The distance from tunnel center to ground surface

The Secondary mode: If the tunnel is constructed close to the surface ($c/d < 2.5$) and confining support is insufficient, the secondary mode may follow after the primary mode. This situation leads to the formation of a rigid ground block which is bounded by two single or multiple shear planes running from the tunnel to the surface. Displacements formed at the ground surface above the opening have a similar order of magnitude as those at the opening (Figure 1.7).

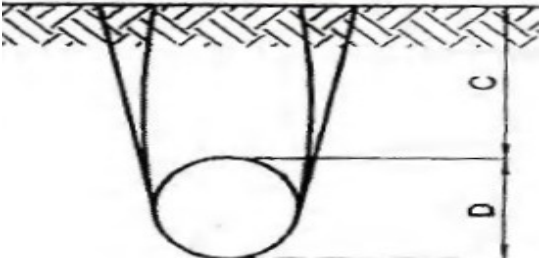


Figure 1.7 : Secondary mode : basic transverse cross-section (Leca, 2007)

At the investigation of Chambon et. al. (1994), for surface settlement, the distance between the tunnel face and surface of the soil, is critical. When the distance is designated with C and the tunnel diameter is designated with D, whether the surface will be affected from the settlement is obtained by the rate of this parameters. If the

C/D ratio is equal to or smaller than 0.5, the surface settlements take place, on the contrary if C/D is higher than 0.5, surface settlements do not take place (Figure 1.9).

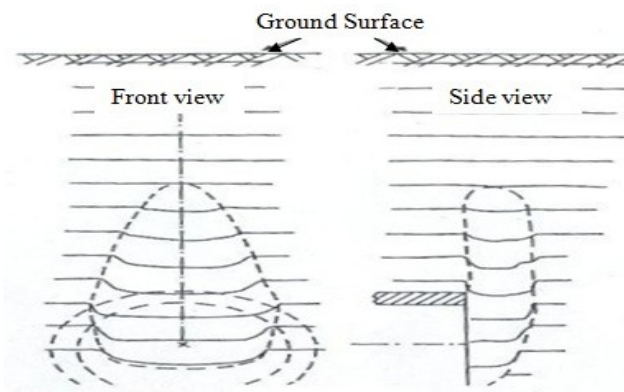


Figure 1.8 : Failure bulb for fully lined tunnel (Chambon et. al., 1991)

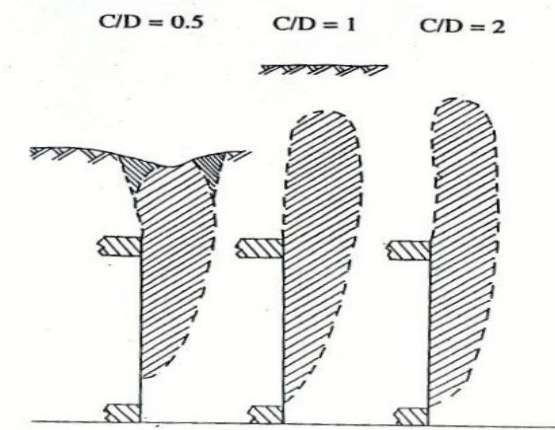


Figure 1.9 : Failure bulbs for different C/D ratios (Chambon et al., 1991)

In addition, the minimum support pressure grows directly in proportion with the diameter (Figure 1.10).

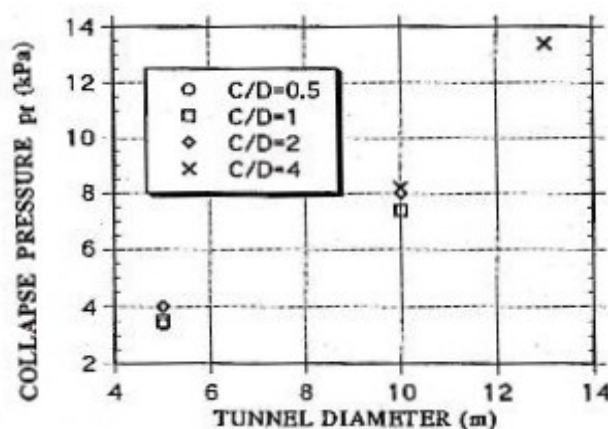


Figure 1.10 : Influence of Tunnel Diameter on Collapse Pressure p_f (Chambon et al., 1991)

As excavations go forward, these mechanisms triggered by the ground response generally cause vertical and horizontal displacements that is likely to build up at the ground surface. As a result it forms what is named as the settlement trough (Figure 1.11).

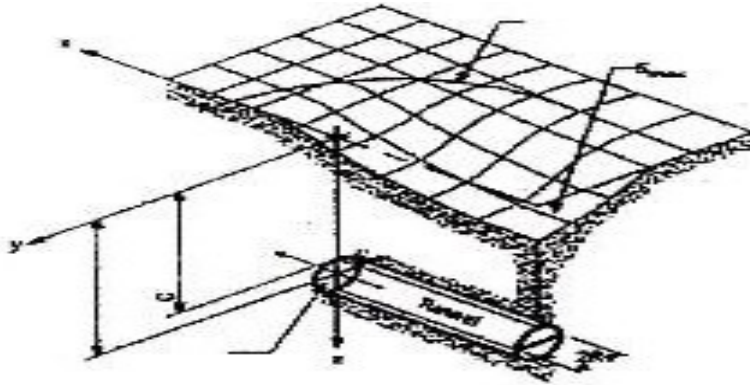


Figure 1.11 : Three-dimesional transverse settlement trough (Attewell et. al.,1986).

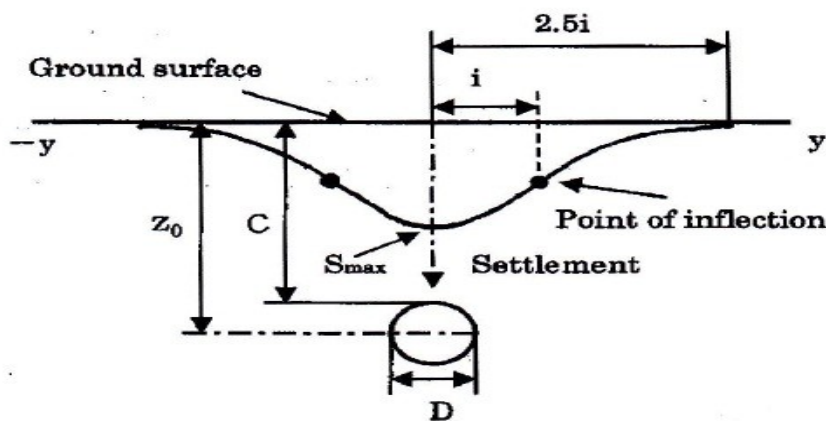


Figure 1.12 : Transverse settlement trough (Sugiyama et. al., 1999)

In 1969, Peck started that the tranverse settlement(Figure 1.12) trough can be described by a Gaussian function and maximum vertical settlement on the tunnel centerline is given by equation 1.3.;

$$S_v(x) = S_{v_{max}} e^{\frac{-x^2}{2i^2}} \quad (1.3)$$

Where $S_{v_{max}}$ is maximum settlement on the tunnel centerline, x horizaontal distance from the tunnel center line, i horizontal distance from the tunnel centerline to the point of inflexion on the settlement trough. i_x can be determined with using below equation 1.4.;

$$I_x = K \cdot Z_0 \quad (1.4)$$

here Z_0 is the distance between tunnel center and ground surface. K can be taken 0.5 for the clay stratum (Figure 1.14), 0.35 for the Gravel-sand stratum (Figure 1.13).

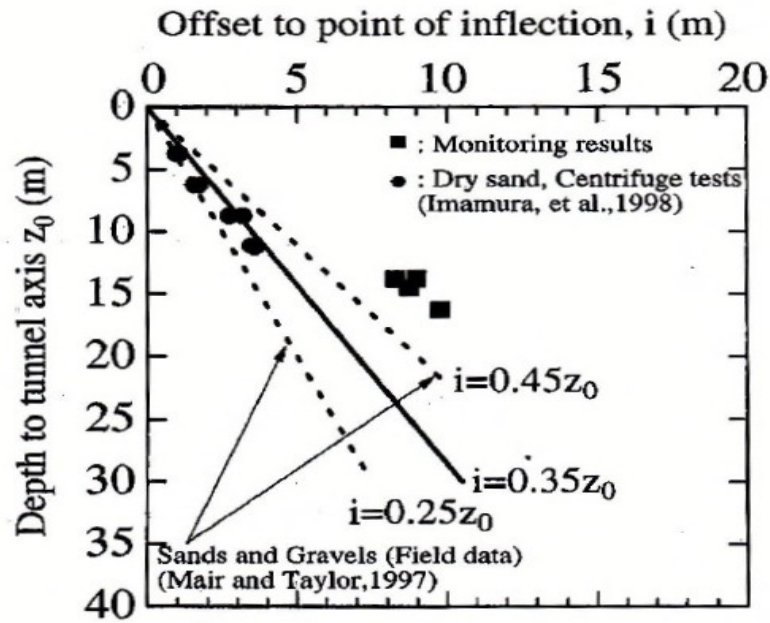


Figure 1.13 : Variation in surface settlement trough width parameter with tunnel depth for tunnels in sands and gravel (Sugiyama et. al., 1999)

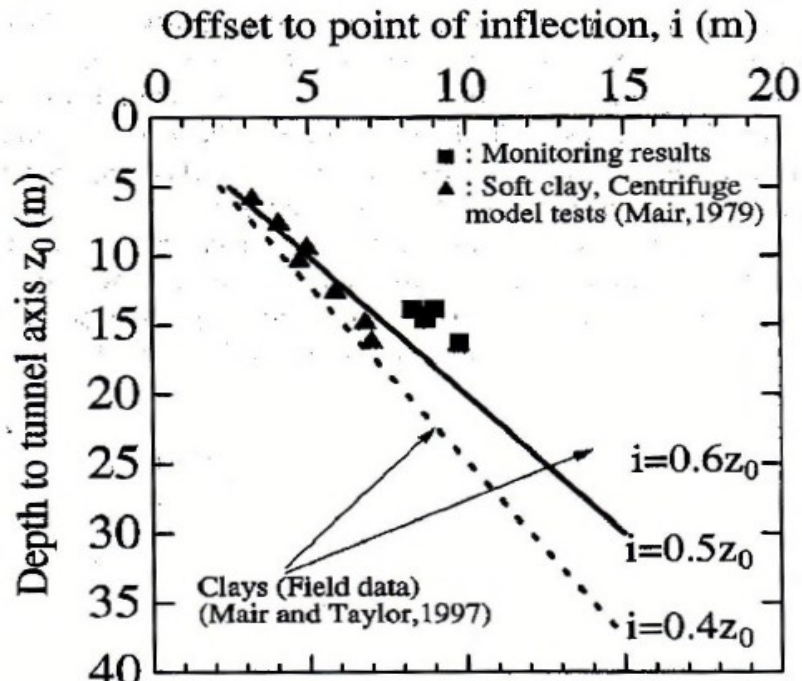


Figure 1.14 : Variation in surface settlement trough width parameter with tunnel depth for tunnels in clays (Sugiyama et. al., 1999)

1.1.5 Causes For Construction Induced Settlements

Displacements along the center-line of the tunnel begin at some distance ahead of the face and carry on increasing unless a complete support system is placed appropriately. Hence, a distinction between the settlements determining the methods of excavation used at the face, and settlements behind the face. In order to describe the steps related to settlements, four main settlement sources can be recognized:

- Settlements connected with the stability at the face
- Settlements connected with the properties and conditions of placing of a temporary support system
- Settlements connected with the cross-sectional sequencing of the excavation
- Settlements connected with the latest lining installation and reaction.

Whatever the used construction method is, the excavation of a tunnel causes displacement around the opening and may expand towards the ground surface. The dislocations of the buildings interact with the ground movement, and the rigidity of existing structures will promote reduction of the magnitude of displacements induced by tunneling.

The lateral displacements of heavily strengthened buildings will be smaller than the foundation ground. When compared to ground distortions, the flexural stiffness of these structures causes distortions to be reduced, especially if continuous foundation supports are used (long strip footings or raft). Stiff structures show a tendency to be exposed to tilt rather than distortion and exhibit a great resistance against shear stress. This reaction form is related to the building height (floor number), the number of openings and type of structure (concrete walls, beams and pillars, etc.).

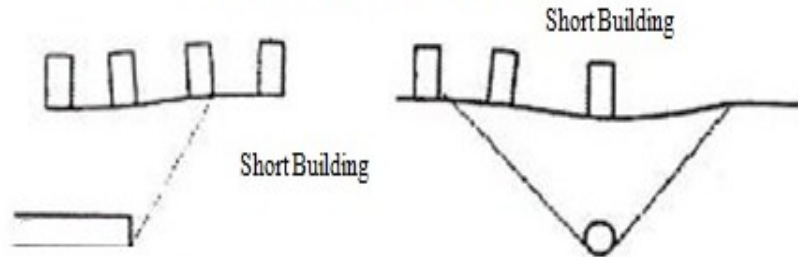
The structure location in regard to the settlement strongly effects the movements experienced (extension and hogging over the convex parts of the settlement; compression and sagging over the concave parts.)

To sum up, it is possible that a structure neighbouring on a tunnel under construction will go through the following movements,

- Uniform settlement
- Differential settlement between supports
- Overall or differential rotation

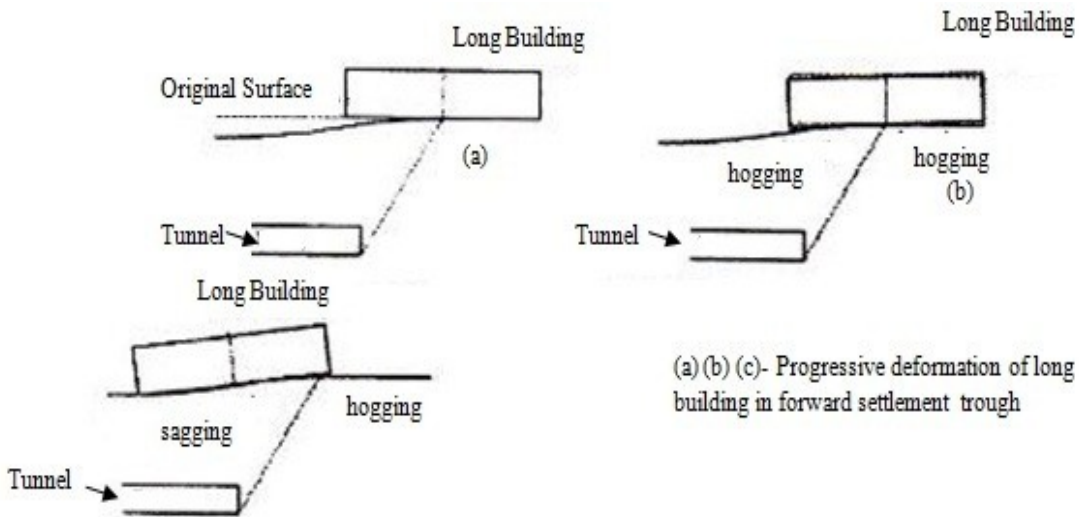
- Overall horizontal displacement
- Differential horizontal displacement in compression or extension (Figure 1.15)

GROUND MOVEMENTS

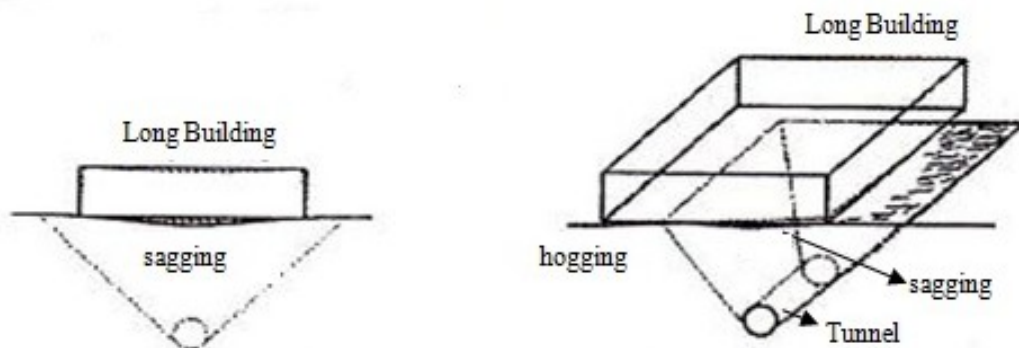


Narrow building rides the forward settlement move with significant sagging or hogging deformation

Narrow building experience as rigid body, but significant sagging or hogging deformation across a transverse settlement



(a) (b) (c) - Progressive deformation of long building in forward settlement trough



Sagging of long building transverse settlement trough

Sagging and hogging of long building in the full trough

Figure 1.15 : Typical idealized building response (Attewell et al., 1986)

There are three categories of the damages which the existing structures experience,

- Architectural damages that affect the visual appearance
- Functional damages that may distort the operation
- Structural damages that affect the structural stability

The chart which represents the British guidelines can be helpful with this assessment of masonry structures.

The purpose of this classification is primarily addressing the practical use and accordingly it is partially based on repair criteria (Table 1.1).

Table 1.1 : Classification of visible damage that may affect standard structures (Leca, 2007)

Damage Type	Damage Degree	Damage Description	Crack width In mm
0	Negligible Damage	Micro-cracks	<0,1
1	Very slight Damage	Architectural	<1
2	Slight Damage	Architectural, To be treated	<5
3	Moderate Damage	Functional	5-15, or several Cracks >3 mm
4	Severe Damage	Structural	15-25
5	Very Severe Damage	Structural	>25

Type 1: It is easy to repair internal cracks during routine renovation Works, as well as some uncommon external cracks which are only perceptible through deep investigation.

Type 2: It is easy to fill internal cracks but the masonry needs to be rehabilitated to make sure adequate tightness, doors and windows may be malfunctioning to a degree

Type 3: Before filling, internal cracks must be opened, the quality and durability of water-tightness as well as insulation may be affected by external cracks, cracks may greatly be inappropriate to residents.

Type 4: Cracking may endanger the safety of residents and structural stability; it is necessary to widely repair and may even include the replacement of wall sections, particularly above the opening, doors and windows are twisted, floors are not horizontal anymore, damaged supporting beams may exist, utilities are broken

Type 5: The building may become unstable and must be rebuilt partly or totally.

The small scale centrifuge model, which is newly designed, provided dependable information about the face collapse of a shallow tunnel. A required support pressure for shield driven tunnels in soft materials, and the ground deformations along the longitudinal section of the tunnel model, can be identified by simulating a loss of tunnel face stability.

The first implementation on the IGT of the digital image correlation ‘Particle Image Velocimetry’ (PIV) technique was successfully conducted. A small model design for the installation of the PIV equipment was carried out. The models could be tested in the geotechnical centrifuge, simulating real stress conditions. Observing ground deformations, beginning and propagation of failure was performed in high resolution and accuracy. Moreover, it was likely to obtain a detailed picture of seeming settlement troughs. Perhaps the first usage of a netbook within a geotechnical centrifuge was applied successfully.

Engineering practice in real world, however, tunneling through dry, cohesionless sand is quite uncommon. Mostly, at sites with coarse-grained soils, parts of the tunnel length can be excavated and constructed within the vadose zone above the groundwater table, where the coarse-grained soil involves sufficient moisture to generate some amount of visible cohesion. This generalisation applies especially for urban areas under which shallow tunnels are possibly to be built. But, in spite of this fact, no physical modelling data come into existence to explain the developing of ground deformations with loss of tunnel face pressure in unsaturated sands.

2. GEOTECHNICAL CENTRIFUGE

Taylor, (1995) explained the the history, principles, laws of the geotechnical centrifuge in his book, called as Geotechnical centrifuge technology. Second section of this thesis is formed by the help of this book.

2.1 Past – Present - Future

A paper with the title ‘De l’equilibre des solides elastiques semblables’ was presented by Edouard Phillips to the Academie des Sciences in Paris in January 1869. In this paper he recognised the limitation of contemporary elastic theory in the analysis of complex structures (Craig,1989). Earlier when he was working in the railway industry, his studies focused on the subjects of the elastic behaviour of steel leaf springs, shock absorbers and beams under both static and dynamic conditions. He encountered insoluble analytical problems and recognized the role of models and of model testing.

Significantly, he recognised the consequence of self weight body forces in a variety of conditions and developed relevant scaling relationships. From this point of view, he developed recognition of the necessity of a centrifuge to attain resemblance of stress between models and prototypes when the same materials were used in one and all.

Field of his early practices was the bridge engineering problems in which British engineers were using bigger and bolder designs at that time. He offered centrifuging a 1:50 linear scale model of the Britannia tubular bridge over the Menai Straits, up to a centrifugal acceleration of 50 g.

Philip Bucky (1931) from Columbia University in the USA appears to be the first person employing centrifuge modelling in one of his papers. His study was related with the integrity of mine roof structures in rock where small rock structures were exposed to increasing accelerations until the rupture. While the work was maintained at Columbia for some time (Cheney, 1988) there was a little or no application of the

models and because this source did not lead to an accepted development, their importance now is practically historical.

The main initial improvement of geotechnical modelling with the centrifuge was materialized in the USSR succeeding independent proposals made by Pokrovskii and Davidenkov in 1932. Several early publications in the Russian Language were available but the first high-profile English Language publication was presented by Pokrovskii and Fiodorov at the First International Conference on Soil Mechanics and Foundation Engineering at Harvard in 1936. As the Second World War developed and followed by the isolation of the Soviet block behind the so-called Iron Curtain little more was heard of this technique.

Dr.A.N. Schofield, from England, had learned about the initial work in the USSR and translated Russian books on the soil mechanics. He saw the potential of and started small scale/low stress model work on structures being undertaken in 1960s at Cambridge University. With the beginning of the new programme, he made up a frame mounted on an existing controlled speed turbine in his own laboratories for the first studies and then stepped up to a larger centrifuge designed by the aerospace and defence industries for environmental testing. In his early works, he focused on problems of slope stability in clay soils and undoubtedly implicated considerations of consolidation.

Centrifuge modelling capacities in many countries were increased to a great degree after 1985. From that day forward recognition of the technique increased among practising engineers and continued increments in the size and number of machines available and also the growth of number of operators.

2.2 Centrifuges In Modelling Principles And Scale Effects

Modelling plays an important role in geotechnical engineering. It is required to reproduce the soil behaviour in respect to strength and stiffness geotechnical modelling. Related to a particular problem there can be a variety of soil behaviour in geotechnical engineering. Two leading reasons determine this: a) it is possible to have a varying soil strata in a site which may influence a particular problem from many aspects, and b) stresses in situ change with increasing depth and as it is well known, soil behaviour is a function of stress level and stress history. Obviously,

reproducing these features is very important in any generalised successful physical modelling. It is for the second reason that centrifuge modelling is widely used in geotechnical engineering. In order to create inertial radial acceleration field which is acting like a gravitational acceleration field but several times stronger than Earth's gravity, soil models positioned at the end of a centrifuge arm are accelerated. The upper surface of the soil model within the container is unstressed and inside the soil body amount of stress increases with depth proportional to the soil density and the strength of the acceleration field. In case the identical soil used in the model as in the prototype and model preparation process maintained carefully because of which the model is exposed to an analogous stress history ensuring that the arrangement of the soil particles is reproduced, at that point for the centrifuge model exposed to an inertial acceleration field of N times the Earth's gravity (g) the vertical stress at depth h_m will be similar to that of the prototype depth h_p where $h_p = N h_m$. In this essential scaling law of centrifuge modelling, likeness of stress is accomplished at homologous points by means of accelerating a model with scale N to Ng .

2.2.1 Scaling Laws For Models

Linear Dimensions

Just as mentioned above, the fundamental scaling law came into existence to meet the need to ensure the model and corresponding prototype stresses are identical. If an acceleration of N times Earth Gravity (g) is put on a material with density ρ , in the model, the vertical stress σ_v at depth h_m (subscript m indicates the model) is obtained by the following equation (2.1):

$$\sigma_{vm} = \rho N g h_m \quad (2.1)$$

In the prototype, (subscript p indicates the prototype) then equation 2.2.

$$\sigma_{vp} = \rho g h_p \quad (2.2)$$

Hence for $\sigma_{vm} = \sigma_{vp}$, then $h_m = h_p N^{-1}$ and for linear dimensions the scale factor (model: prototype) is $1:N$ (Table 2.1). Because the model represents a linear scale of the prototype, scale factor for displacements will also be $1:N$. Therefore the scale factor of strains is $1/1$ and so the part of the soil stress-strain curve mobilised in the model will be the same as that of the prototype.

Table 2.1 : Scaling factors for centrifuge modelling (Ferstl, 1998)

Physical Value or Event	Dimension in Prototype	Dimension in Centrifuge Model at (N*g)
Gravity	1	N
Length	1	1/N
Displacement	1	1/N
Area	1	1/N ²
Volume	1	1/N ³
Stress	1	1
Strain	1	1
Force	1	1/N ²
Velocity	1	N
Acceleration	1	N ²
Mass	1	1/N ³
Energy	1	1/N ³
Density	1	1
Time (consolidation)	1	1/N ²
Frequency	1	N

The earth's gravity does not change between the practical limits of soil depth in civil engineering. At any time a produced acceleration field is used for centrifuge modelling, slight variations in acceleration exists. This is caused by the inertial acceleration field (N*g) is calculated by $\omega^2 r$, where ω is the angular rotational speed and r is the radius to any element in the soil model. If implementer pays attention to select the radius where the gravity scale factor N is determined, remaining is a minor problem. Comparison of the vertical stresses distributions is shown in Figure 2.1, where they were plotted against corresponding depth, graph is exaggerated for clarity. The analogy is accurate at two thirds of the model depth. Taylor claimed

that in case the ratio of the ratio of model height and effective centrifuge radius h_m/R_e is less than 0.2, the maximum error $h_m/6R_e$ in the stress profile is less than 3% of the prototype stress, meaning the error is minor.

Taylor made the argument that if the ratio of model height and effective centrifuge radius h_m/R_e (where $R_e = R_t + h_m/3$) is less than 0.2, the maximum error $h_m/6R_e$ in the stress profile is less than 3% of the prototype stress and therefore minor. The correspondent point in this study was always tried to keep up at the tunnel axis. This can be seen exactly when $C/D=0.5$ at one-third of the soil sample depth.

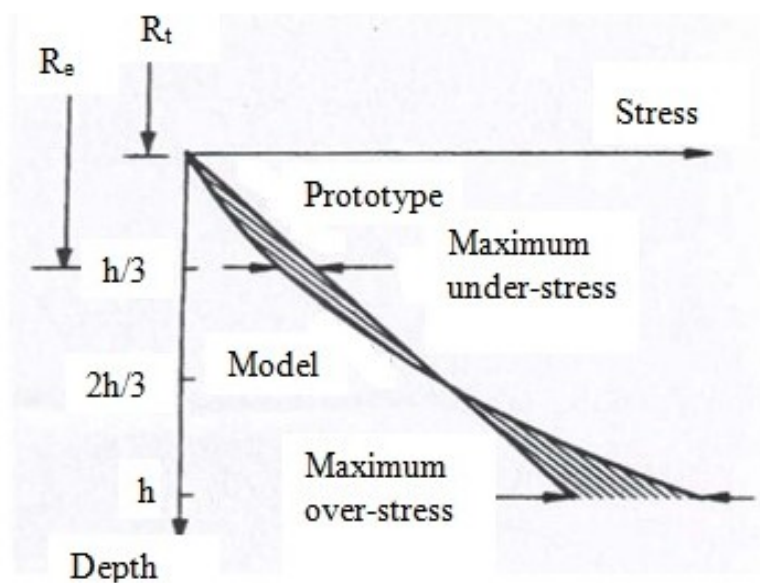


Figure 2.1: Comparison of stress variations on depth in a centrifuge model and its corresponding prototype (Taylor, 1995)

2.2.2 Scale Effects

In studies carried out with a physical model, reproducing all details of the prototype is rarely possible, so making some approximations is needed. It is necessary to keep in mind that model studies are not perfect and in order to evaluate extend of any shortcomings, named scale effect, their nature must be questioned. One of the most popular issue of concern about centrifuge modelling is how can centrifuge modelling be justified if the size of soil particles are not reduced by a factor of N . If the model size is increased to the prototype size in the mind's eye, increasing the particle size jointly might seem to be sensible. Hence a fine sand used in a 1:100 scale model would be representing a gravel. But according to the same logic, a clay would be

representing a fine sand. This argument is clearly flawed because a clay has very different stress-strain characteristics when compared to a fine sand. If an attempt was made at high acceleration and thus at very small scale to model a prototype which is mostly consist of a coarse soil (gravel), a problem could come up. In that case, the soil grain size would be important when compared to that of the model and it is not expected that the model would mobilise the same stress-strain curve as the case in the prototype. By this means in some cases particle size effects may be significant and should be questioned.

2.2.3 Rotational Acceleration Field

Though, a centrifuge is an enormously convenient method for producing an artificial high gravitational acceleration field, the rotation around a fixed axis leads some problems. Since the direction of the acceleration field is towards the centre of rotation, related to the vertical distance of the sample across its width, a change appears in the acceleration direction. Hence a lateral acceleration component comes out. Ensuring that the main cases occur along the radius will minimize the error of the acceleration field. Tendency of acceleration forces depends on the location in the centrifuge model. The resultant force of earth gravity and radial acceleration is considered to be perpendicular to the model surface. This is a further source of an incorrect centrifuge gravity field.

This is not true because there is a frictional resistance in the pivots of the swinging basket. The theoretical upswing angle will always be larger than the real upswing angle. Using a model mass which is adjusted as eccentric, this error can be compensated. ‘Modelling of models’ is a convenient method for controlling scale effects. If no prototype is available to verify the test results, this method is particularly useful. Centrifuge models produced in different scales are tested with suitable acceleration values. Hence, they match to the same prototype. These models should exhibit the same behaviour and support a check on the modelling process.

3. PARTICLE IMAGE VELOCIMETRY (PIV)

In order for understanding the eventual failure mechanism of a geotechnical structure, measuring the plane ground deformations is essential. In consequence of these observations solutions for ultimate load are validated. After the tests accomplished, generally the quite big displacements were found by excavation in the soil of the model. Owing to this, diagnosing the failure mode became possible. But the understanding of settlements and initial ground movements at a much lower strain range is required in order for serviceability state design. Combining the reduced dimensions in geotechnical models and correspondingly a reduction in the area size of related displacements, the measurement of pre-failure soil deformations is formidable task. Experienced strain ranges of various geotechnical processes can be seen in Figure 3.1

A range of 0.01% - 1% involves pre-failure and serviceability deformations. Catastrophic event like the collapse of a tunnel, which caused by greater deformations can also be seen. To achieve a successful deformation measurement even the smallest strain throughout the field must be able to get controlled. Presume that a common centrifuge model has an area of interest of 300x200mm, the pre-failure deformation of 0.01% in an area of 10% of the model, movement detection must be of a size of 2 μ m.

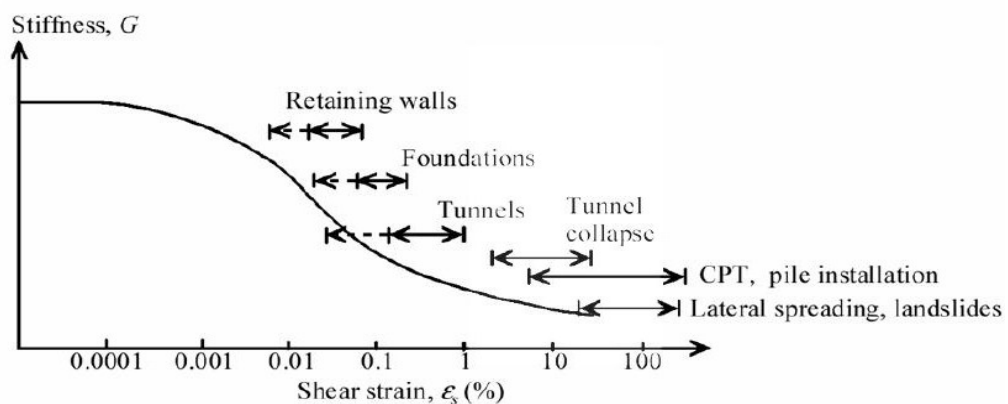


Figure 3.1 : Typical strain ranges experienced in geotechnical engineering (Mair, 1993)

Relatively new visual system named particle image velocimetry (PIV) which is used for visualizing the small ground movements during tunnel face stability loss was used. It can offer to have displacement information over the whole observed area with high accuracy and a very high resolution. Its principle of operation based upon texture measurement that does not benefit from any target markers within the soil. Instead it is using advantage of the soil texture itself. Using a regular digital camera a series of digital photos taken and these images constitutes the underlying data for the calculation. In order to get real displacement values, a calibration for coordinate translation is required.

The concluding displacement and strain field analyses in this thesis were done with GeoPIV8 .

3.1 Step by Step how PIV works

For the visualisation of flow fields, originally developed as a measuring system offering quantitative investigation of plane displacements and velocimetry in experimental fluid mechanics, Particle Image Velocimetry PIV (synonymous with Digital Image Correlation, DIC) was introduced by Adrian in 1991. During the recent years, the principles of PIV has been applied growingly to other research groups to obtain displacement data, much by the virtue of the developments in digital photography. Moreover, it goes into service in geotechnical applications because it provides displacement and strain fields observation on a grain scale level over the whole model without disturbing the soil specimens (not only the movement at a single point).

Hence a series of digital images are obtained with geotechnical model tests. In the calculations with post processing software the first images are separated into small patches by overlaying a mesh. Each patch has a unique texture by means of arrangement and brightness of each pixel in it. By this way a displacement vector field is generated.

Provided the surface contains convenient texture, the use of PIV is practicable. White et.al., (2001) have shown that natural sand meets this need to apply PIV owing to different coloured grains and light and shadows between neighbouring grains when the soil becomes enlightened. When using homogeneous clay, by adding tracer-

particles in a different colour, a texture has to be flagged on the clay surface. PIV track the texture (i.e. the spatial variation of brightness) within a soil image throughout a series of images. To do that, the initial image is divided into a mesh to create PIV test patches. A few sand grains are involved in each patch and a certain distribution of grey or coloured values determines the characteristics of each patch. Taking a single of these patches into account, it is located at coordinates (u_1, v_1) in image 1 (Figure 3.2). To position the new location of this patch in the following image, the correlation between the patch obtained from image 1 (time = t_1) and the greater search area equal to and around the patch from the same site of image 2 (time = t_2) is evaluated. The degree of match is calculated at each position, and at the end a map of ‘degree of match’ is generated over the entire zone. The location of the highest correlation found shows the changed location of the patch (u_2, v_2) . To acquire a convincing adjustment, the correlation peak has to climb over the random noise distortion of the correlation plane. By running an interpolation around the highest integer peak, the exact location of the correlation peak is established to sub-pixel precision (White et. al., 2003). This image processing algorithm is resumed for the complete mesh of patches within the first image, and then repeated for each image pair composing the series. Thus complete trajectories of each test patch is produced by following each patch through all the pictures. In Figure 3.3 schematic flowchart is shown. The trajectories in one image show the movements which are developed during taking this and the following image.

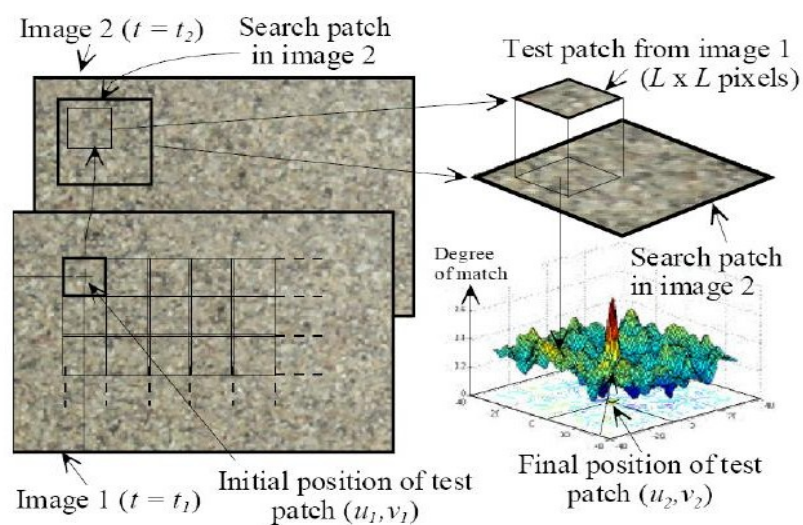


Figure 3.2 : Principles of PIV analysis (White et. al., 2002)

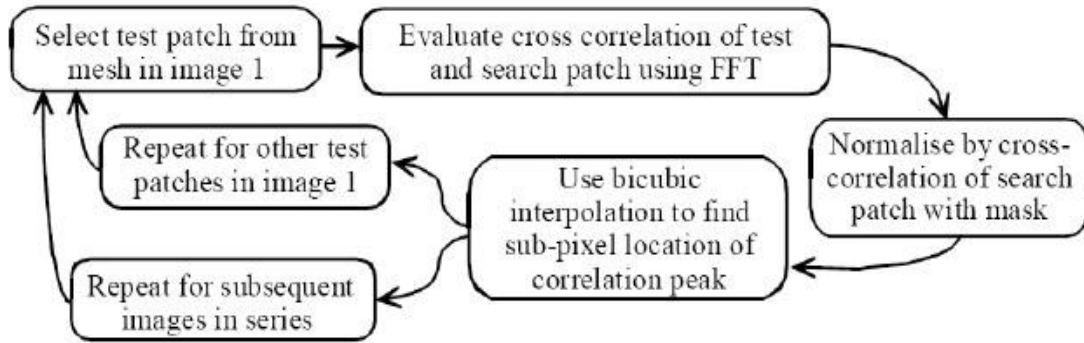


Figure 3.3 : Flowchart of the GeoPIV analysis procedure (White et. al., 2002)

If the patch in the following frame cannot be found by the software, because of the disappearing of wanted peak in the random noise distortion, a ‘wild vector’ comes out. Confirming the performance of a measurement system can be assessed by regarding the errors related to accuracy and precision. The systematic variation between a measured and the true value is entitled as accuracy. It is dependent upon the computation process used to convert image-space to object-space coordinates. On the other hand, the random difference between numerous measurements of the same quantity is called precision. The process used to construct the displacement field determines it. One of the random errors connected to the precision of image-based displacement measurement systems is human error in film measurement and another one is alteration in lighting in centroiding techniques.

The accuracy of a PIV software (GeoPIV) is determined by White et. al. (2003). An experimental device being composed of a translating container enabled a non-deforming plane of soil to be translated horizontally underneath a rigidly fixed camera. By use of a micrometer small known increase of movement were applied to the soil container. Using PIV software the resultant series of images was analysed. The precision was assessed by checking the displacement vectors obtained from a grid of PIV patches overlying the soil. the displacement vectors need to be the same so as to the soil translates as a rigid body. The precision of the practice is indicated by the random variation within the measured vectors.

The precision happens to be a strong function of patch size, L , and a weak function of image content. A larger patch size increases the precision, but at the same time reduces the number of measurement points that can be involved within an image.

Patches containing a larger area get out of focus on the displacement field in area of high strain gradient. Steering a middle course is necessary.

3.2 Close Range Photogrammetry

Deformation measurement systems based upon image analysis composed of two phases. First, the displacement field between two or more images is generated. Second, this field is turned from image-space (coordinates in terms of mm on the photograph or pixels in the image) into object-space (real coordinates on the soil). Displacement field in image-space coordinates is generated using the PIV software. The image-space to object-space conversion is a discrete process and must be performed right after the PIV analysis. The accuracy of resultant measurements connected with the technique used to convert image-space coordinates to object-space coordinates. In order to render the image-space to object-space conversion more accurately, the transformation procedure can be performed by assuming the image scale constant or by using close range photogrammetry.

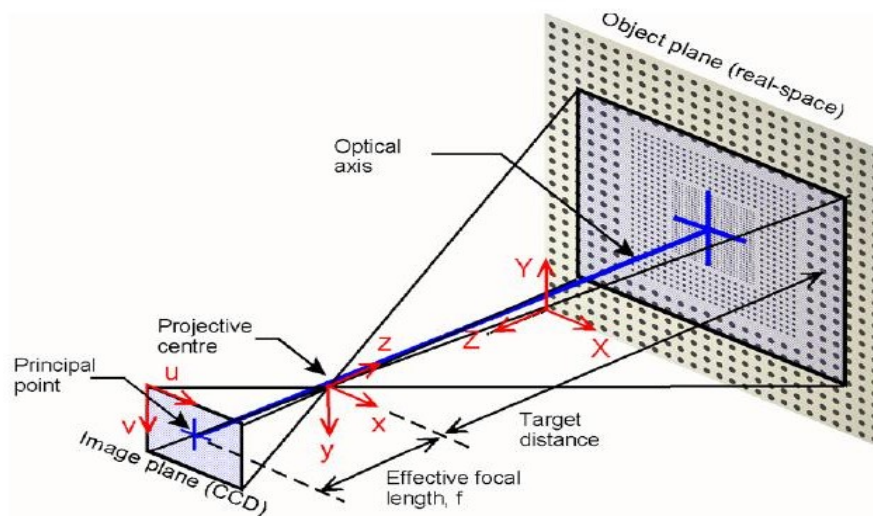


Figure 3.4 : Calibration of different coordinate systems (Thusyanthan, 2008)

When one particular scaling factor is used, the spatial variation in image scale causes errors. Because of that, some corrections must be done to improve the precision. This image distortion correction process is called camera calibration. A mathematical framework, rather than a constant scaling factor, is used for stating the transformation (u,v). Basis of this framework resides the principles of close range

photogrammetry, assuming a number of sources in image distortion (White and et. al., 2002).

3.2.1 Non-coplanarity

The coordinate systems of the CCD and the object plane are rotated relatively with the Euler angles θ , Φ and ϕ between them. Hence the normals to the image plane and object plane are not parallel. Take (2003) stated that during centrifuge testing at 100g, even the increased self weight of a typical digital camera causes a declination of 3° of the CCD plane. Even if the increased acceleration field does not exist, an accurate alignment is difficult, may be causing a 1-2% spatial variation in image scale. Although, when the planned gravity-level is reached no further movements should take place, all images are taken on an equal basis.

3.2.2 Radial and tangential lens distortion

The pinhole camera model which is signified by the light ray beams running straight through a single point to form a perspective designation of the object, is an approximation. Distortion of the radial lens leads to the radial deviation of the rays from the normal to the lens. This effect is generally called fish eye.

Because the curvature centres of the lens surfaces are not superbly collinear, for cameras especially containing multiple lenses an additional error shows up. This distortion causes decentring, which is apply both in radial and tangential components.

3.2.3 CCD non-squareness

This small error is a linear scaling factor, so it can be easily implicated into the coordinate transformation. The height to width pixel ratio is generally of 1 ± 0.004 and assumed to be constant over the entire digital camera sensor.

3.2.4 Refraction through the viewing window

When the object is behind a viewing window a further variation in image scale comes up. The refractions of the light rays caused by this create obvious change in object size. The resultant distortion rely on the thickness and refractive index of the window, which does not change throughout the picture, and the slope of the rays to the normal of the window, which does change throughout the picture. When modelling this refraction GeoPIV8 Snell's Law is used.

This entire calibration process is based on object points with known object coordinates. This is why so called window markers are drawn on the inner side of the transparent perspex window. Size of them should be about 3-5mm in diameter and for a good recognizability a high contrast colour support needed. In the PIV software, calculation of centre of the points is performed by using a centroiding technique (Figure 3.5). From now on the marker coordinates are generated in object-space and image-space. By that means the non-linear image scale caused by the fish-eye effect (near distance image taking) can be corrected by relating the analogous real object coordinates.

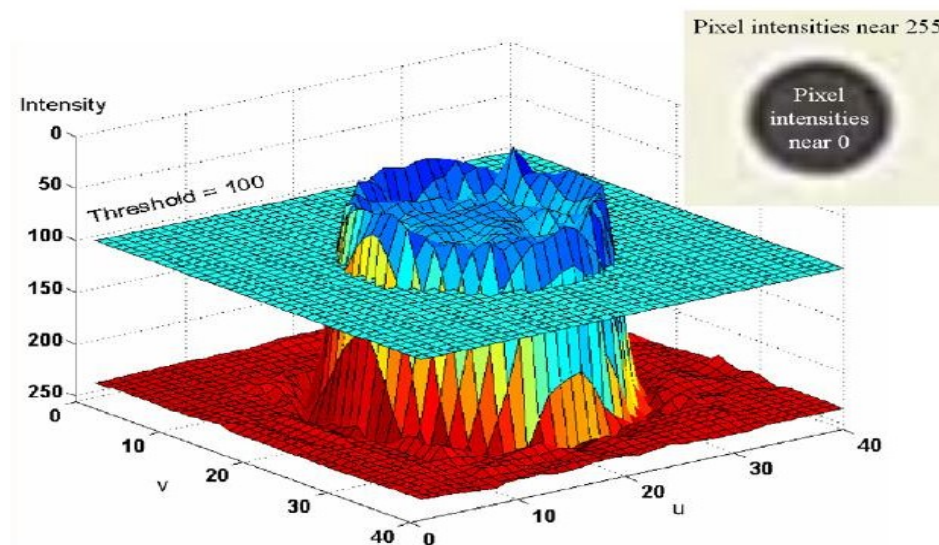


Figure 3.5 : Centroiding of window markers (Thusyanthan, 2008)

When the window markers are used alone it may not give sufficiently satisfying results. In practical terms markers were drawn by hand, so they cannot give the desired accuracy in the size of a few micrometers. A mylar film with a calibration pattern can be used in order to prevent this problem. The system can be calibrated quite accurately by taking a picture of the mylar hang onto the perspex and check against it with a window markers' image (Figure 3.4).

3.3 GEOPIV8

GeoPIV is a Matlab module which applied PIV to geotechnical testing, developed by White and Take at University of Cambridge. In this chapter the detailed use of GeoPIV described, including measuring displacement fields from digital images, the efficiency of the software, general errors and how to prevent them. For GeoPIV8 the

Matlab version R2007b or higher is required. White (2002) and Take (2003) described the development and performance of the software in depth. This Matlab module requires a launcher and an initial mesh file. These input files are produced in ASCII format by the user. The mesh file involves the pixel coordinates of the patches. It can be created by either writing manually or being generated by the m-file 'geoMESHuv8'. The launcher file contains the basic information needed for the analysing process. This information include the name of the implemented mesh, size of the search zone in pixels, the location and names of the images, leapfrog, display settings during calculation and use of bicubic sub-pixel interpolation. Size of the search zone has to be larger than the biggest anticipated displacement. The output files can be changed by the user in Matlab or a spreadsheet to produce displacement and strain data and are in ASCII format as well.

Data needed by the program for the PIV process is supplied by the launcher and mesh input files and the images. Coordinates and sizes of the initial grid of PIV patches are contained by the mesh file. This grid of patches is applied to the first image and each patch is tracked through the following images. The analysis is carried out with the GeoPIV8.m file by reaching the above-mentioned data. Previous and new image coordinate origins of the patches and also the u, v displacement in pixels are involved in the ASCII output files. Possibly emerged wild vectors are deleted and the displacements combined prior to starting post-processing. In this way, with the third step using short range photogrammetry the data can be calibrated through conversion from image to object space coordinates. Then plots of the X, Y displacement and strain field can be created.

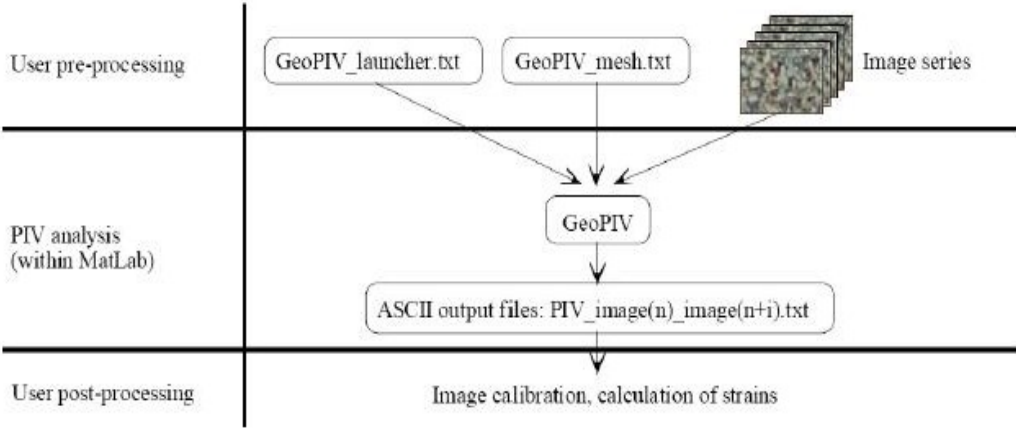


Figure 3.6 : GeoPIV software usage (White et. al., 2002)

4. EXPERIMENTAL SET UP

All tests were conducted in the IGT Beam Centrifuge at the Universität für Bodenkultur BOKU (University of Natural Resources and Applied Life Sciences), Vienna. The model box was designed to be used in the experiments explained in this thesis, but also were considered in the design prospective projects, particularly those using the geoPIV method. All equipments was designed by Dipl.-Eng. Gregor Idinger.

4.1 Description Of IGT Beam Centrifuge

The only centrifuge existing in Austria is the geotechnical centrifuge residing in the laboratory of the IGT (Institute für Geotechnik; Institute of Geotechnical Engineering). The centrifuge was manufactured by Trio-Tech, CA in 1989. It has been used in numerous research projects such as earth pressure and foundation problems since its installation. The beam centrifuge, Model 1231 Standard Heavy Duty, has a diameter of 3.0m, a load capacity of 10 tonne, 56 slip rings and the driving force is supplied by a 15HP DC motor (Table 4.1). The geotechnical centrifuge shown in Figure 4.1.

Table 4.1 : Technical specifications of IGT centrifuge (TRIO-TECH, 1988)

Diameter of Centrifuge (m)	3.0
Radius to swinging basket axis (m)	1.30
Radial acceleration (g)	0 to 200
Angular Velocity (1/min)	0 to 400
Max. Load Capacity (t)	10
Max. Model Weight (kg)	90
Max. Model Dimensions WxDxH (mm)	540x560x560
Total Weight (t)	2.041

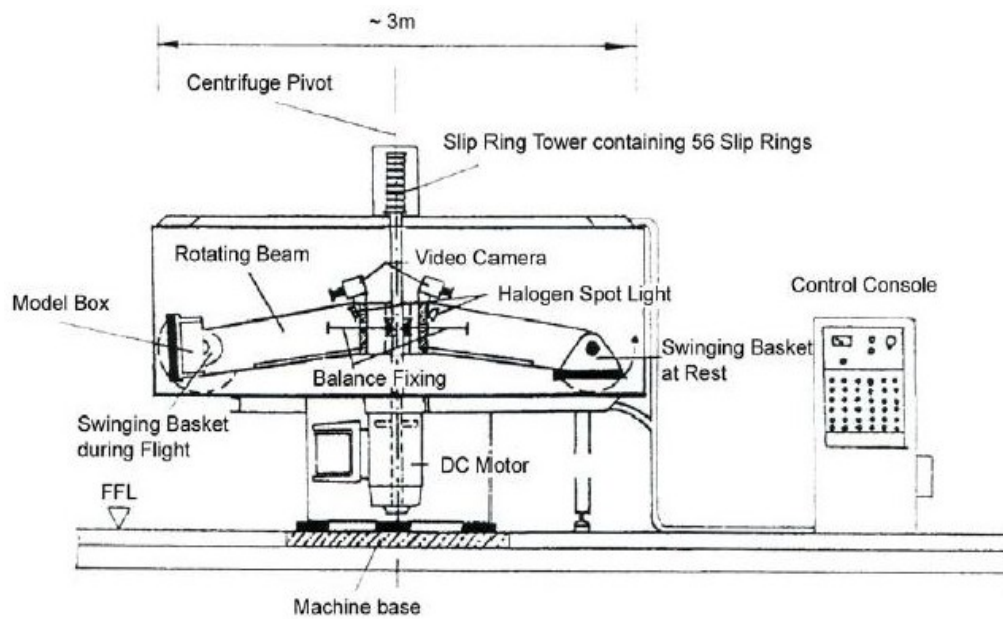


Figure 4.1 : Schematic sketch of Trio-Tech 1231 Geotechnical Centrifuge (Ferstl, 1998)

Attached to the motor, a symmetrical high strength aluminium beam is rotated. Swing platforms are placed at both ends of this rotating arm. The model box is mounted on one of these swinging platforms, and to provide symmetry an equal counterweight is placed on the opposite end. So as to accomplish an exactly even configuration the beam can get loosened and used as a balance. In the course of flight the beam has to be turned back to the fixed position. Small iron rods with a weight of exactly 14.5 grams are inserted to an aluminium box as a counterweight. There is a slip ring tower on top of the centrifuge enclosure, containing 56 electrical slip rings. These junctions are required for data transmission. Which include transducer measuring signals, video signals, computer signals (TCP/IP) for process control and data collection and also for a power supply connection of diverse assembled instruments using low current and voltage (e.g. illumination). Rings rated at 5AMP (shielded individually), 12V and 24V are delivered to the centrifuge without a significant loss. Along with the electrical slip rings, for water and air pressure special supplies do exist. After the signals leave the centrifuge passing through the slip rings, they arrive to a decoder in the centrifuge control room. So that both in centrifuge arm and control room, the cables are connected to DB15 plugs. After the centrifuge is started during the flight staying in the centrifuge room is not permitted. A personnel guard for the centrifuge is assigned in the form of a surrounding aerodynamic

enclosure as an additional safety measure to contain components and test specimens accidentally loosened during flight, and also for minimizing perturbations of the rotating arm because of the variations in air drag. Moreover, it has to be under ground level. There is an unseat switch to use in the event of emergency, for example mass lost causing unbalanced beam, use of which should be avoided though.

All the tests are performed distant from the control room. The centrifuge is managed using a control console. The angular velocity is supplied either manual or, for an exact acceleration value, by a computer-programmed remote signal in revolutions per minute (RPM) to reach the desired acceleration. The present value is shown by digital digits. The velocity is held on a constant with a variation of $\pm 0.1\%$.

A compact video camera and a light source (low-voltage halogen spot light) are mounted near the centrifuge axis to observe the behaviour of the tested specimen, directed to the swinging basket with the model box placed in centrifuge(Figure 4.1). The video signal is sent through the slip rings to a monochrome display residing in the control room. Accordingly as well as the upswing angle of the swinging basket, unexpected effects can also be controlled. Electromagnetic interference can only let the camera be used during start-up process. In the contrary case measuring signals operating at low voltage are disturbed.

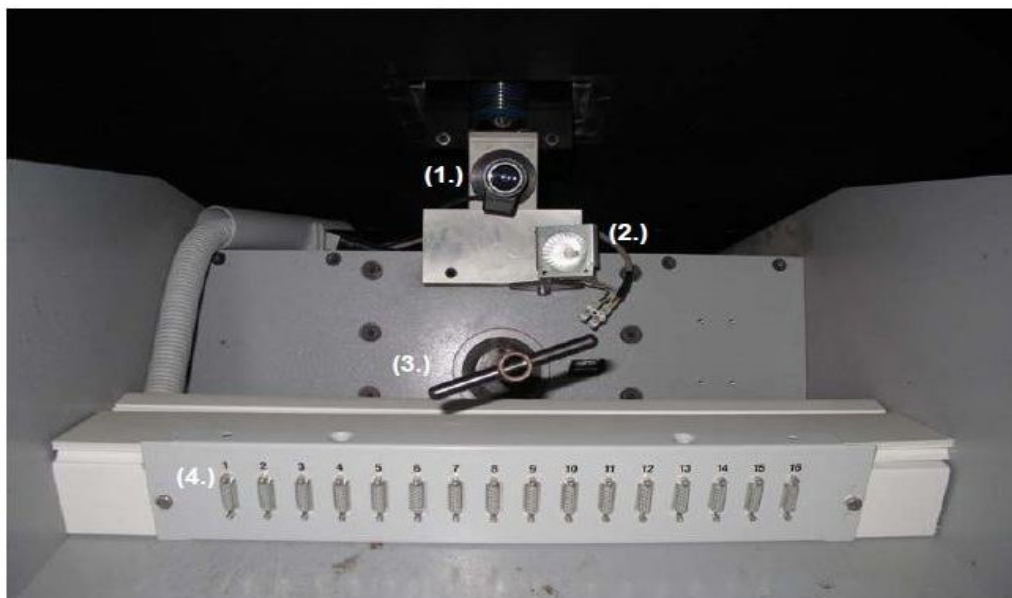


Figure 4.2 : Centrifuge equipment: (1.) video camera, (2.) halogen light, (3.) balance fixing and (4.) DB15 plug bar (Idinger, 2010)

Other slip rings are split up to 16 DB15 (15 pins) plugs (Figure 4.2) as follows: 11-15 power supply, 1-5 full bridge, 6-10 half bridge, 16 analog camera. A slip ring full bridge composed of 4 wires, a half bridge of 3 wires. Power supply plugs composed of two wires, arriving and leakage current. An analog connection was mounted for a miniature video camera. An analogous DB15 plug bar is installed in the control room.



Figure 4.3 : IGT beam centrifuge: (1.) slip ring tower, (2.) high strength steel enclosure, (3.) rotating arm, (4.) DC motor (Idinger,2010)



Figure 4.4 : Rotating beam - model at the back and box with counterweights at front (Idinger,2010)

The acceleration field forming force acting on the model box placed on the swinging platform depends on the rotation radius and angular velocity in RPM (Table 4.2). The distance from centrifuge rotation axis to the swing axis of the basket is 1.30 metres and during flight to the longitudinal tunnel axis 1.42 metres. For the applied angular velocity this value is the calculation basis. Tests were performed at 75g.

Table 4.2 : RPM at certain model factors g for r=1.42m (radius to tunnel axis)

g (-)	RPM [[1/min]]	RPS [1/sec]	Rotation Speed [km/h]	g (-)	RPM [[1/min]]	RPS [1/sec]	Rotation Speed [km/h]
5	61.05	1.02	35.05	45	183.15	3.05	105.16
10	86.34	1.44	49.57	50	193.05	3.22	110.85
15	105.74	1.76	60.72	75	236.44	3.94	135.76
20	122.10	2.04	70.11	100	273.02	4.55	156.77
25	136.51	2.28	78.38	125	305.24	5.09	175.27
30	149.54	2.49	85.86	150	334.38	5.57	192.01
35	161.52	2.69	92.74	175	361.17	6.02	207.38
40	172.67	2.88	99.15	200	386.10	6.44	221.70

4.2 Design Of The Model

The model box was designed for Dipl. Eng.Gregor Idinger's thesis. The whole mechanism with every detail was designed by him, with the aim to build a test set-up adequate for the PIV technology. As shown in Figure 4.5, the main items include an aluminium box with one transparent perspex window (1.), a digital camera (4.) and a sufficient illumination (3.). Three massive aluminium plates constitute the basic model box. An extra side wall with a cut-out for the actuator was constructed for the tunnel tests. The model box is planned to be used for future (PIV) experiments after the tunnel test.

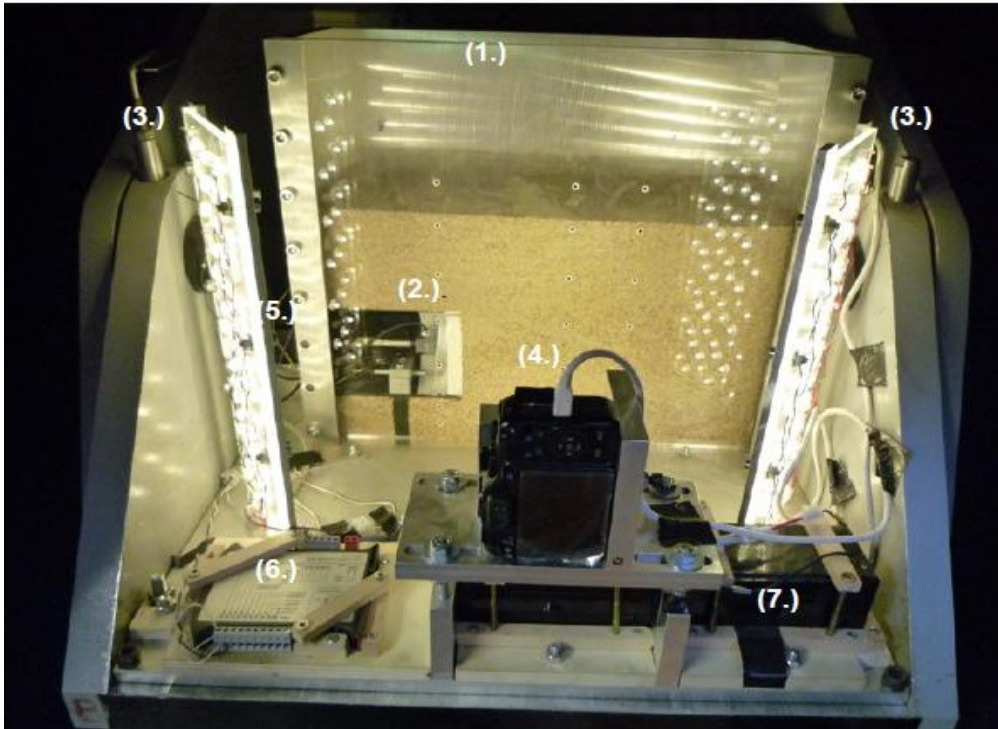


Figure 4.5 : Model box mounted on swing basket before the start of test ($C/D=1.0$), 1. Model box, 2. tunnel, 3. LED lights, 4. camera, 5. engine, 6. engine driver, 7. Batteries (Idinger, 2010)

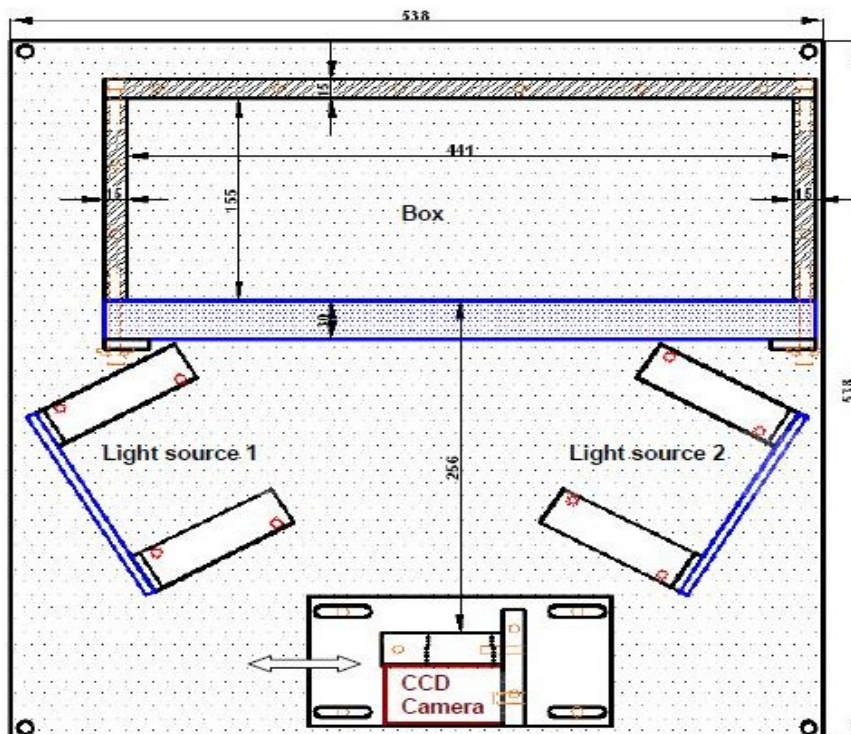


Figure 4.6 : Sketch of PIV-model assembly, top view (Idinger, 2010)

4.3 Tunnel Model

The mechanism cutting vertically through the tunnel axis which can be seen on previous pictures was modeling the problem in half to gain the soil deformations in the longitudinal axis. Because the greatest deformations occur in this section, analysing the stability at this level is a particular issue of concern. It should be noticed that surface of the less structured perspex reduces the friction and accordingly effects the path of the grains.

When modeling the TBM, a cylindrical aluminium half-shell Ø100mm with a thickness of 3mm was used. It is stiff enough to avoid deformations during the acceleration of the gravity field, as is the prototype segment lining. On the axis lying 100mm above the bottom of the box, the model tunnel protruded 130mm into the soil.

There are two choices to simulate the loss of face support pressure. First method is reducing the pressure of an air-filled balloon through remote control valve. An aluminium plate is placed as the tunnel face. This flexible system is advantageous by means of that the effect over the earth pressure increasing with depth is observable by the inclination of the face plate. The second method is reducing support pressure by driving a rigid piston inward the tunnel. Independently of the preferred method, when starting the instability process by decreasing the support pressure, right after that a constant reduced earth pressure will be measured. This measured value arise from the load of the weak failure zone ahead the tunnel face and can be said to be the the least required support pressure. It means when this pressure is supplied to support the system against the soil, equilibrium will be achieved and no failure will occur.

In this thesis the second type was preferred for the tunnel model because it provides an easier realization and is specified in detail accordingly.

As shown in Figure 4.7, the piston was formed of an aluminium tunnel face, a linear actuator which is for carrying out the displacement and a load cell for measuring the acting pressure. In order to connect the actuator and the load cell a steel rod with windings on both sides was installed completing the piston axis. The diameter of the face plate was preferred to be smaller than the inner diameter of the shell to attain a friction reduction in the displacement.

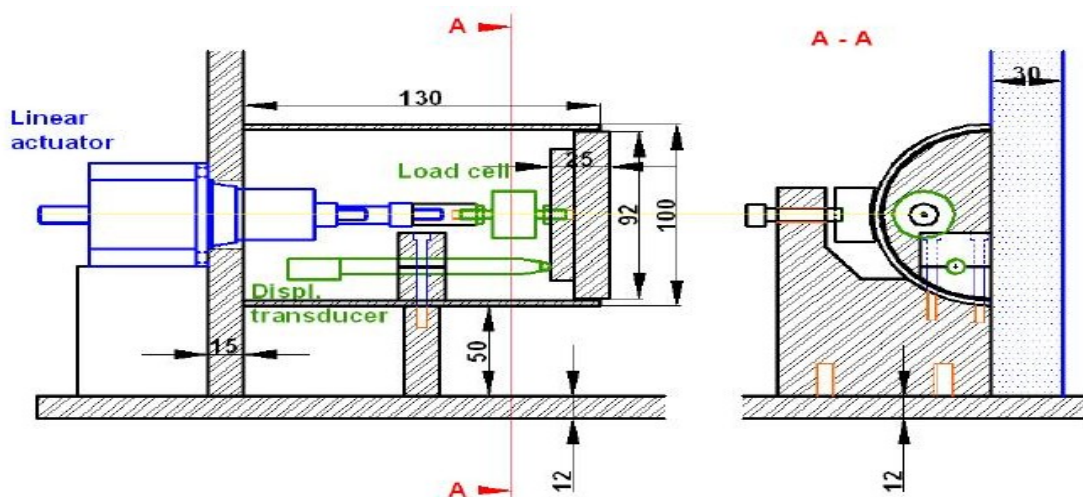


Figure 4.7 : Sketches of tunnel model, frontal view and cross-section (Idinger, 2010)

Accordingly, to prevent any soil to lead in, the gap between tunnel and semi-circled tunnel face must be closed. In the contrary case, it would let an obstruction for the piston in, cause disruption on the high-precision instruments and mistaken the measured data. A distance of 50mm to the box floor is enough to avoid any effect at the tunnel face. So as to reach a tight state in the beginning, teflon sheets were standed to the aluminium face to fill the gap completely. Even so, at 75g a high friction between piston and tunnel comes out due to the peeled sheets. Kirsch (2009) suggested three different methods for sealing: a thick film of bearing grease in the gap, bearing grease along with a nonpermanent cling foil to cover the gap or a tunnel face completely wrapped with the cling foil. The third method was giving the best results, so it was implicated in the experiment mechanism.

The same sealing problem appeared on the contact zone tunnel perspex. Therefore the tunnel cylinder was pushed against perspex by using a screw. So as to assure a good contact and consequently keep the soil from entering the gap between window and tunnel, felt was adhered to the tunnel contact faces. In addition, as a supplemental measure the risk of scratching the window was reduced. Since the two restraint screws fixing the displacement transducer to the tunnel bracket were enough achieve this function, it was found that the additional screw fixing was not needed.

Besides obtaining a tight tunnel, minimizing the friction between the piston and tunnel was a harder challenge. Despite the existence of a gap of 1mm friction showed up. This was found to be caused by rising piston self-weight in flight. Because of the

total piston length of 130 mm, the aluminium semi-circle mounted at the end was forced downward. The friction should be reduced by Teflon sheets adhered to inner surface of the tunnel and perimeter of piston. In the friction measuring tests, it was found that the Teflon sheets had a negative effect on the friction. This can be explained by deformations on the sheets caused by the slippery tunnel face. A roller bearing as guidance would come in useful but it is hard to apply because the space inside the tunnel model is not large enough.

The effective earth pressure acting on the tunnel face is measured with the load cell operating behind the semi-circular tunnel face. It should be stated that via this measurement setting the earth pressure distribution over the tunnel face is not evaluated. By dividing the measured force according to the area of the semi-circle, an average pressure is obtained.

In order to control the piston displacement a displacement transducer is mounted. Since the action is provided by a step engine the sensor is not necessarily needed. That is because every investigation about single rotation step is converted to a defined displacement. Even so, the data obtained by the displacement transducer was helpful for observing the test process.

4.3.1 Instrumentation

The test instruments are introduced in this chapter: the elements of the tunnel model – linear actuator, load cell, displacement transducer and the PIV system elements – CDD camera and lighting. In appendix I, a schematic view of the entire instrumentation of the experiment is given.

4.3.1.1 Linear Actuator

A linear actuator was used for the purpose of attaining the horizontal displacement of the piston. This step engine converts the rotation into a longitudinal motion. By reason of the awaited tunnel collapse takes place within a shift of a compartment of one millimetre, displacement resolution was required to be high. The linear actuator by Haydon (57000 series) meet this requirement. One step, a rotation of 1.8° , equals to a movement of 0.0105mm, or $10.5\mu\text{m}$. The bipolar, captive, 12VDC low current, with a maximum stroke of 31.8mm was chosen. A thrust of 91kg is applied.

The linear actuator is driven by single steps in the tests. Hence a high signal coming from a computer, have to reach the engine. A driver unit which is matching the

current of the engine, is connected between the engine and computer, to identify these signals. The required 24VDC power for the driver is achieved by two 12V lead accumulators.

A high signal is sent through the com port gateway to the STEP+ input on the driver using a program written in Basic. The STEP- input is used as grounding. Values of interval and total step number are entered in the program. Piston speed is selected as 5sec/step and interval as '1000'.

4.3.1.2 Transmitter

4.3.1.2.1 Load Cell

The U9B 1kN load cell by Hottinger Baldwin Messtechnik (HBM) was used. Compression (positive) and tensile forces (negative) can be measured, with an accuracy of $\pm 0.00012\text{kN} = 0.12\text{N} \approx \text{load of } 0.012\text{kg} = 12\text{g}$. It was installed in the piston axis behind the aluminium face. Adjusting the piston axis through the application point of the tunnel face was not possible, hence the resultant earth pressure put across moments to the load cell. Even so, they can be neglected because they are small in magnitude.

For the connection of centrifuge and control room, a full bridge is needed. Measuring cables, the Spider8 and the Catman software by HBM were used.

4.3.1.2.2 LVDT Transducer

Because the space inside the tunnel is not large enough, the HBM miniature LVDT (Linear Variable Differential Transformer) transducer WI with a range of 10mm was used. It measures axial displacements with an accuracy of $\pm 0.000625\text{mm} = 0.625\mu\text{m}$. In order to ensure a displacement of 5mm, the transducer was fixed in the lower half of the tunnel, contacting the aluminium face with its tip carbide ball.

4.3.1.2.3 Spider8

This is a component which performs multi-channel electronic PC measurement for parallel and dynamic measurement data acquisition over a computer. It is capable of converting the electronic signal received from the transmitter to physical variables.

4.3.1.2.4 Catman

This is the data acquisition software used. Data are recorded with a frequency of 1Hz. A peculiarly designed measurement setup was used for the tunnel tests. The resultant values were saved in a spread sheet so as to be adjusted.

4.3.1.3 Camera

One of the reasons for the breakthrough of PIV analysis is fast development of CCD camera technology. In recent years high-resolution digital cameras are getting more economic. Now for a well-done patch tracking almost every model has a sufficient resolution. Many different models have been used in centrifuge tests up to and some even over 100G and passed without any damage (White et.al., 2005). For close-range photogrammetry beneath a high sensitive sensor in order to take a frame as big as possible, a wide angle objective is desired. In this tests distance is 256mm, the FOV covered an area of approximately 360x240mm.

Canon G10 was purchased for the experiments. Resolution of pictures taken 2592x3456 pixels, are corresponding to a size of 8.9MP and a memory requirement around 3MB, for each one. Accordingly, one test involves up to 400 pictures and needed a storage capacity of more than 1GB. Pictures are saved in the camera memory and in a hard drive. One millimetre has a size of about 12 pixels in the preferred resolution. According to this, for a normal coarse sand grain with a diameter of 1mm approximately 113 pixels are needed. The camera must be attached tightly to a rigid component connected to the model box and observed soil, so as to ensure a constant image frame during flight. To achieve that, a customized module was designed, seen in Figure 4.10. Placed on a platform the upright camera is fixed to a vertical aluminium plate by a 1/4'' tripod screw. Increasing gravity may cause the camera objective to move downwards. To prevent this movement it is placed to a tightly fitting aluminium block. With 0.15 mm Teflon sheets the final position was arranged.

It is important to release the trigger over a long period. This is required to provide a photo series over the whole experiment. Setting a weight onto the trigger button is the published easiest way, so that it is pressed down during flight and thereby releasing the button. No extra equipment is required for this. But since the camera position is vertical this is not a proper solution. Therefore as a solution a special

remote control software was obtained, and a connection to a computer within the centrifuge was provided.

4.4 Illumination

A good lighting is required to take suitable pictures for the PIV analysis. Since the only usable light source (the small spotlight located near the centrifuge centre) was too weak and was not even working during recording and transmitting data, a new illumination system was necessary. Two options were existing: enlightening the whole centrifuge interior or mounting fixed spotlights to the model box. In the first option uneven illuminance were the drawback, so two lights were inserted on the mounting plate. By this means no relative movement to the camera lenses appear and the lights provide constant conditions. Thus there were no concerns for the on spatial variation in brightness based PIV analysis.

Different angles were tested to find the appropriate position to the observed part. The purpose was to reduce the reflection of the light sources to the minimum while still achieving a bright and homogeneous light. The aluminium faces were painted black to eliminate reflections from heading to glass.

Light-emitting diodes (LED) have several advantages among the various available illumination option: high energy-efficient, long lifetime, low heat emissions, no expected effects in an increased gravity field. Single 5mm warm-white LED with luminosity of max. 20.000mcd was chosen. By this way, for a constant illumination they could be adjusted manually shifted in an offset of 25mm. Roughened diode heads were serving the purpose of protecting diffuse light conditions. An apparatus with 33 LED each was placed on both sides to the model. The diodes were placed through perspex driven holes and covered with hot glue. In order to provide the required stiffness, the 5mm perspex plates were attached to two L-brackets. Small circuits involving 3 and 2 diodes were soldered together to support electricity. To reduce current suitable resistances needed. Since low ampere is needed electricity could be supplied over a slip ring.

4.5 Soil

For the experiments, two different types of sand are used in dry form. As known, unless the sands are not in water, they cannot be compressed much. Both sands are placed on the experiment equipment in a loose form and by using in two different experiments, it is investigated that how they affect the results of ground changes.

4.5.1 Soil 1 (S1)

The first ground is coarse grained silica sand which is produced according to DIN 1164/58 norm sand II rules which is named as the Norman Sand. The soil is used in the experiments dry and loose form. Because the ground has a uniform grain diameter distribution, it is rarely observed in natural ground conditions. The properties of the ground is shown in the below mentioned table (Table 4.3).

Table 4.3 : Parameters of soil S1

Specific weight ρ_s [g/ cm ³]	2.65	Coefficient of Uniformity C_u	1.4
Density range ρ_{min}, ρ_{max} [g/cm ³]	1.44 – 1.62	Coefficient of Curvature C_c	1.03
Void Ratio e_{min}, e_{max}	0.607– 0.844	Friction angle ϕ [°]	34
Relative Density (%)	32	Cohesion c [kN/ m ²]	0

4.5.2 Soil 2 (S2)

2nd ground is the mixture of fine sands with different grain diameters. This ground is also used in a dry and loose form in order to make a comparison. The properties of the ground is shown in the below mentioned table (Table 4.4).

Table 4.4 : Parameters of soil S2

Specific weight ρ_s [g/ cm ³]	2.65	Coefficient of Uniformity C_u	3.25
Density range ρ_{min}, ρ_{max} [g/cm ³]	1.47 – 1.62	Coefficient of Curvature C_c	1.94
Void Ratio e_{min}, e_{max}	0.640 – 0.804	Friction angle ϕ [°]	35
Relative Density (%)	25	Cohesion c [kN/ m ²]	0

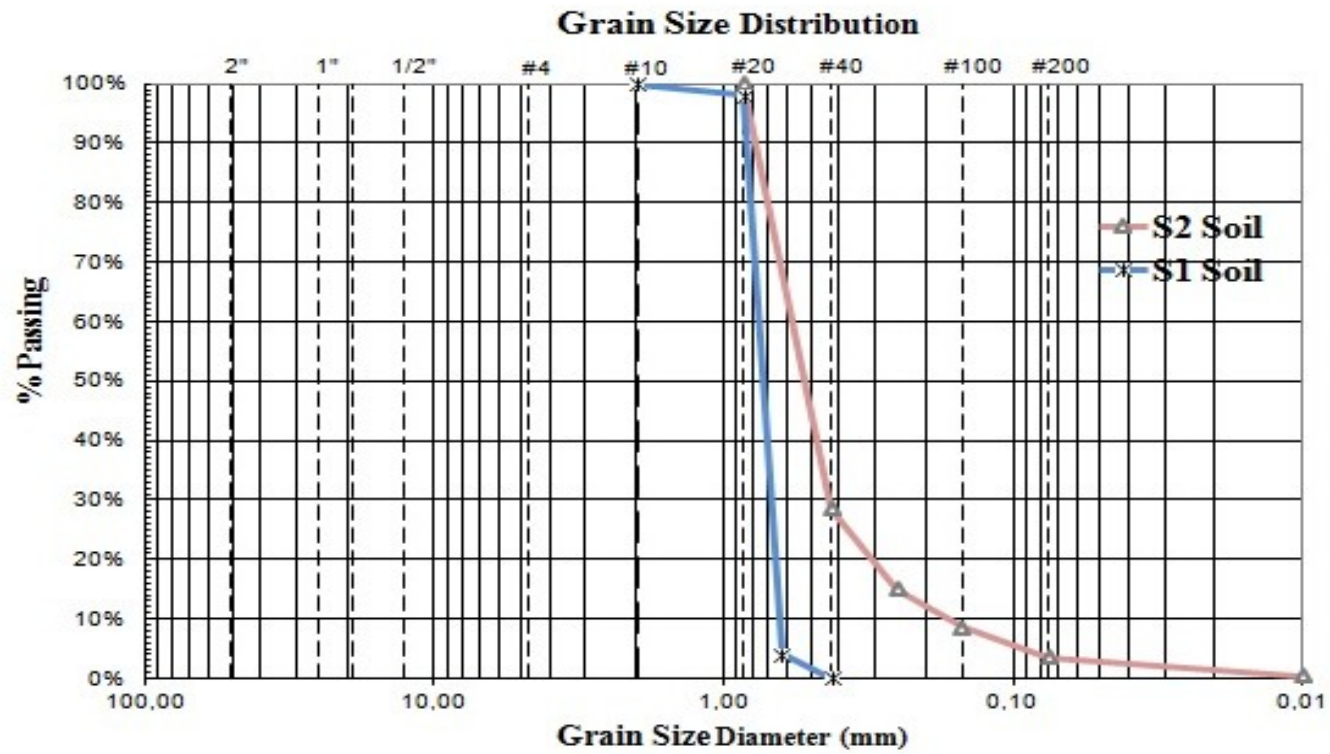


Figure 4.8 : Grain size curve of S1 and S2 soils

4.6 Typical Test Procedure

All steps of performing a single centrifuge test is listed in this chapter. By this way it should be guidance for future centrifuge tests, especially if the PIV model box is used.

4.6.1 Assembling Of The Model Box

Centrifuge room: The perspex has to be disassembled to bring together the elements of the piston which is reducing the face support. The sidewall with the cut-out for the linear actuator is required for the tunnel test. The measurement equipments are inserted through this hole. A milled edge is installed to the big engine hole for their cables. After the the steel rod, load cell can be screwed to the actuator. Screws have to be tight. Then the actuator can be placed into the hole and fixed to the side wall. As a measure for downward movements of the actuator, a support piece is placed underneath. The semicircled tunnel face is installed to the load cell. After doing this the piston is ready and the tunnel halfshell is placed. When the displacement transducer is fixed by its restraint to the tunnel bracket, after the sensor is arranged in the right position by touching the face, the rigid tunnel state is achieved. Hence the tunnel model is ready, the perspex can be mounted again.

4.6.2 Mounting The Model Box To The Centrifuge Swinging Basket

Centrifuge room: the assembly crane is used when inserting the model box into the centrifuge. The two blue steel devices and the two winding rods are required to hang the model box on the hook on the model. Refraining canting the model mounting plate, the model is placed onto the swinging platform carefully. Now, to fix the model to the platform the four holes have to be adjusted. Next the heaving devices are demounted.

4.6.3 Linear Actuator

Centrifuge room: The actuator is connected to the stepper motor driver DS1041. Cables order: pink/white: FA-, pink: FA+, green: FB+, green/white FB-. There was no need for Shield wiring. The step input cables are connected to STEP+ and STEP- contacts and the DB15 plug bar (half bridge or power supply), respectively. Then, the driver can be connected to the two in series 12V batteries and the piston brought to the start position. The UDP30 device is connected to the driver to change direction

of the linear actuator: direct = inside (adjusting for tunnel experiment), inverse = outside (going back to initial position).

Control room: The step input cables are connected to the COM port device of the DOS computer and the selected DB15 channel. Basic program is started when starting the actual test, the interval set to '1000' (5sec) and then 500 steps are transmitted, completing a total 5mm displacement.

4.6.4 Embedding The Soil

Centrifuge room: The model box can be filled with soil either before placing the centrifuge or inside the centrifuge when already mounted, with the centrifuge roof opened. The total weight has to be measured before filling the soil. Besides it can be compacted in layers of 4 centimetres, for example with a proctor compaction device. The perspex must be protected. If the soil is embed on the swinging platform it can be fixed against tilting. After leveling the soil surface the remaining soil is weighted again. The density can be calculated, because the difference is inside the box, the volume is also known. After that, the counterweight is adjusted and filled with the steel rods. The rotation arm is set untighten and used as balance for an accurate balance. Afterwards the arm must be tightened again.

4.6.5 Transmitter

Centrifuge room: Load cell and displacement transducer cables can be connected to their channel (full bridge, channel 1-5) on the DB15 plug bar.

Control room: Cables are connected to in one end the same DB15 plug and on the other end to the Spider8. The Spider on its part is connected to a Windows computer. After the spider is turned on, the Catman program is started. Spider channels are scanned and from the database, settings of used devices loaded. Signals are set null (original load negligible). Previous data must be deleted. The data frequency is set to 1 and then the prepared program is opened.

4.6.6 Camera

Centrifuge room: The camera is connected to the data computer which is placed on a platform near the centrifuge axis. This device is connected per Ethernet through the sliprings (full bridge, channel 1-5) to the control computer. The data computer starts the WinVNC software and is remote controlled which can be closed and fixed. After

the camera is combined with the PSRemote software the objective comes out, therefore the camera can be fixed on that position. With the purpose of minimizing movements during flight Teflon sheets are put between object and aluminium.

Control room: Starting the vnc viewer software by entering the data computer's IP-address its desktop can be controlled. The camera is started with PSRemote and the time lags are selected (in this tests 6sec).

4.6.7 Illumination

Centrifuge room: Two LED unit circuits are connected and plugged to the DB15 bar (channel 3).

Control room: The cable is plugged to a power socket.

4.6.8 Spin-up

Centrifuge room: The centrifuge door (and roof) is closed, the power in the control room is necessarily turned on twice. And then the centrifuge room must be evacuated until the experiment is over.

Control room: The centrifuge rotation was entered manually. Spin-up was begun by 5g step, up to 75g. 5 more minutes are awaited for consolidation of the sand, then the test is started.

4.6.9 Initialising Actual Test

Control room: The program is written in Basic activates the piston movement by on the DOS computer. The time interval between two steps was selected 5 sec, or a time factor of 1.000. A total displacement of 5 mm 500 steps are required, because one step is equal to a displacement of 10.5 μ m.

4.6.10 Post-processing – Measurement Data

During spin-up is deleted the first measurement data part taken. That record was only for checking the spin-up process. Before the first step the displacement is set null. After the correction with the calibrated friction value, the load cell data is converted to pressure.

4.6.11 Post-Processing - GeoPIV8

Pictures must be taken in recognisable intervals. In these tests every 25th picture was chosen. That implies a gap of about 4 minutes or a face displacement of 0.5mm. The PIV launcher file is prepared, a mesh of 32x32 pixels is defined with 'geoMESHuv8' in the Matlab command window. After performing the PIV analysis, 'geoPIV8', the recorded displacements of every image pair are added, 'consolidate8'. Wild vectors, if present, are removed with 'geoWILD'. Before plotting the results a correcting must be applied to image distortion and coordinates have to be transformed from image-space to real object-space. Next, following steps must be tracked:

Before the experiment centroiding the window markers and centroiding mylar targets ('geoCENTROID8'). After running 'GeoPIV8' on both with a copy of the same picture each, the window marker result is consolidated. Now using the mylar launcher file and a text file of 3 columns involving the x and y coordinates of the mylar targets the window markers are calibrated. By this way, the real X and Y coordinates of the window markers are obtained. To calibrate the PIV attachment this has do be done once. Once the PIV analysis of the selected images done, a PIV calculation on the window markers over all images after the window markers are centroided again. At last, using the consolidated image data, the launcher file of the window markers and the XY coordinates of the markers the image can be calibrated and provide the X and Y coordinates of all patches. For a better explanation a schematic summary is found in appendix II.

After defining the data with 'geoSTRAIN8', now results can be plotted by 'qq' (vector field) or 'plotstrainsuv' (strain contours).

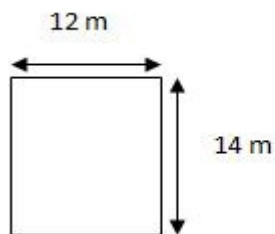
5. RESULTS

In this section, the results of 7 experiments are assessed. In these experiments, the changes in the surface settlements and tunnel surface pressure are examined by changing some of the parameters. These parameters are the loading on the ground surface (a building is present or not etc), different surface conditions, supports made during the tunnel construction and finally how the layer on the tunnel is affected by its change.

In the experiments, the surface soil samples used are under loose and dry conditions. Except the 6th and 7th experiments, C/D=0.5 and it is constant in the other two experiments, C/D=1 is used.

During the experiments the surcharge load used as 2 kg. But actually, it equals to almost 924t (corresponding to a building which has 5 stories).

$$\text{Building Weight} = \text{Number Of Floor} \times \text{Area Of Floor} \times 1,1 \text{ [Ton/m}^2\text{]}$$



5 Floor

$$BW = 5 \times 12 \times 14 \times 1,1 = 924 \text{ Ton}$$

$$\text{Mass} = 1 / [N^3] = 924 / [75^3] \approx 2 \text{ kg}$$

Table 5.1 : Conditions Of Experiments

EXPERIMENT NO	RELATIVE DENSITY (%)	MATERIAL	OVERBURDEN RATIO	SURCHARGE LOAD	TEXTILE
1	32	S1	C/D=0.5	----	----
2	32	S1	C/D=0.5	X	----
3	25	S2	C/D=0.5	----	----
4	25	S2	C/D=0.5	X	----
5	32	S1	C/D=0.5	----	X
6	32	S1	C/D=1.0	----	----
7	32	S1	C/D=1.0	----	X

5.1 Experimental Results

5.1.1 Experiment 1

The conditions of experiment 1 is shown in Table 5.2:

Table 5.2 : The conditions of experiment 1

EXPERIMENT NO	RELATIVE DENSITY (%)	MATERIAL	OVERBURDEN RATIO	SURCHARGE LOAD	TEXTILE
1	32	S1	C/D=0.5	----	----

The model box is filled with S1 soil, the soil surface is flattened by a spatula. Then typical test procedure, which is explained in section 4.6, is completed, The camera is started with PSRemote and the time lags are selected (in this tests 6sec). Before the program activates the piston movement by on the DOS computer, the first pictures is taken by camera. On Figure 5.1, the piston is not started to moving, that means total displacement is zero .

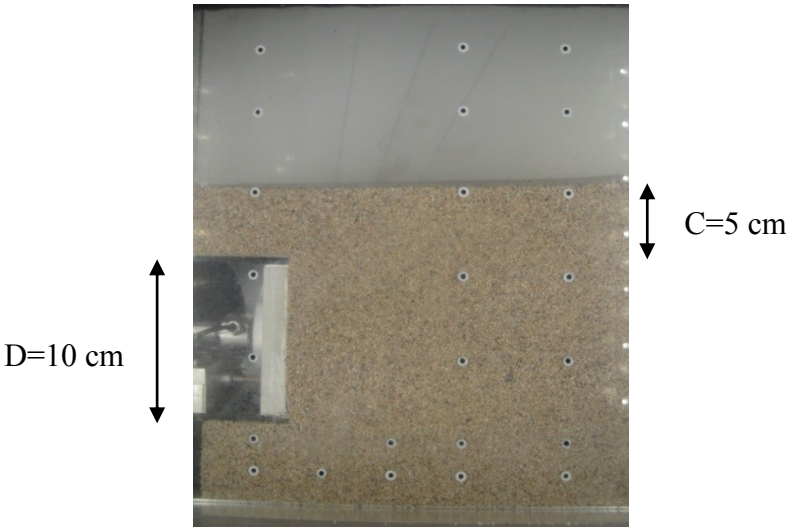


Figure 5.1 : The first picture (when the experiment started)

After the total displacement reach to the 500th step or 5 mm displacement , the last picture is taken by the camera. Figure 5.2 shows the ground surface settlement after the moving of 5 mm at the tunnel face.

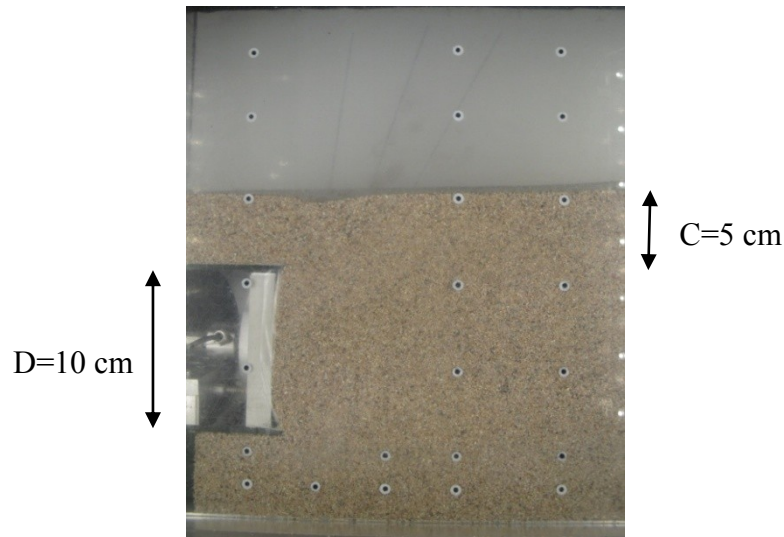


Figure 5.2 : The picture, after 5 mm of tunnel face displacement

During the test, A picture is saved every six second thus the amount of ground surface settlement is determined using the PIV program.

5.1.1.1 Vector Field

In order to understand the eventual failure mechanism of a geotechnical structure, measuring the plane ground deformations is essential. The pictures are compared with the helping of PIV program, and the deformations are shown in this section.

The first experiment is done using with Norman Sand without any surcharge load at 75g. In Figure 5.3, shows the affected area by the movement of the tunnel face between the 0 mm and 0.5 mm.

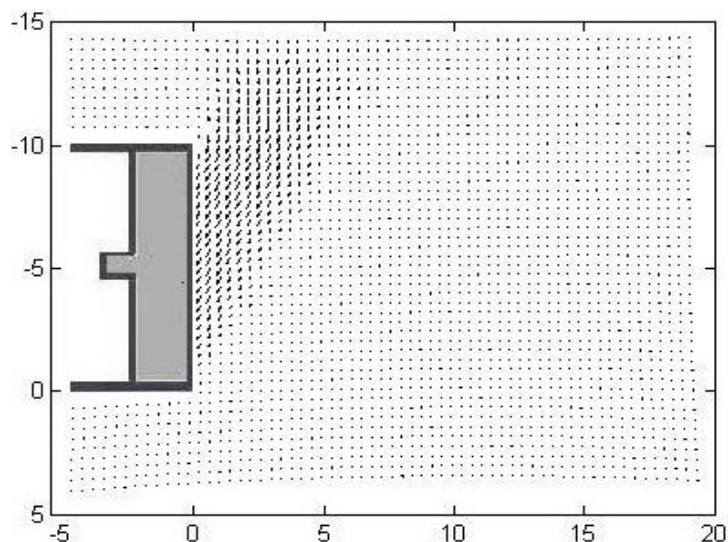


Figure 5.3 : $C/D=0.5$ S1 loose: vector field of resultant ground movement at 0.5mm face

In Figure 5.4 shows the affected area by the movement of the tunnel face between the 0 mm and 5 mm.

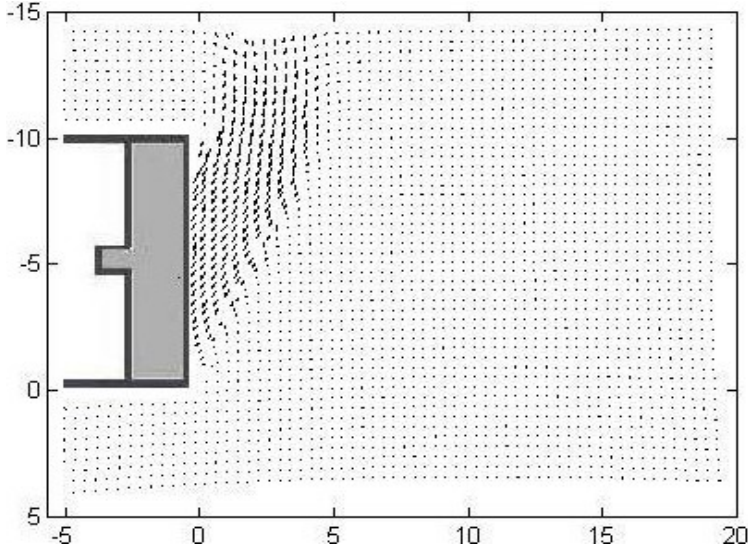


Figure 5.4 : C/D=0.5 S1 loose: vector field of resultant ground movement at 5mm face

5.1.1.2 Contours of Resultant Maximum Shear Strain

The pictures compares helping of PIV program, and the maximum shear strains are shown below in Figure 5.5.

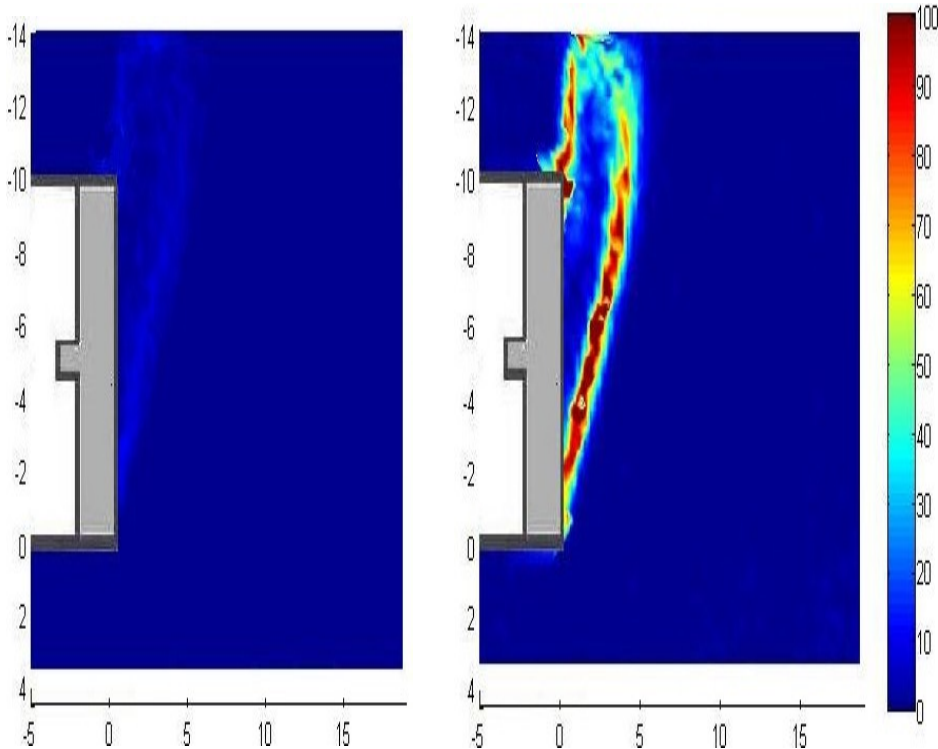


Figure 5.5 : C/D=0.5 S1 loose: a)contours of resultant max. shear strain after 0.5 mm face b) contours of resultant max. shear strain after 5mm face

Picture on the left shows the shear strains which affected by the movement of the tunnel face between the 0 mm and 0.5 mm, picture on the right shows the affected area by the movement of the tunnel face between the 0 mm and 5 mm.

5.1.1.3 Surface Settlement

In the case when Norman Sand is used without any surcharge load, the maximum surface settlement is 5 mm (Figure 5.6).

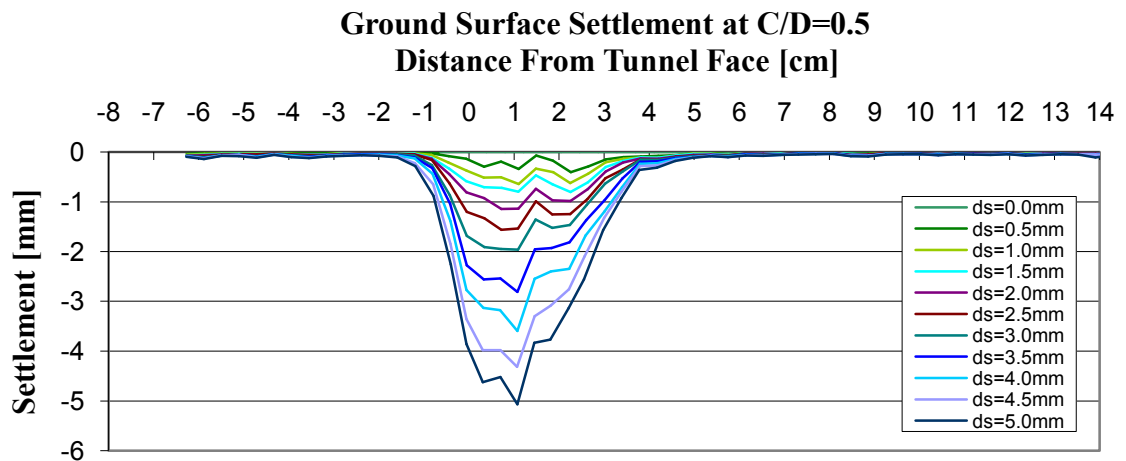


Figure 5.6 : C/D=0.5 S1 loose: surface settlement after $\Delta s=0.5\text{mm}$ face displacement, total face displacement $ds=5\text{mm}$; max. settlement: 5 mm

5.1.1.5 Support Pressure

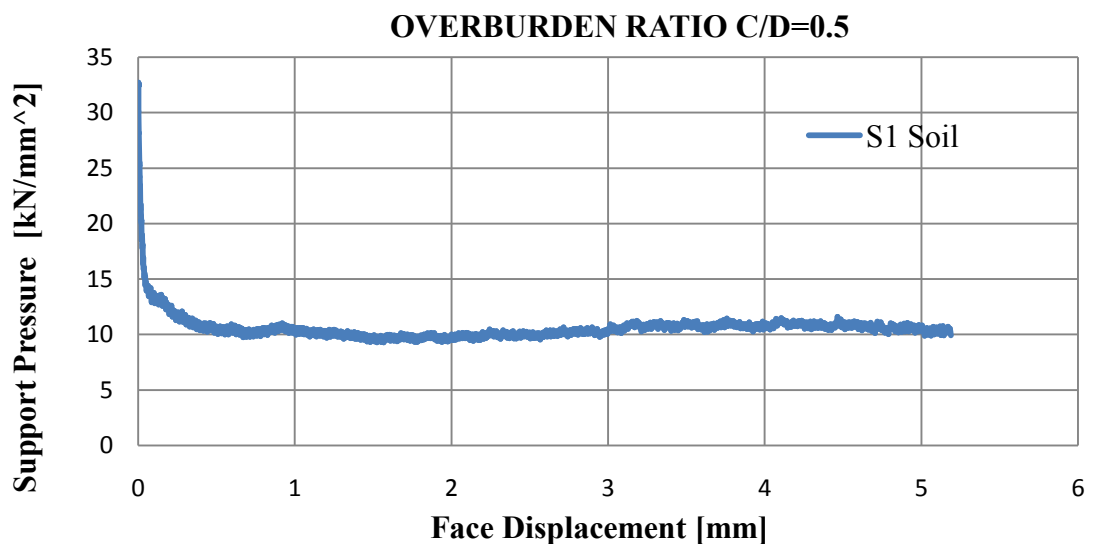


Figure 5.7 : C/D=0.5 S1 loose: support pressure over face displacement; five millimetres; mean pressure after failure: $p_f=10.0\text{kN/m}^2$

In the 1st experiment (no surcharge load, norman sand, C/D=0.5), maximum support pressure formed during the experiment is measured as 32.5 kN/m² and minimum support pressure is measured as 10 kN/m².

5.1.2 Experiment 2

The conditions of experiment 2 is shown in Table 5.3:

Table 5.3 : The conditions of experiment 2

EXPERIMENT NO	RELATIVE DENSITY(%)	MATERIAL	OVERBURDEN RATIO	SURCHARGE LOAD	TEXTILE
2	32	S1	C/D=0.5	X	----

The model box is filled with S1 soil, the soil surface is flattened by a spatula, the building model is placed on ground surface. Then typical test procedure, which is explained in section 4.6, is completed, The camera is started with PSRemote and the time lags are selected (in this tests 6sec). Before the program activates the piston movement by on the DOS computer, the first pictures is taked-n by camera. On Figure 5.8, the piston is not started to moving, that means total displacement is zero.

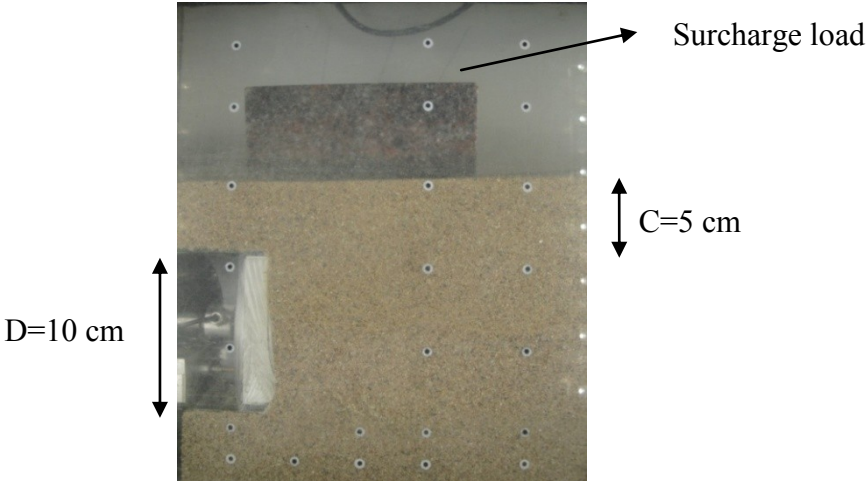


Figure 5.8 : The first picture (when the experiment started)

After the total displacement reach to the 500th step or 5 mm displacement, the last picture is taken by the camera. Figure 5.8 shows the ground surface settlement after the moving of 5 mm at the tunnel face.

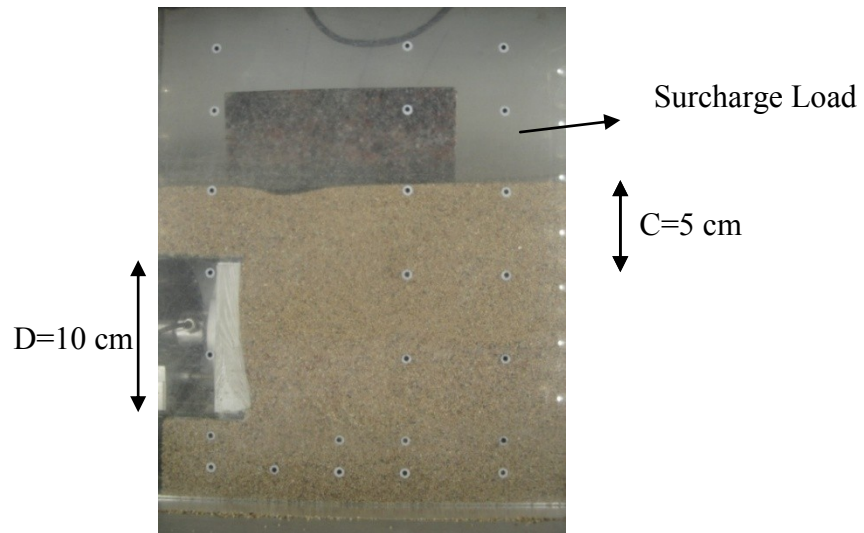


Figure 5.9 : The picture, after 5 mm of tunnel face displacement

During the test, A picture is saved every six second thus the amount of ground surface settlement is determined using the PIV program.

5.1.2.1 Vector Field

In order to understand the eventual failure mechanism of a geotechnical structure, measuring the plane ground deformations is essential. The pictures compared with the helping of PIV program, and the deformations are shown in this section.

The second experiment is done using with Norman Sand , then surcharge load is placed on ground surface. Experiment 2 is performed at 75g. Figure 5.10, shows the affected area by the movement of the tunnel face between the 0 mm and 0.5 mm.

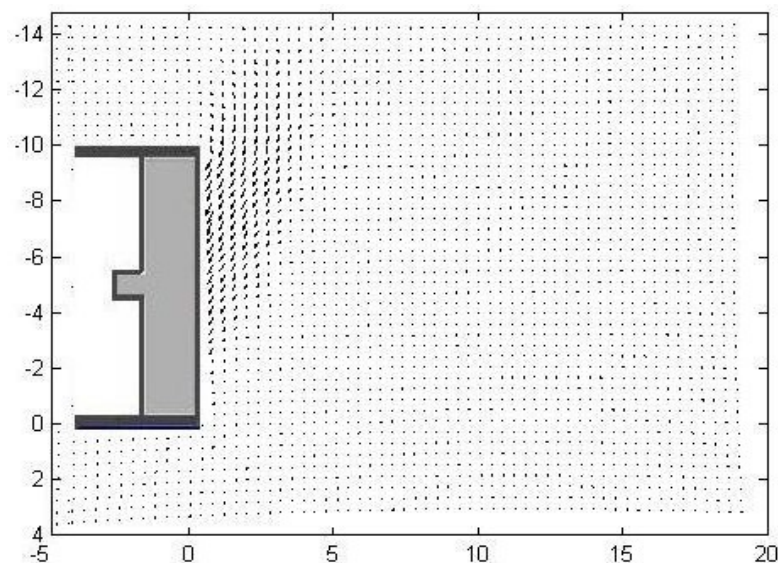


Figure 5.10 : $C/D=0.5$ S1 loose, with surcharge: vector field of resultant ground movement at 0,5mm face

Figure 5.11, shows the affected area by the movement of the tunnel face between the 0 mm and 5 mm.

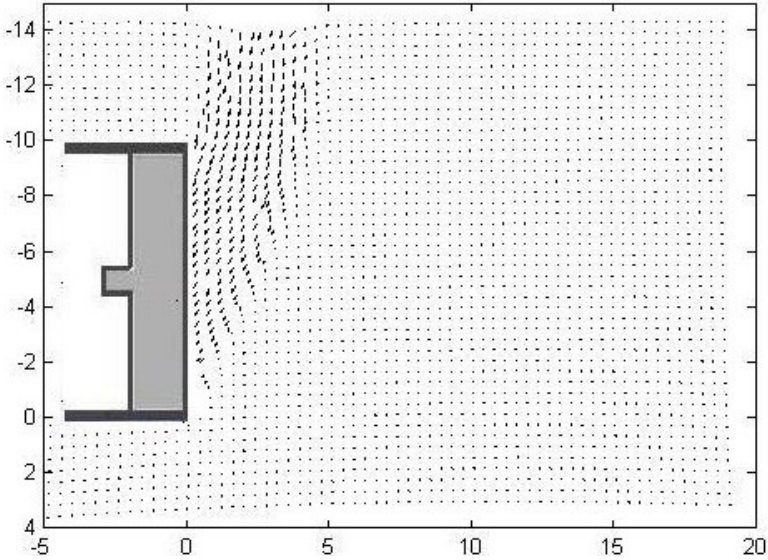


Figure 5.11 : C/D=0.5 S1 loose, with surcharge: vector field of resultant ground movement at 5 mm face

5.1.2.2 Contours of Resultant Maximum Shear Strain

The pictures compares helping of PIV program, and the maximum shear strains are shown below in Figure 5.12.

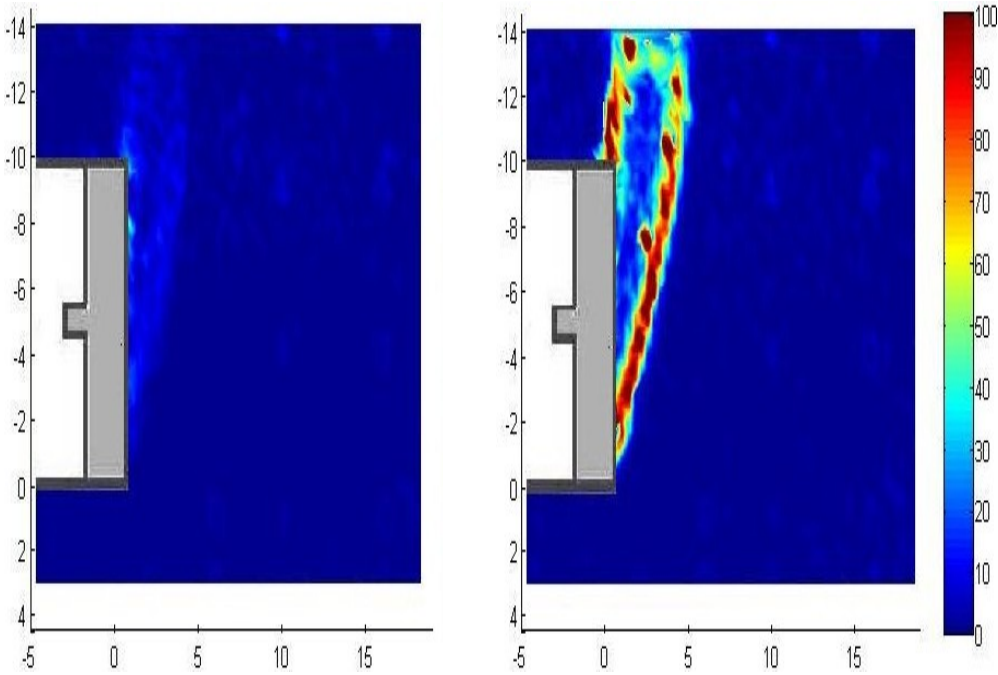


Figure 5.12 : C/D=0.5 S1 loose(with surcharge): a)contours of resultant max. shear strain after 0,5mm face b)contours of resultant max. shear strain after 5mm face

Picture on the left shows the shear strains which affected by the movement of the tunnel face between the 0 mm and 0.5 mm, picture on the right shows the affected area by the movement of the tunnel face between the 0 mm and 5 mm.

5.1.2.3 Surface Settlement

In the case when Norman Sand is used with surcharge load, the maximum surface settlement is 5.5 mm, the width of the surface settlement is approximately 50 mm (Figure 5.13).

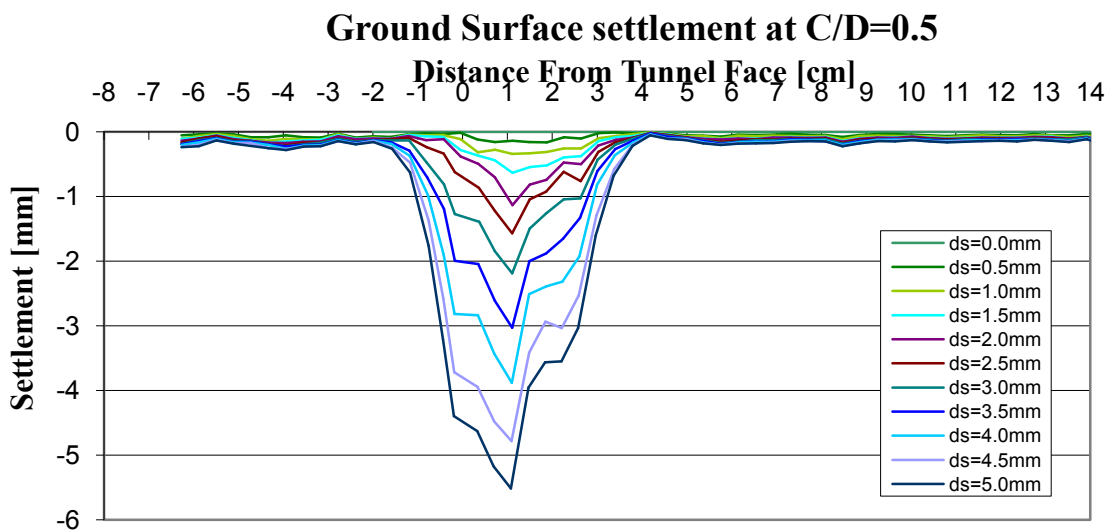


Figure 5.13 :C/D=0.5 S1 loose(with surcharge): surface settlement after $\Delta s=0.5$ mm face displacement, total face displacement $ds=5$ mm; max. settlement: 10.2 mm

5.1.2.5. Support Pressure

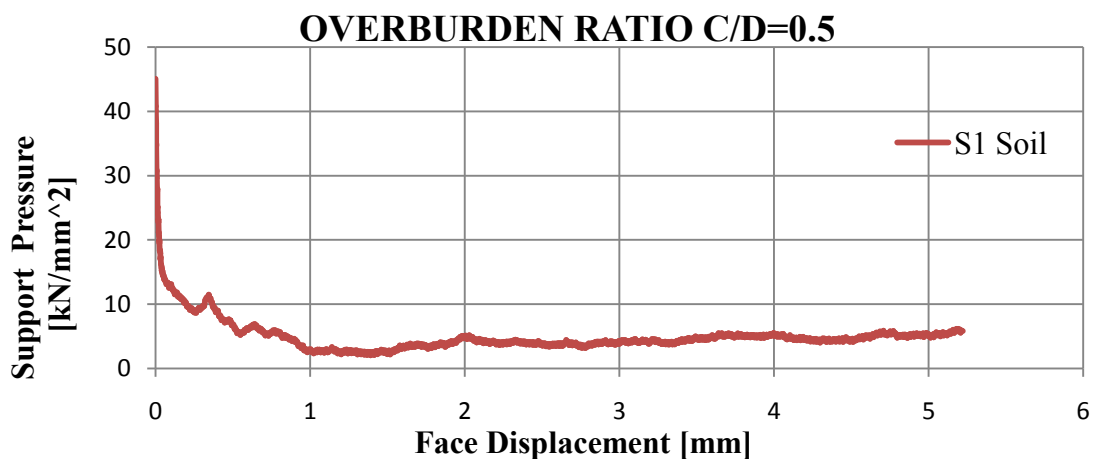


Figure 5.14 : C/D=0.5 S1 loose (with surcharge): support pressure over face displacement; five millimetres; mean pressure after failure: $pf=5.0$ kN/m²

In the 2nd experiment (surcharge load present, norman sand, C/D=0.5); the developed maximum support pressure is measured as 45 kN/m² and minimum support pressure is measured as 5 kN/m²

5.1.3 Experiment 3

The conditions of experiment 3 is shown in Table 5.4:

Table 5.4 : The conditions of experiment 3

EXPERIMENT NO	RELATIVE DENSITY (%)	MATERIAL	OVERBURDEN RATIO	SURCHARGE LOAD	TEXTILE
3	25	S2	C/D=0.5	----	----

The model box is filled with S2 soil,the soil surface is flattened by a spatula.Then typical test procedure, which is explained in section 4.6, is completed, The camera is started with PS Remote and the time lags are selected (in this tests 6sec).Before the program activates the piston movement by on the DOS computer, the first pictures is taken by the camera. On Figure 5.15, the piston is not started to moving, that means total displacement is zero .

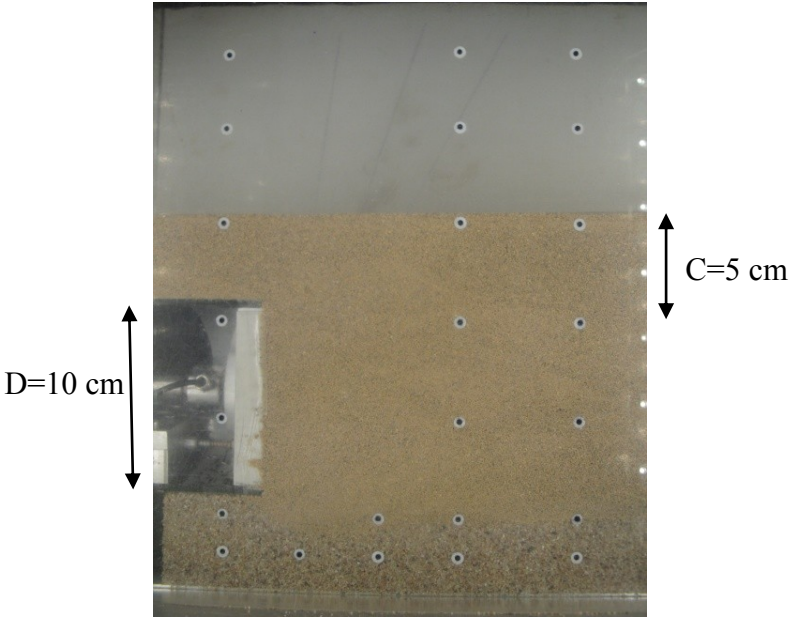


Figure 5.15 : The first picture (when the experiment started)

After the total displacement reach to the 500th step or 5 mm displacement, the last picture is taken by the camera. Figure 5.16 shows the ground surface settlement after the moving of 5 mm at the tunnel face.

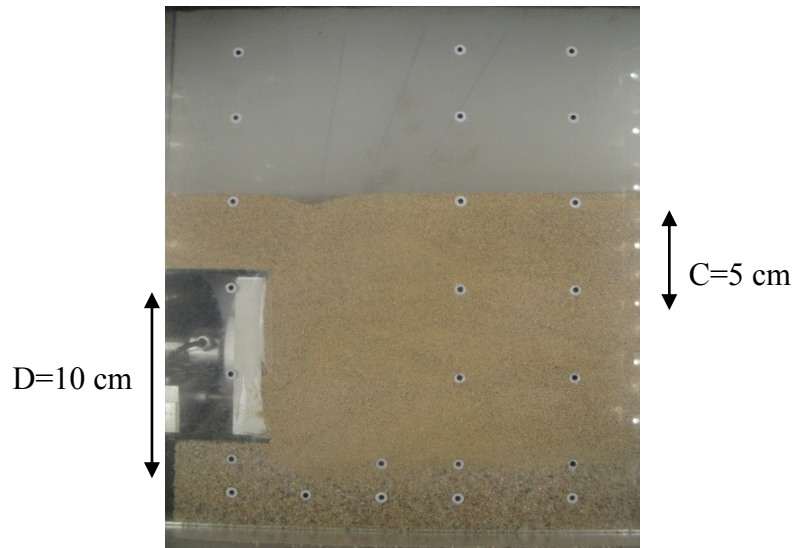


Figure 5.16 : The picture, after 5 mm of tunnel face displacement
 During the test, A picture is saved every six second thus the amount of ground surface settlement is determined using the PIV program.

5.1.3.1 Vector Field

In order to understand the eventual failure mechanism of a geotechnical structure, measuring the plane ground deformations is essential. The pictures are compared with the helping of PIV program, and the deformations are shown in this section.

The third experiment is done using with S2 Soil without any surcharge load at 75g. Figure 5.17, shows the affected area by the movement of the tunnel face between the 0 mm and 0.5 mm.

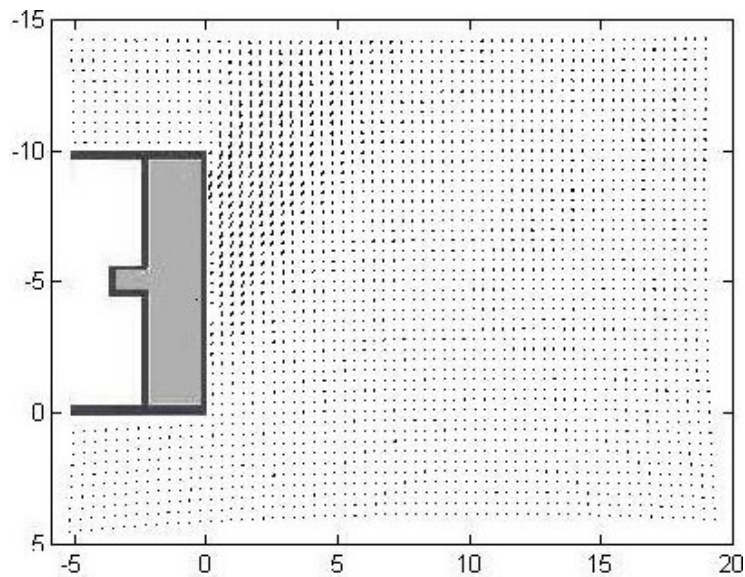


Figure 5.17 : C/D=0.5 S2 loose: vector field of resultant ground movement at 0.5 mm face

Figure 5.18, shows the affected area by the movement of the tunnel face between the 0 mm and 0.5 mm

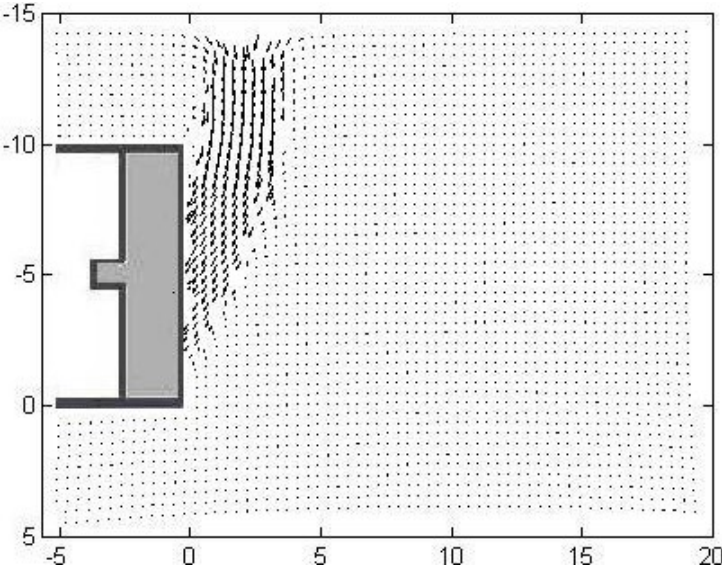


Figure 5.18 : C/D=0.5 S2 loose: vector field of resultant ground movement at 5mm face

5.1.3.2 Contours of Resultant Maximum Shear Strain

The pictures compares helping of PIV program, and the maximum shear strains are shown below in Figure 5.19.

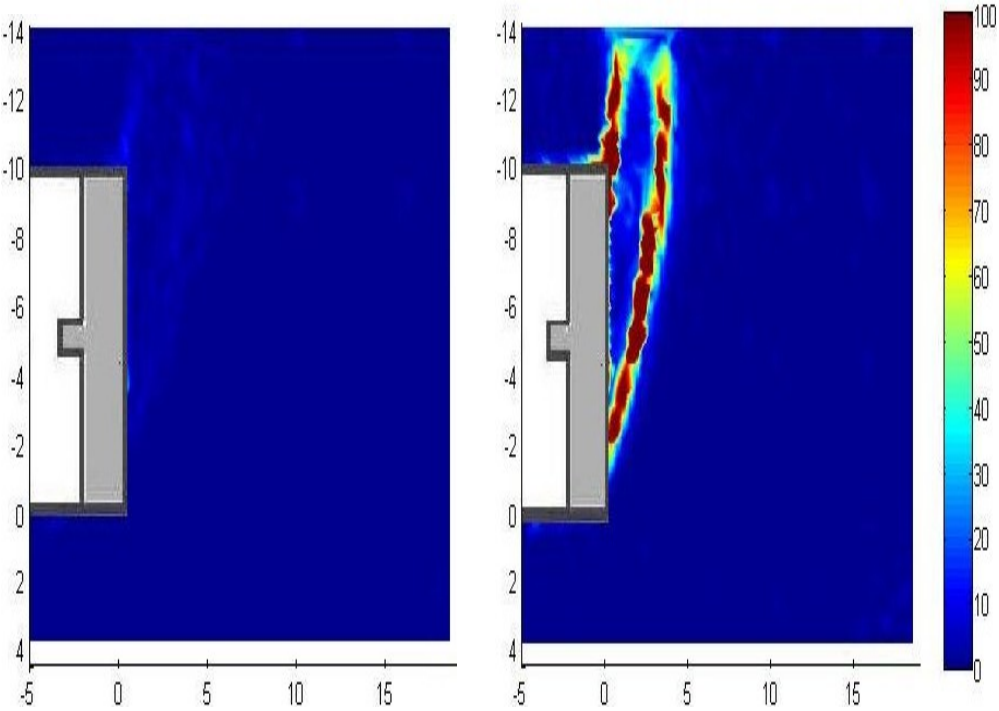


Figure 5.19 : C/D=0.5 S2 loose: a)contours of resultant max. shear strain after 0.5mm face b)contours of resultant max. shear strain after 5 mm face

Picture on the left shows the shear strains which affected by the movement of the tunnel face between the 0 mm and 0.5 mm, picture on the right shows the affected area by the movement of the tunnel face between the 0 mm and 5 mm.

5.1.3.3 Surface Settlement

In case experiment 3, when no surcharge load is present, the maximum surface settlement is 7.3 mm (Figure 5.20).

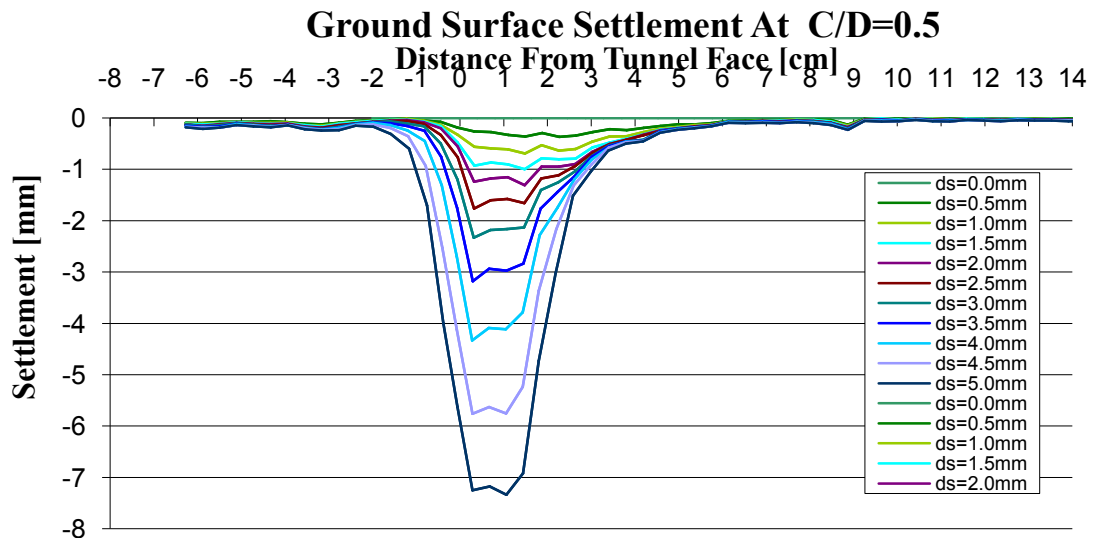


Figure 5.20 : C/D=0.5 S2 loose: surface settlement after $\Delta s=0.5\text{mm}$ face displacement, total face displacement $ds=5\text{mm}$; max. settlement: 7.3 mm

5.1.3.4 Support Pressure

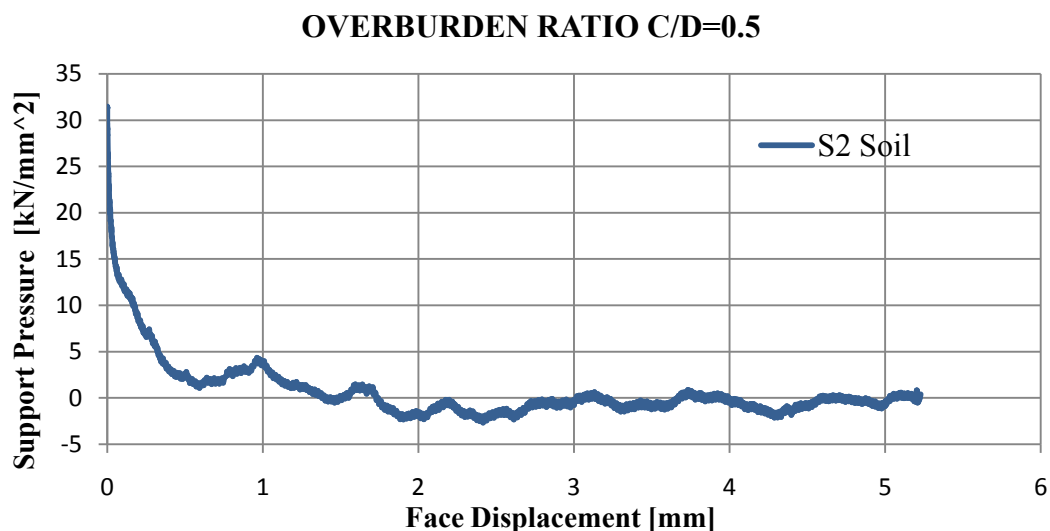


Figure 5.21 : C/D=0.5 S2 loose: support pressure over face displacement; five millimetres; mean pressure after failure: $p_f=0.0\text{kN/m}^2$

In the 3rd experiment (no surcharge load, fine sand, C/D=0,5); the maximum support pressure formed during the experiment is measured as 31.5 kN/m² and the minimum support pressure is measured as 0 kN/m².

5.1.4 Experiment 4

The conditions of experiment 4 is shown in Table 5.5:

Table 5.5 : The conditions of experiment 4

EXPERIMENT NO	RELATIVE DENSITY(%)	MATERIAL	OVERBURDEN RATIO	SURCHARGE LOAD	TTEXTILE
4	25	S2	C/D=0.5	X	----

The model box is filled with S2 soil,the soil surface is flattened by a spatula, the building model is placed on ground surface.Then typical test procedure, which is explained in section 4.6, is completed, The camera is started with PS Remote and the time lags are selected (in this tests 6sec).Before the program activates the piston movement by on the DOS computer, the first pictures is taken by the camera. O Figure 5.22, the piston is not started to moving, that means total displacement is zero

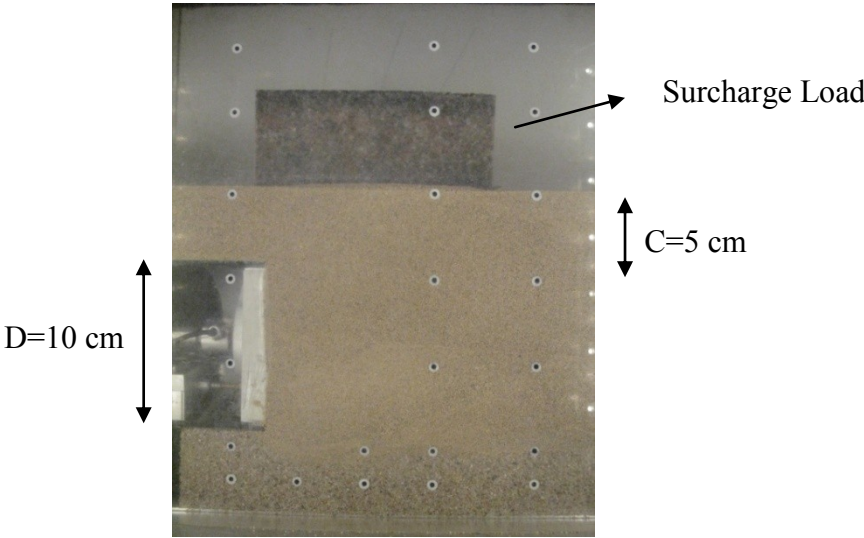


Figure 5.22 : The first picture (when the experiment started)

After the total displacement reach to the 500th step or 5 mm displacement, the last picture is taken by camera. Figure 5.23 shows the ground surface settlement after the moving of 5 mm at the tunnel face.

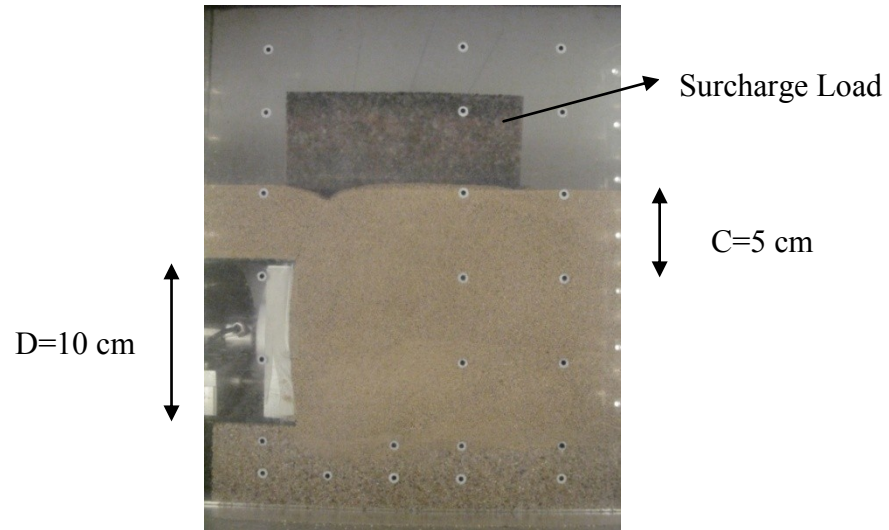


Figure 5.23 : The picture, after 5 mm of tunnel face displacement

During the test, A picture is saved every six second thus the amount of ground surface settlement is determined using the PIV program.

5.1.4.1 Vector Field

In order to understand the eventual failure mechanism of a geotechnical structure, measuring the plane ground deformations is essential. The pictures are compared with the helping of PIV program, and the deformations are shown in this section.

The fourth experiment is done using with S2 Soil with surcharge load at 75g. Figure 5.24, shows the affected area by the movement of the tunnel face between the 0 mm and 0.5 mm.

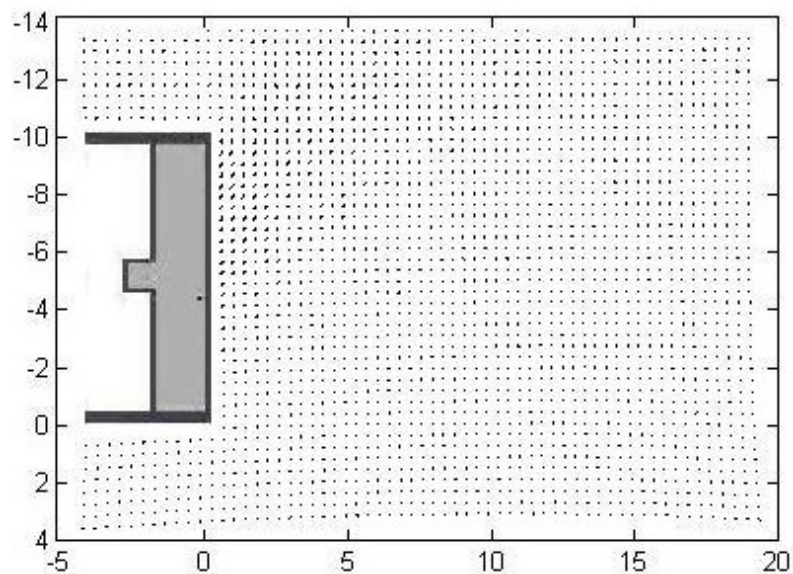


Figure 5.24 : $C/D=0.5$ S2 loose, with surcharge: vector field of resultant ground movement

Figure 5.25 shows the affected area by the movement of the tunnel face between the 0 mm and 5 mm.

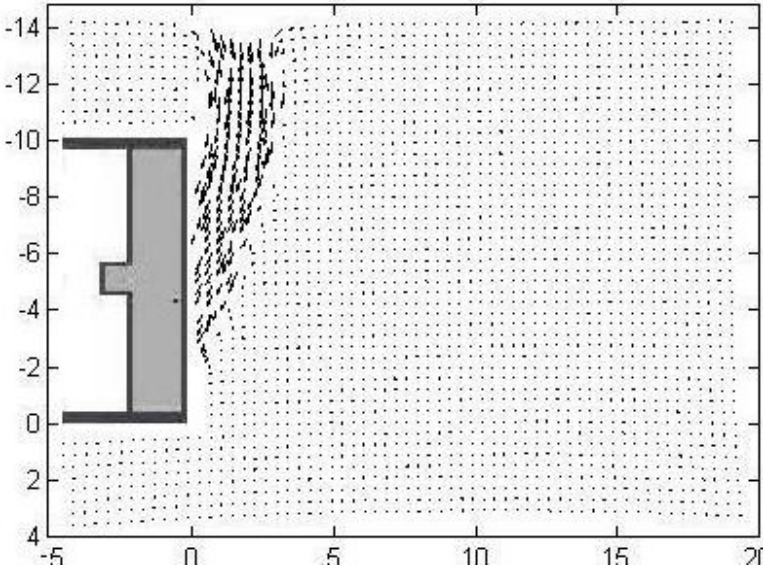


Figure 5.25 : C/D=0.5 S2 loose, with surcharge: vector field of resultant ground movement at 5mm face

5.1.4.2 Contours of Resultant Maximum Shear Strain

The pictures compares helping of PIV program, and the maximum shear strains are shown below in Figure 5.26.

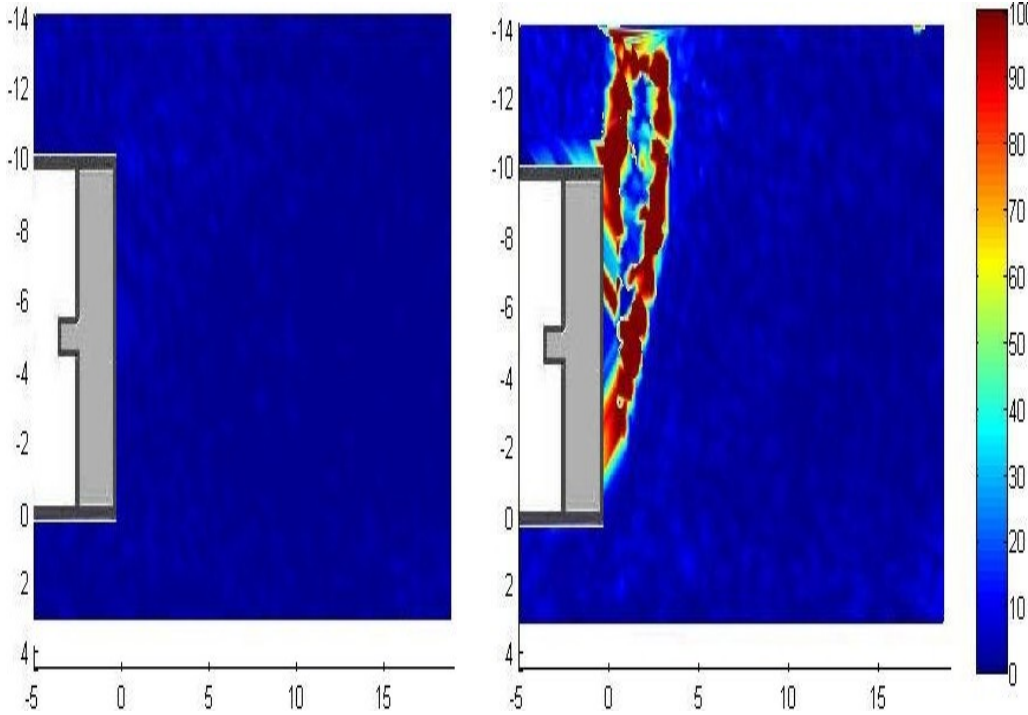


Figure 5.26 : C/D=0.5 S2 loose(with surcharge): a)contours of resultant max. shear strain after 0.5mm face b)contours of resultant max. shear strain after 5mm face

Picture on the left shows the shear strains which affected by the movement of the tunnel face between the 0 mm and 0.5 mm, picture on the right shows the affected area by the movement of the tunnel face between the 0 mm and 5 mm.

5.1.4.3 Surface Settlement

In the Experiment 4, when the surcharge load is added, surface settlement has reached to 10.2 mm .

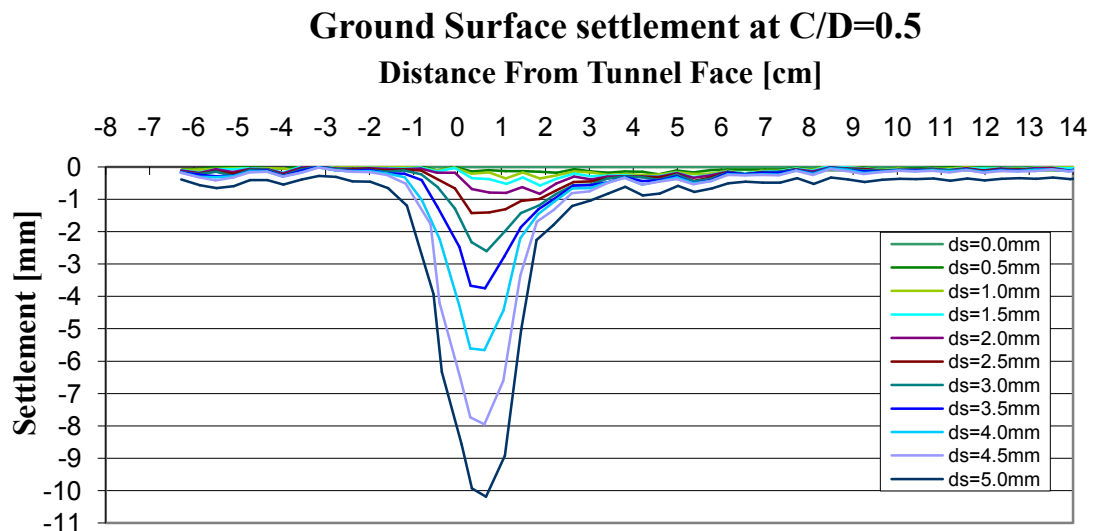


Figure 5.27 : C/D=0.5 S2 loose(with surcharge): surface settlement after $\Delta s=0.5\text{mm}$ face displacement, total face displacement $ds=5\text{mm}$; max. settlement: 10,2 mm

5.1.4.4 Support Pressure

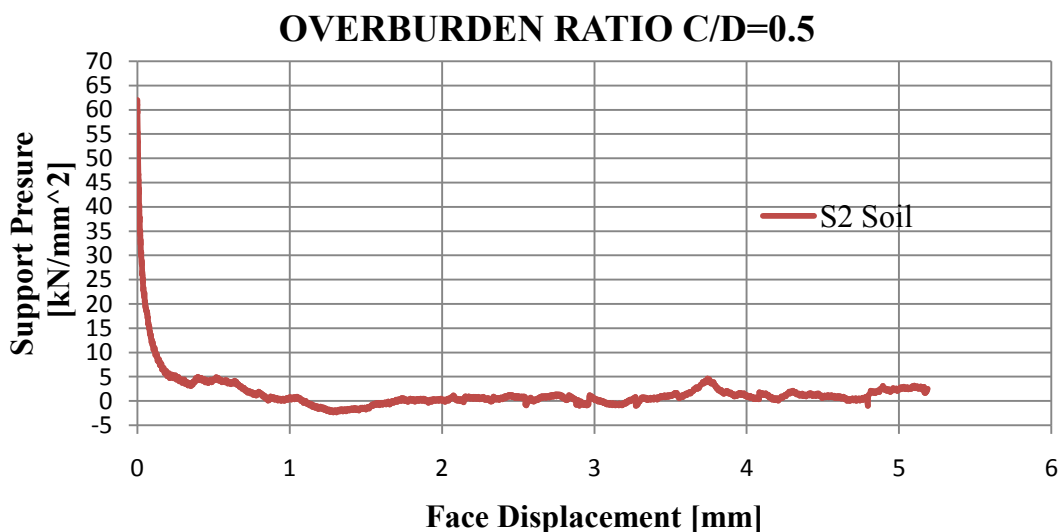


Figure 5.28 : C/D=0.5 S2 loose (with surcharge): support pressure over face displacement; five millimetres; mean pressure after failure: $p_f=0.0\text{kN/m}^2$

In the 4th experiment (surcharge load is present, fine sand, C/D=0,5), the developed maximum support pressure is measured as 61 kN/m² and the minimum support pressure is measured as 0 kN/m².

5.1.5 Experiment 5

The conditions of experiment 5 is shown in Table 5.6:

Table 5.6 : The conditions of experiment 5

EXPERIMENT NO	RELATIVE DENSITY(%)	MATERIAL	OVERBURDEN RATIO	SURCHARGE LOAD	TEXTILE
5	32	S1	C/D=0.5	----	X

The model box is filled with S1 soil,the soil surface is flattened by a spatula then geotextile material is put on the tunnel surface, typical test procedure, which is explained in section 4.6, is completed, The camera is started with PSRemote and the time lags are selected (in this tests 6sec).Before the program activates the piston movement by on the DOS computer, the first pictures is taken by the camera. On Figure 5.29, the piston is not started to moving, that means total displacement is zero

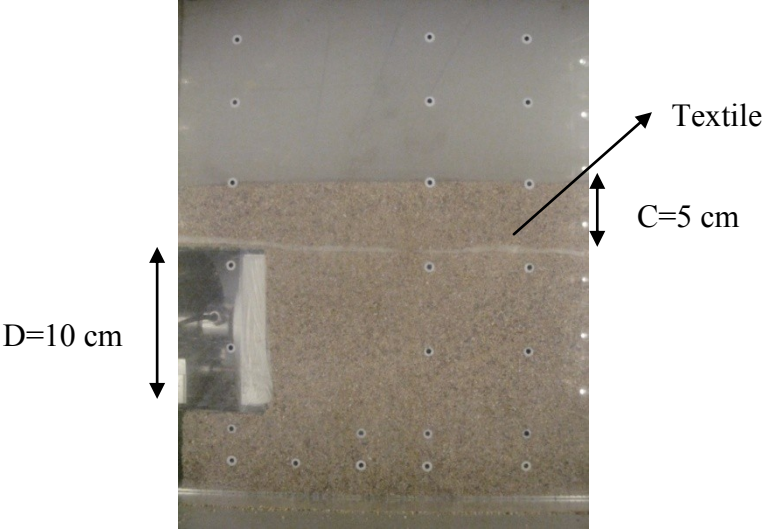


Figure 5.29 : The first picture (when the experiment started)

After the total displacement reach to the 500th step or 5 mm displacement, the last picture is taken by the camera. Figure 5.30 shows the ground surface settlement after the moving of 5 mm at the tunnel face.

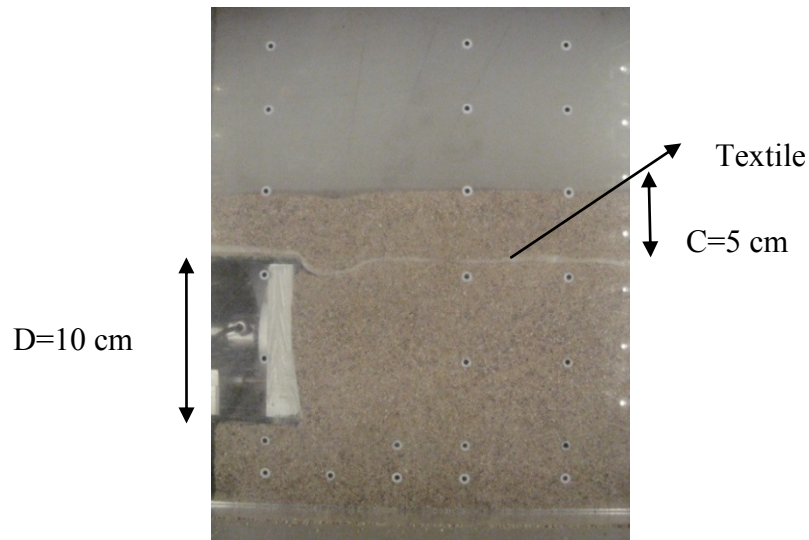


Figure 5.30 : The picture, after 5 mm of tunnel face displacement

During the test, A picture is saved every six second thus the amount of ground surface settlement is determined using the PIV program.

5.1.5.1 Vector Field

In order to understand the eventual failure mechanism of a geotechnical structure, measuring the plane ground deformations is essential. The pictures comparer with the helping of PIV program, and the deformations are shown in this section.

The fifth experiment is applied with S1 Soil and textile placed on tunnel line at 75g. Figure 5.31 shows the affected area by the movement of the tunnel face between the 0 mm and 0.5 mm

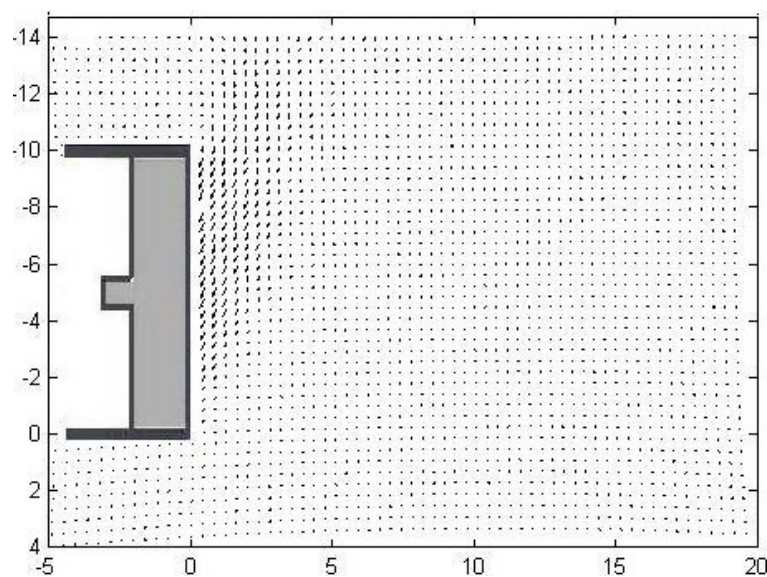


Figure 5.31 : $C/D=0.5$ S1 loose, with textile: vector field of resultant ground movement at 0,5mm face

Figure 5.32 shows the affected area by the movement of the tunnel face between the 0 mm and 5 mm.

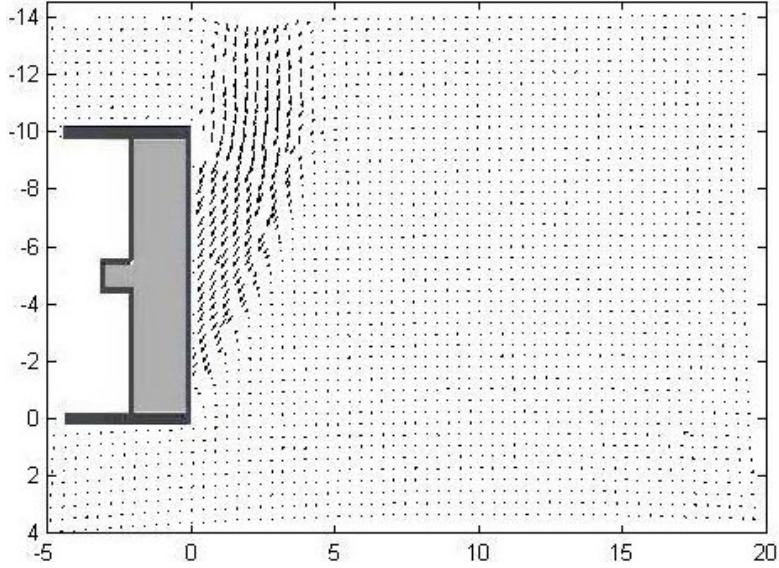


Figure 5.32 :C/D=0.5 S1 loose, (with textile) vector field of resultant ground movement at 5mm face

5.1.5.2 Contours of Resultant Maximum Shear Strain

The pictures compares helping of PIV program, and the maximum shear strains are shown below in Figure 5.33.

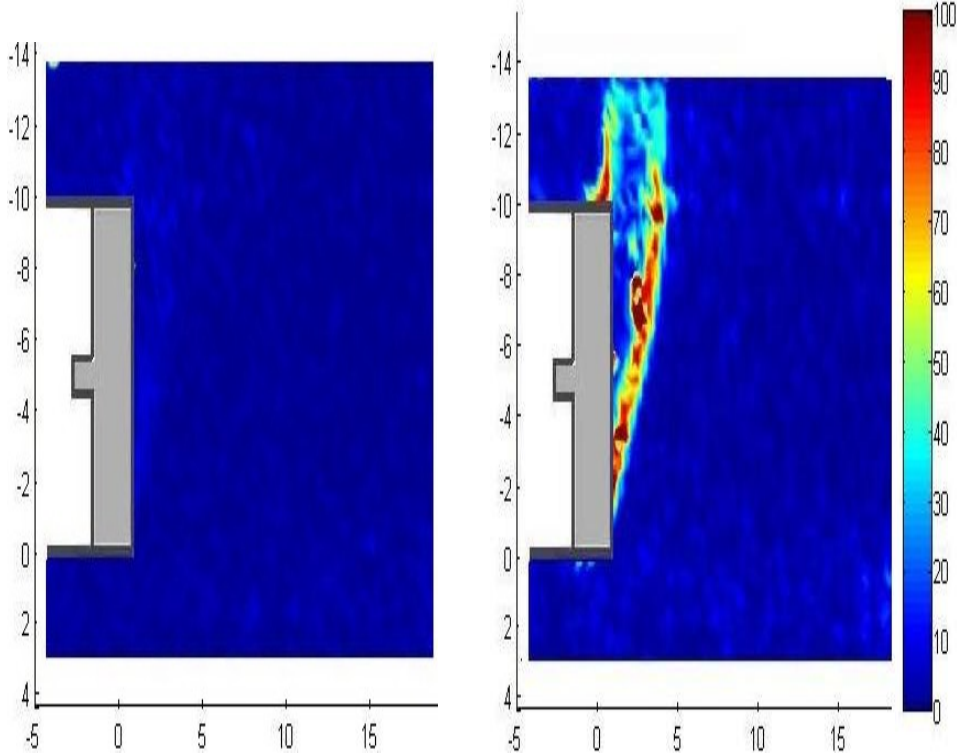


Figure 5.33 : C/D=0.5 S1 loose(with textile): a)contours of resultant max. shear strain after 0.5mm face b)contours of resultant max. shear strain after 5mm face

Picture on the left shows the shear strains which affected by the movement of the tunnel face between the 0 mm and 0.5 mm, picture on the right shows the affected area by the movement of the tunnel face between the 0 mm and 5 mm.

5.1.5.4 Surface Settlement

In the 5th experiment, the maximum surface settlement(Figure 5.34) is about 4.5 mm.

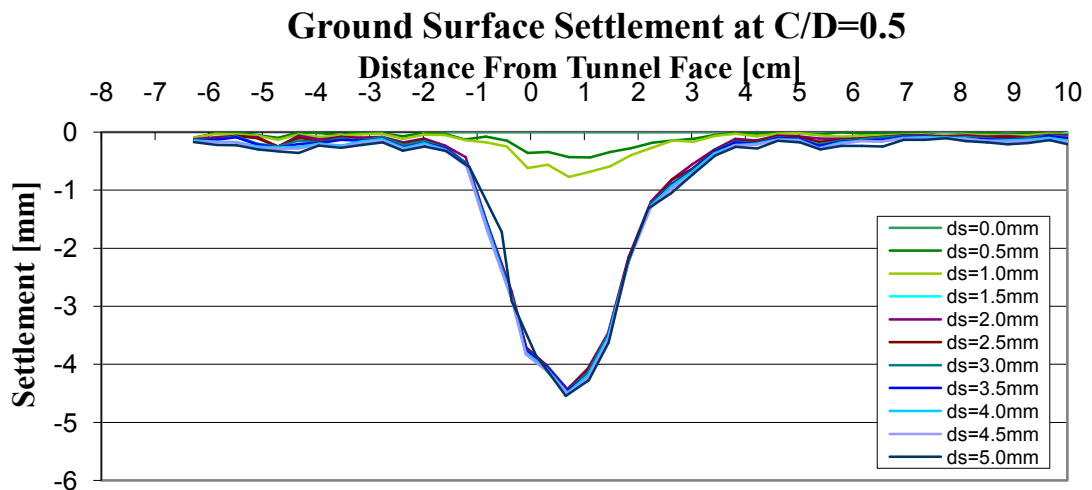


Figure 5.34 : C/D=0.5 S1 loose(with textile): surface settlement after $\Delta s=0.5\text{mm}$ face displacement, total face displacement $ds=5\text{mm}$; max. settlement: 4.5 mm

5.1.5.4 Support Pressure

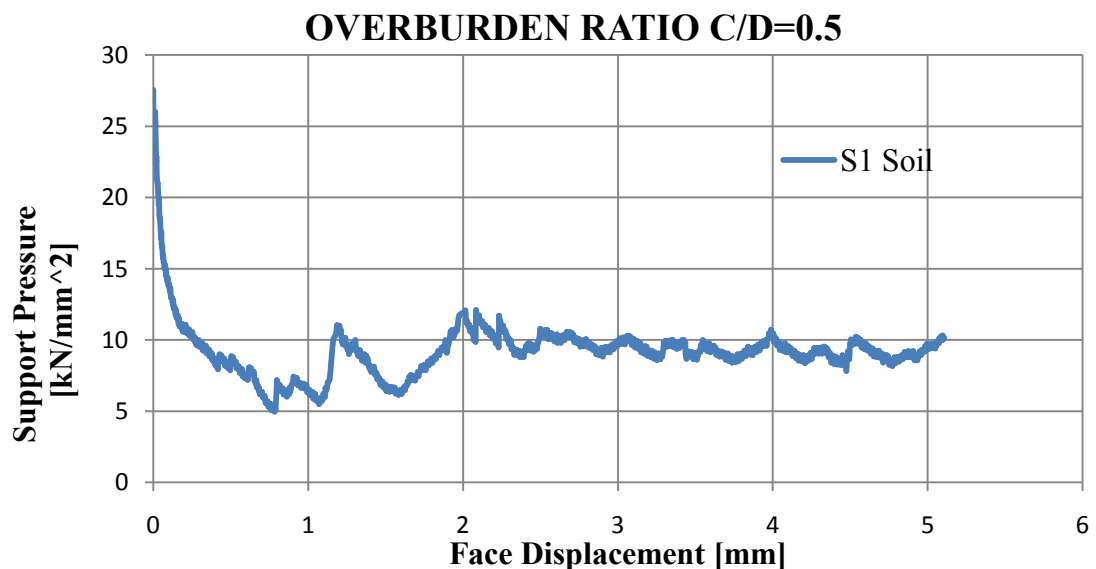


Figure 5.35 : C/D=0.5 S1 loose(with textile): support pressure over face displacement; five millimetres; mean pressure after failure: $p_f=10.0\text{kN/m}^2$

In the 5th experiment the maximum support pressure is measured as 32.5 kN/m² and minimum support pressure is measured as 5 kN/m²

5.1.6 Experiment 6

The conditions of experiment 6 is shown in Table 5.7:

Table 5.7 : The conditions of experiment 6

EXPERIMENT NO	RELATIVE DENSITY(%)	MATERIAL	OVERBURDEN RATIO	SURCHARGE LOAD	TEXTILE
6	32	S1	C/D=1.0	----	----

The model box is filled with S1 soil,the soil surface is flattened by a spatula, typical test procedure, which is explained in section 4.6, is completed, The camera is started with PSRemote and the time lags are selected (in this tests 6sec). Before the program activates the piston movement by on the DOS computer, the first pictures is taken by the camera. On Figure 5.36, the piston is not started to moving, that means total displacement is zero.

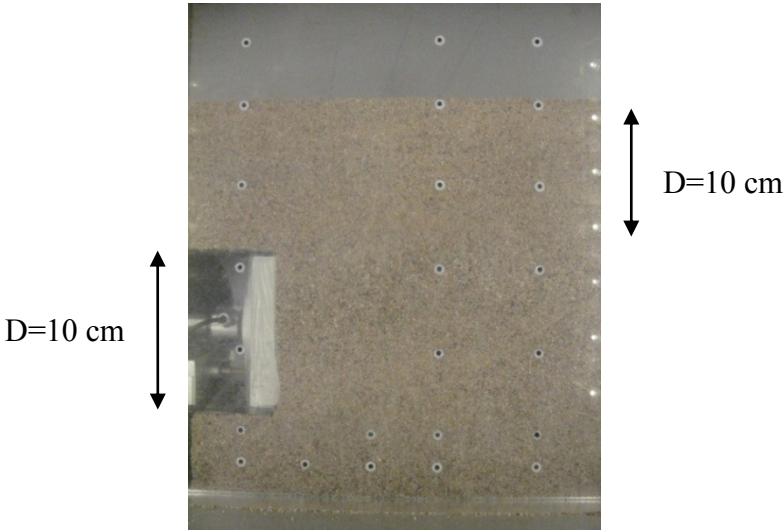


Figure 5.36 : The first picture (when the experiment started)

After the total displacement reach to the 500th step or 5 mm displacement , the last picture is taken by the camera. Figure 5.37 shows the ground surface settlement after the moving of 5 mm at the tunnel face.

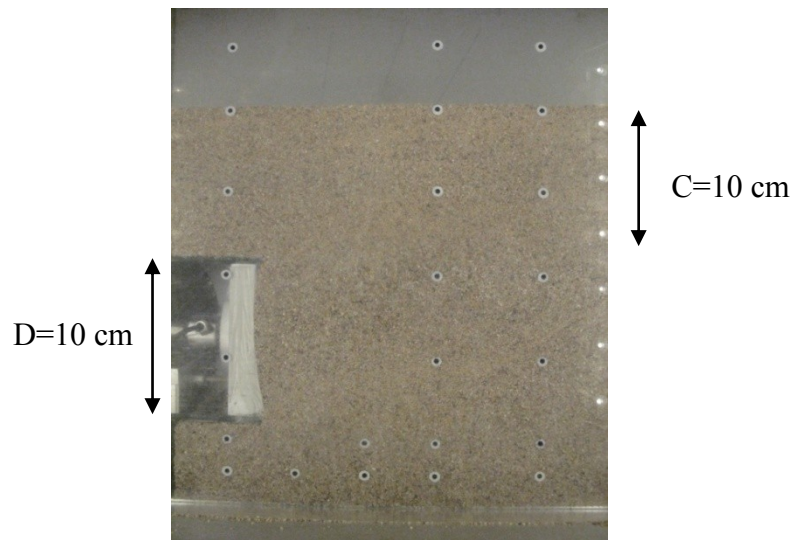


Figure 5.37 : The picture, after 5 mm of tunnel face displacement
 During the test, A picture is saved every six second thus the amount of ground surface settlement is determined using the PIV program.

5.1.6.2 Vector Field

In order to understand the eventual failure mechanism of a geotechnical structure, measuring the plane ground deformations is essential. The pictures are compared with the helping of PIV program, and the deformations are shown in this section..

The sixth experiment is done using with S1 Soil and overburden ratio is 1.0 at 75g. Figure 5.38 shows the affected area by the movement of the tunnel face between the 0 mm and 0.5 mm.

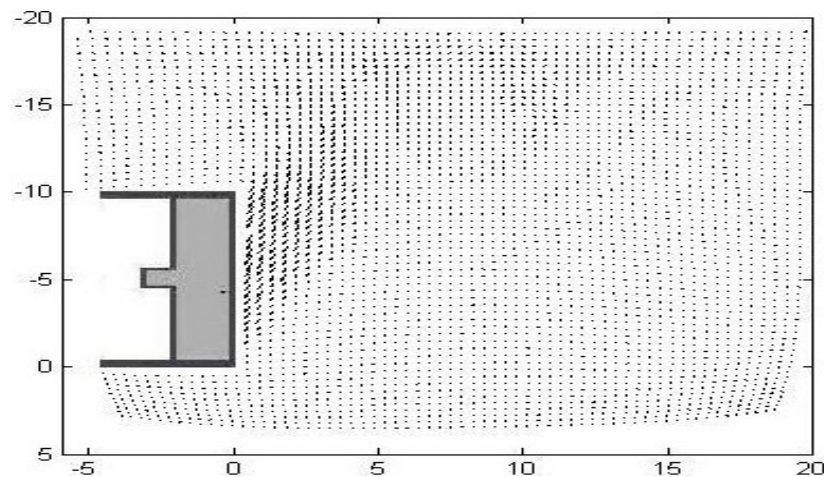


Figure 5.38 : $C/D=1.0$ S1 loose: vector field of resultant ground movement at 0,5mm face

Figure 5.39 shows the affected area by the movement of the tunnel face between the 0 mm and 5 mm.

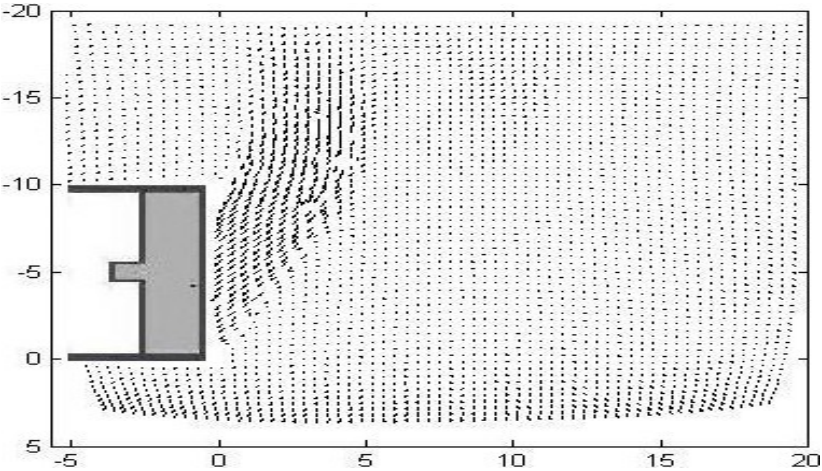


Figure 5.39 : C/D=1.0 S1 loose: vector field of resultant ground movement at 5mm face

5.1.6.2 Contours of Resultant Maximum Shear Strain

The pictures compares helping of PIV program, and the maximum shear strains are shown below in Figure 5.40.

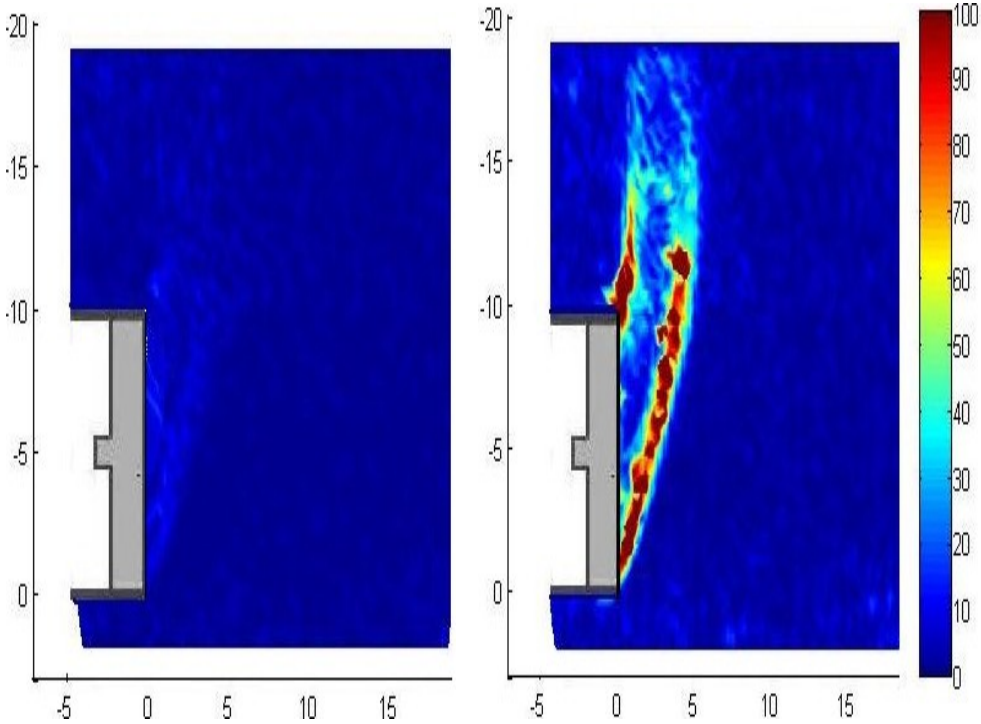


Figure 5.40 : C/D=1.0 S1 loose a)contours of resultant max. shear strain after 0.5mm face b)contours of resultant max. shear strain after 5mm face

Picture on the left shows the shear strains which affected by the movement of the tunnel face between the 0 mm and 0.5 mm, picture on the right shows the affected area by the movement of the tunnel face between the 0 mm and 5 mm.

5.1.6.3 Surface Settlement

In the 6th experiment, maximum surface settlement is 1,4 mm.

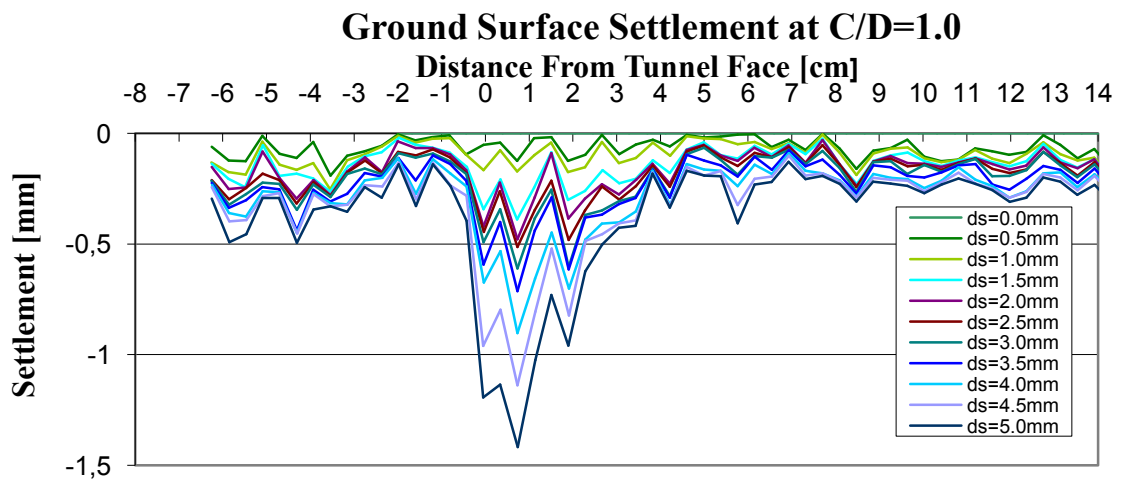


Figure 5.41 : C/D=1.0 S1 loose: surface settlement after $\Delta s=0.5\text{mm}$ face displacement, total face displacement $ds=5\text{mm}$; max. settlement: 1.4 mm

5.1.6.4 Support Pressure

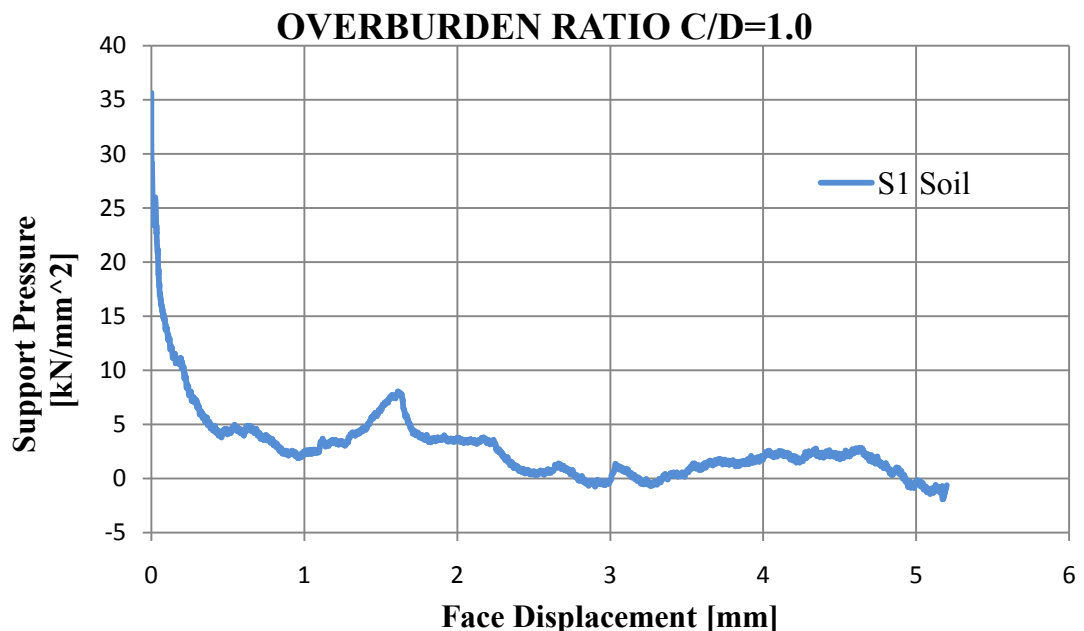


Figure 5.42 : C/D=1.0 S1 loose: support pressure over face displacement; five millimetres; mean pressure after failure: $p_f=0.0\text{kN/m}^2$

In the 6th experiment (no surcharge load, norman sand, C/D=1.0), the developed maximum support pressure is measured as 33 kN/m² and the minimum support pressure is measured as 3 kN/m².

5.1.7 Experiment 7

The conditions of experiment 7 is shown in Table 5.8:

Table 5.8 : The conditions of experiment 7

EXPERIMENT NO	RELATIVE DENSITY(%)	MATERIAL	OVERBURDEN RATIO	SURCHARGE LOAD	TEXTILE
7	32	S1	C/D=1.0	----	X

The model box is filled with S1 soil, the soil surface is flattened by a spatula then geotextile material is put on the tunnel surface, typical test procedure, which is explained in section 4.6, is completed, The camera is started with PS Remote and the time lags are selected (in this tests 6sec). Before the program activates the piston movement by on the DOS computer, the first pictures is taked by camera. At the Figure 5.43, the piston is not started to moving, that means total displacement is zero

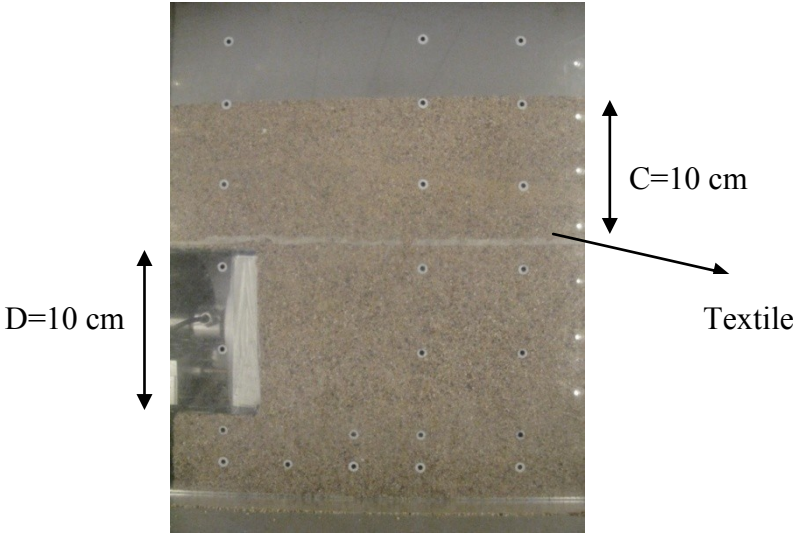


Figure 5.43 : The first picture (when the experiment started)

After the total displacement reach to the 500th step or 5 mm displacement , the last picture is taken by the camera. Figure 5.44 shows the ground surface settlement after the moving of 5 mm at the tunnel face.

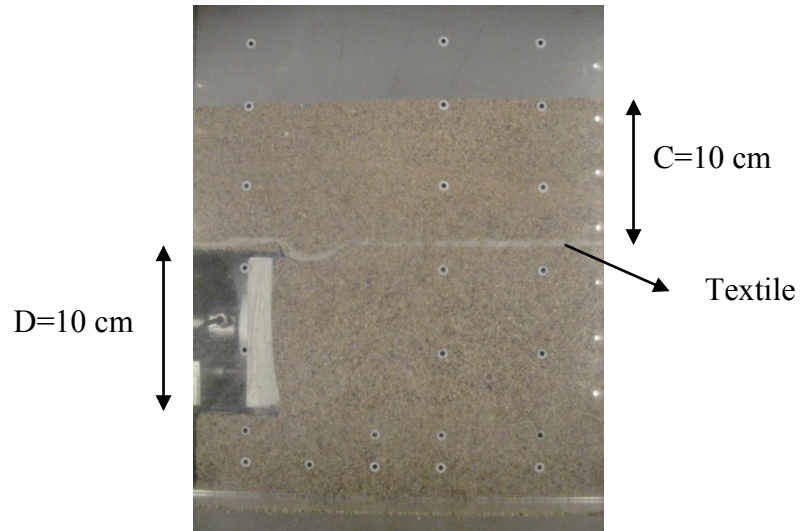


Figure 5.44 : The picture, after 5 mm of tunnel face displacement
 During the test, A picture is saved every six second thus the amount of ground surface settlement is determined using the PIV program.

5.1.7.1 Vector Field

In order to understand the eventual failure mechanism of a geotechnical structure, measuring the plane ground deformations is essential. The pictures are compared with the helping of PIV program, and the deformations are shown in this section.

The seventh experiment is done using with S1 Soil and textile placed on tunnel line at 75g. Figure 5.45 shows the affected area by the movement of the tunnel face between the 0 mm and 0.5 mm.

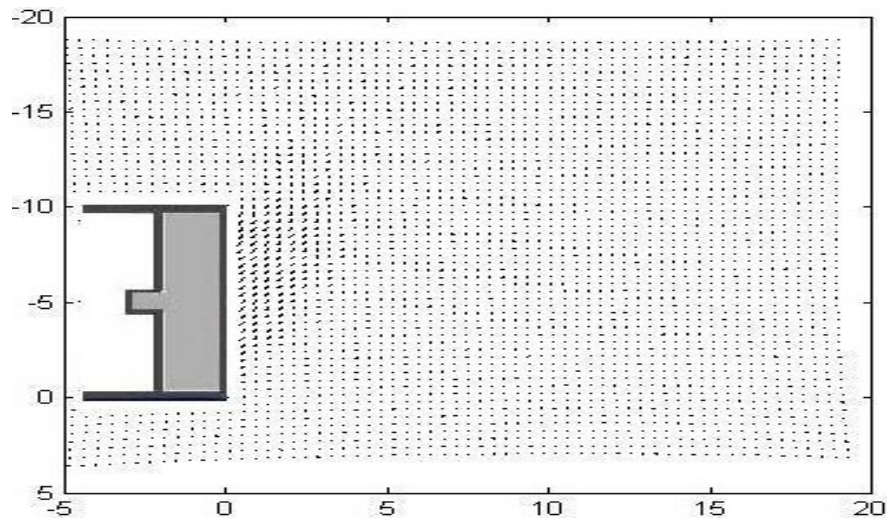


Figure 5.45 : $C/D=1.0$ S1 loose, with textile: vector field of resultant ground movement at 0.5mm face

In Figure 5.46 shows the affected area by the movement of the tunnel face between the 0 mm and 5 mm.

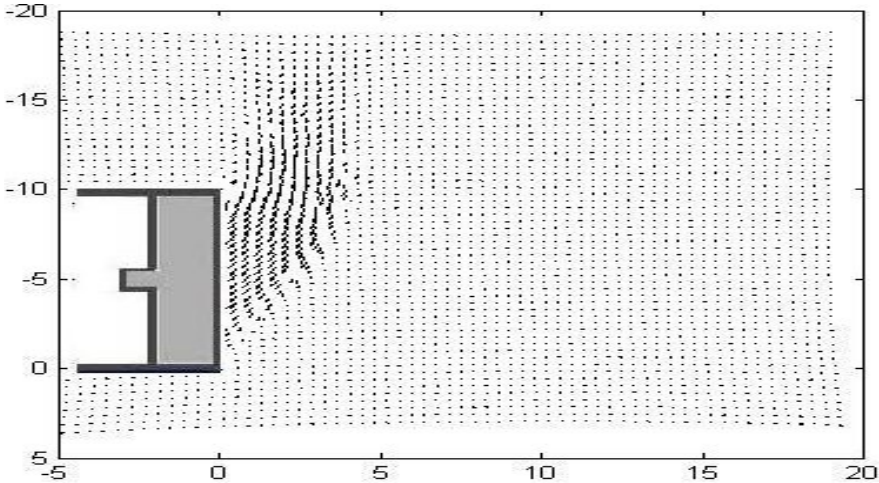


Figure 5.46 : C/D=0.5 S1 loose, (with textile) vector field of resultant ground movement at 5mm face

5.1.7.2 Contours of Resultant Maximum Shear Strain

The pictures compares helping of PIV program, and the maximum shear strains are shown below in Figure 5.47.

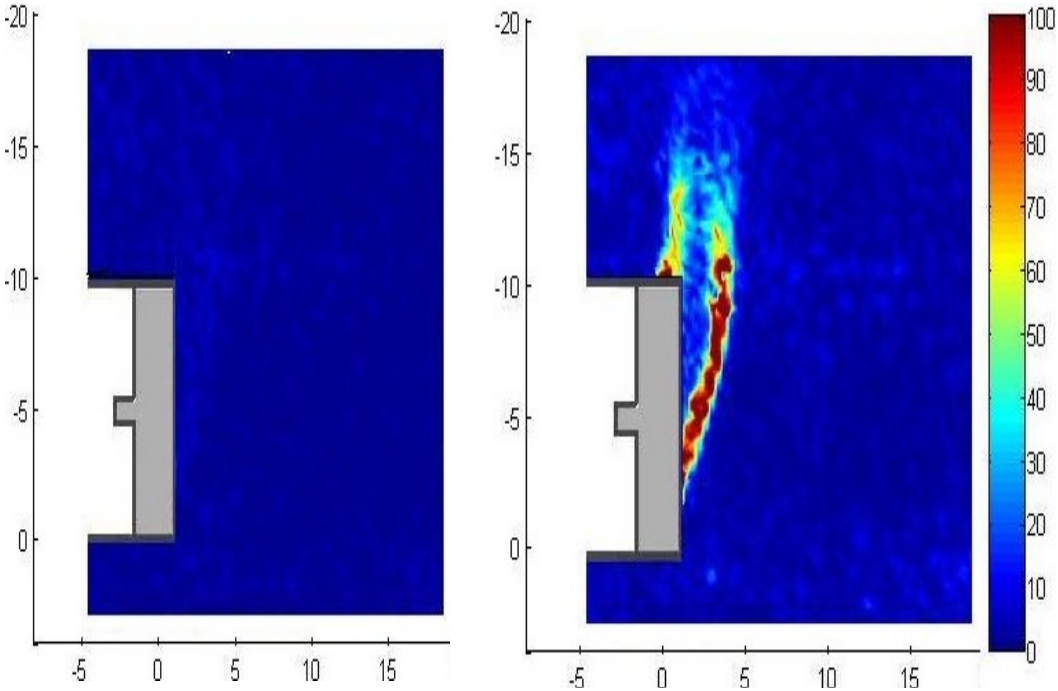


Figure 5.47 : C/D=1.0 S1 loose(with textile): a)contours of resultant max. shear strain after 0.5mm face b)contours of resultant max. shear strain after 5mm face

Picture on the left shows the shear strains which affected by the movement of the tunnel face between the 0 mm and 0.5 mm, picture on the right shows the affected area by the movement of the tunnel face between the 0 mm and 5 mm.

5.1.7.3 Surface Settlement

In the 7th experiment, as a result of using geotextile; maximum settlement decreases up to 1,1mm.

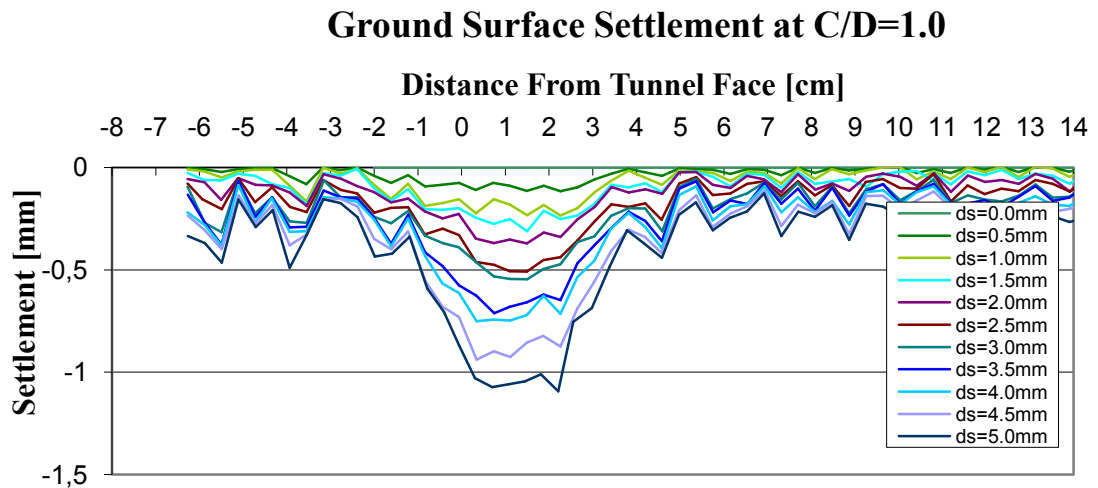


Figure 5.48 : C/D=1.0 S1 loose (with textile): surface settlement after $\Delta s=0.5\text{mm}$ face displacement, total face displacement $ds=5\text{mm}$; max. settlement: 1,1 mm

5.1.7.4 Support Pressure

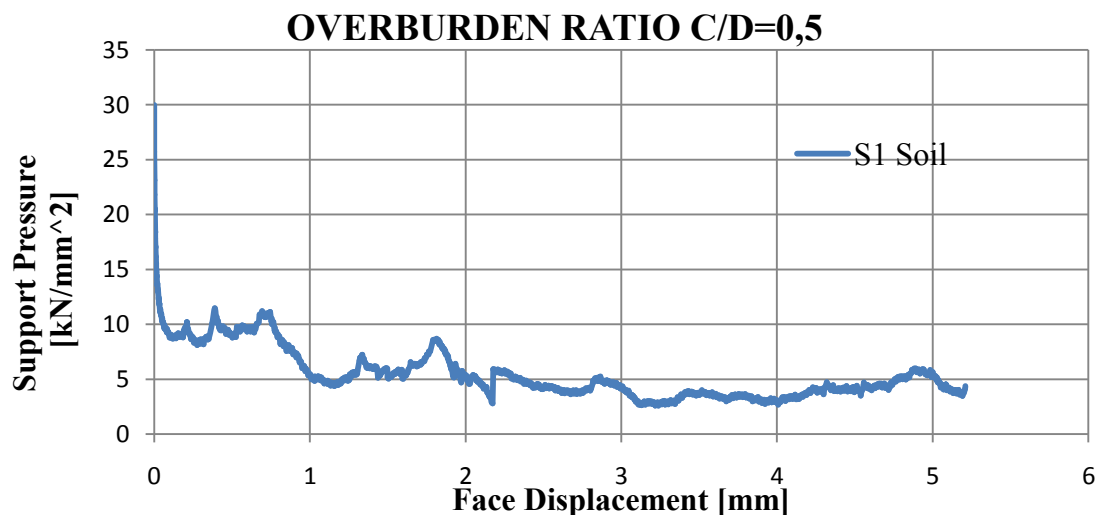


Figure 5.49 : C/D=1.0 S2 loose(with textile): support pressure over face displacement; five millimetres; mean pressure after failure: $p_f= 5.0\text{kN/m}^2$

In the 7th experiment the maximum support pressure is measured as 30 kN/m² and the minimum support pressure is measured as 5 kN/m².

5.2 Compararison Of Experiments

5.2.1 Experiment 1- Experiment 2 S1, C/D=0.5

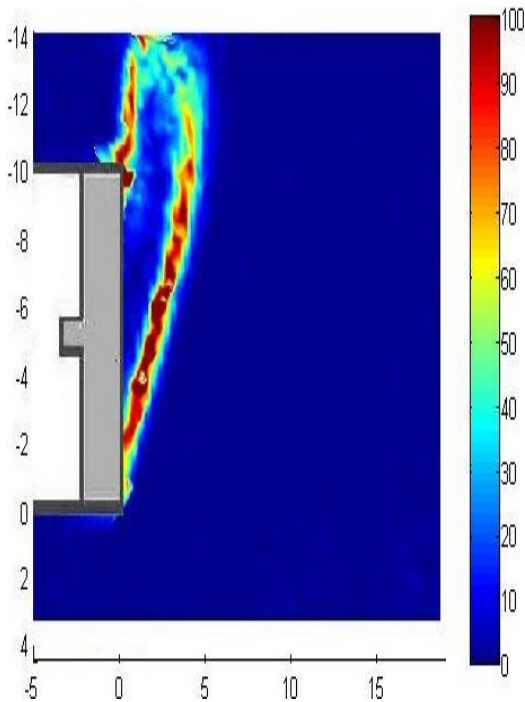
In this section, the 1st and 2nd experiments’ results are compared according to changing of maximum shear strain, ground surface settlement and surface support. Both experiments are done in the same conditions, but in the 2nd experiment the surcharge load added to ground surface (Table 5.9).

Table 5.9 : The comparing conditions of experiment 1 and experiment 2

EXPERIMENT NO	RELATIVE DENSITY(%)	MATERIAL	OVERBURDEN RATIO	SURCHARGE LOAD	TEXTILE
1	32	S1	C/D=0.5	----	----
2	32	S1	C/D=0.5	X	----

5.2.1.1 Contours of Resultant Maximum Shear Strain

a) no surcharge



b)with 2 kg surcharge

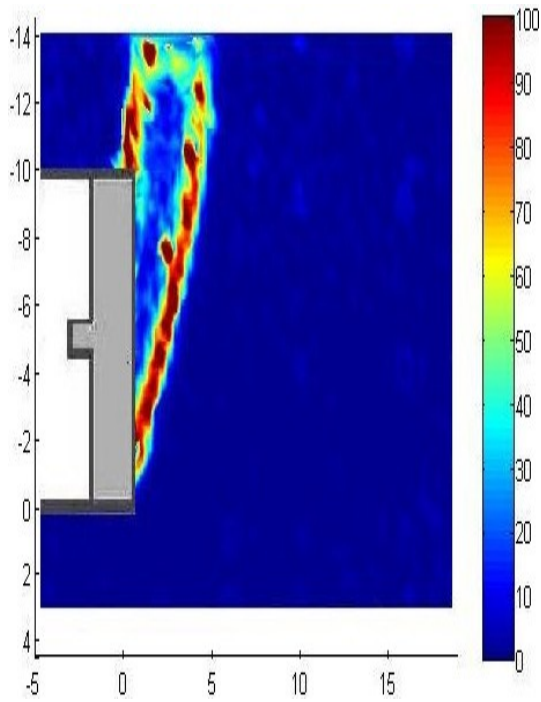


Figure 5.50 : C/D=0.5 S1 loose contours of resultant max. shear strain after 5mm face a)with no surcharge b)with 2 kg surcharge

Picture on the left shows the contours of resultant maximum shear strain without surcharge load, however, picture on the right is the contours of resultant maximum shear strain after surcharge load is added. Resultant maximum shear strain is increased obviously by adding the surcharge load.

5.2.1.2 Surface Settlement

The maximum ground surface settlement increased due to the surcharge load, the difference between the settlements is approximately 0.5 mm.

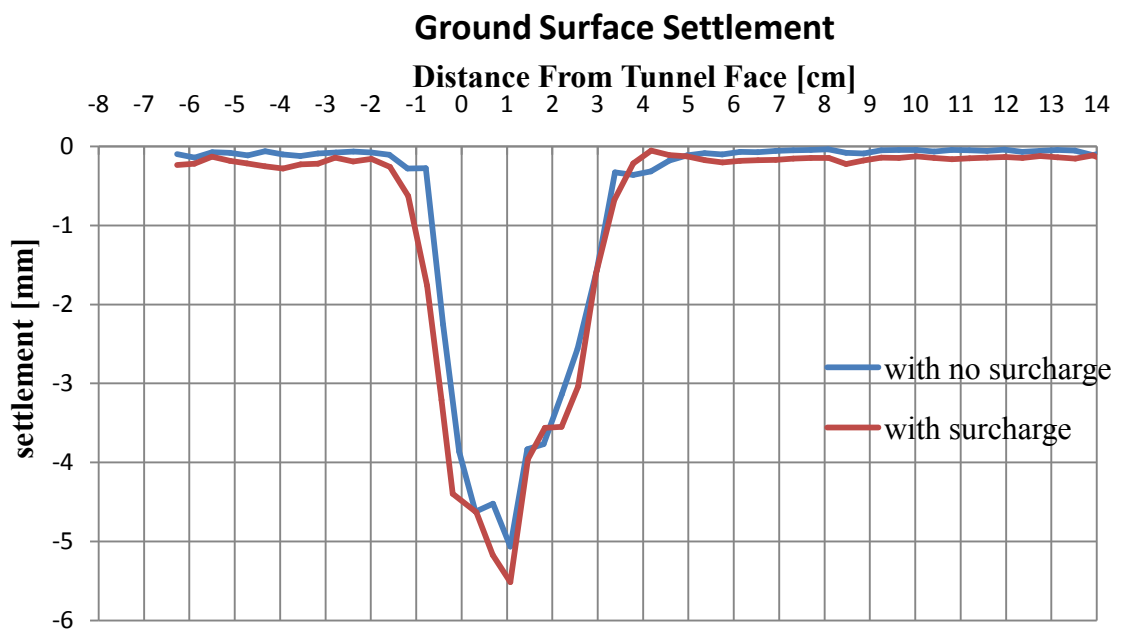


Figure 5.51 : C/D=0.5 S1 loose: surface settlement after total face displacement ds=5mm;a) with no surcharge load max. settlement: 5.0 mm b) a)with surcharge load max. settlement: 5.5 mm

5.2.1.3 Surface Support

A required support pressure for shield driven tunnels in soft materials, and the ground deformations along the longitudinal section of the tunnel model, can be identified by simulating a loss of tunnel face stability. Therefore, in this section the effects of the surcharge load on the support pressure investigated. When there is not any surcharge load, the maximum value of the support pressure is equal to 32.5 kN/mm², the minimum value is 10 kN/mm². After the effects of the surcharge load, maximum value of support pressure increased to 45 kN/mm², the minimum value of support pressure decreased to 5 kN/mm².

OVERBURDEN RATIO C/D=0,5

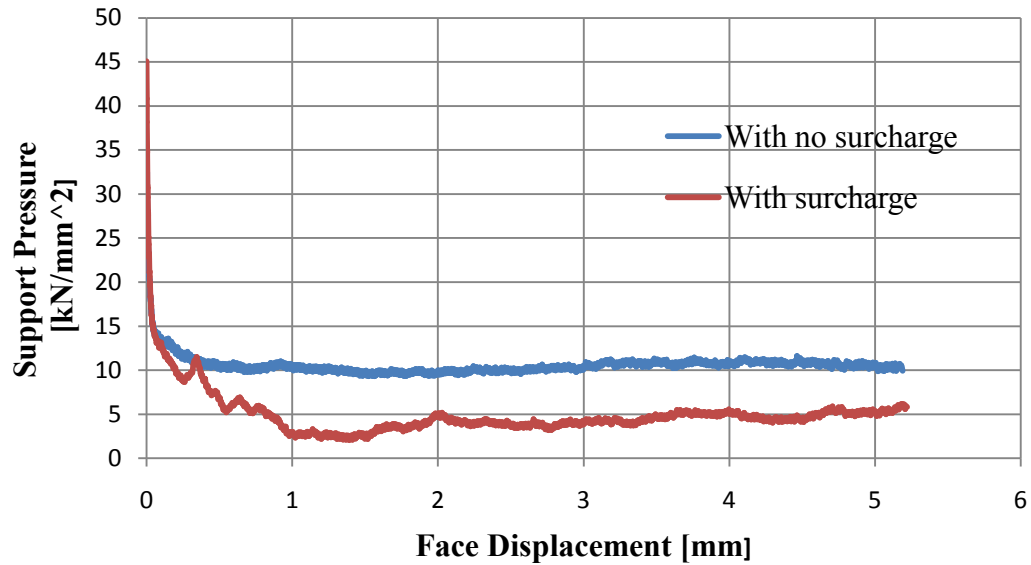


Figure 5.52 : C/D=0.5 S1 loose: support pressure over face displacement; five millimetres; mean pressure after failure: a) with no surcharge $p_f=10.0\text{kN/m}^2$ b) with surcharge $p_f=5.0\text{kN/m}^2$

5.2.2 Experiment 3- Experiment 4 S2, C/D=0.5

In this section, the 3rd and 4th experiments' results compared according to changing of maximum shear strain, ground surface settlement and surface support. Both experiments are performed in the same conditions, but in the 4th experiment the surcharge load is placed on the ground surface (Table 5.10).

Table 5.10 : The comparing conditions of experiment 3 and experiment 4

EXPERIMENT NO	RELATIVE DENSITY(%)	MATERIAL	OVERBURDEN RATIO	SURCHARGE LOAD	TEXTILE
3	25	S2	C/D=0.5	----	----
4	25	S2	C/D=0.5	X	----

5.2.2.1 Contours of Resultant Maximum Shear Strain

a) no surcharge

b) with 2 kg surcharge

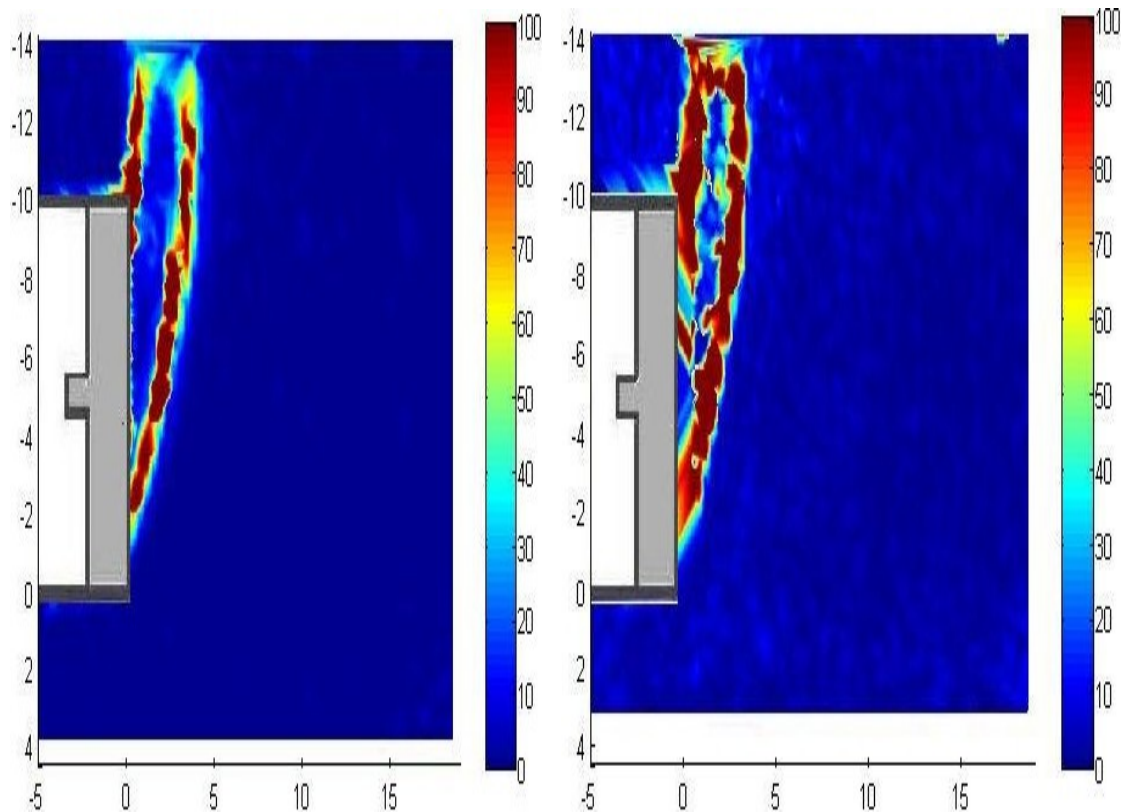


Figure 5.53 : $C/D=0.5$ S2 loose contours of resultant max. shear strain after 5mm face a)with no surcharge b)with 2 kg surcharge

Picture on the left shows the contours of resultant maximum shear strain without surcharge load, however, picture on the right is the contours of resultant maximum shear strain after surcharge load is added. Resultant maximum shear strain is increased obviously by adding the surcharge load .

5.2.2.2 Surface Settlement

The maximum ground surface settlement increased due to the surcharge load, the difference between the settlements is approximately 3.0 mm.

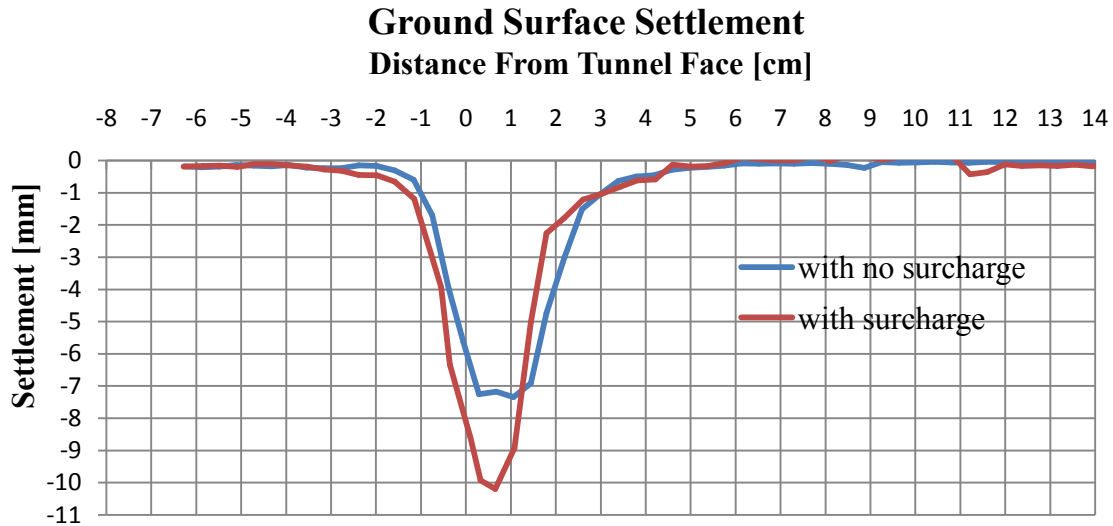


Figure 5.54 : C/D=0.5 S2 loose: surface settlement after total face displacement $d_s=5\text{mm}$; a) with no surcharge load max. settlement: 7.3 mm b) a)with surcharge load max. settlement: 10.2 mm

5.2.2.3. Surface Support

In this section the effects of the surcharge load on the support pressure investigated. When there is not any surcharge load, the maximum value of the support pressure is equal to 31.5 kN/mm^2 , the minimum value is 0 kN/mm^2 . After the effects of the surcharge load, maximum value of support pressure increased to 62.5 kN/mm^2 , the minimum value of support pressure is also equal to 0 kN/mm^2 .

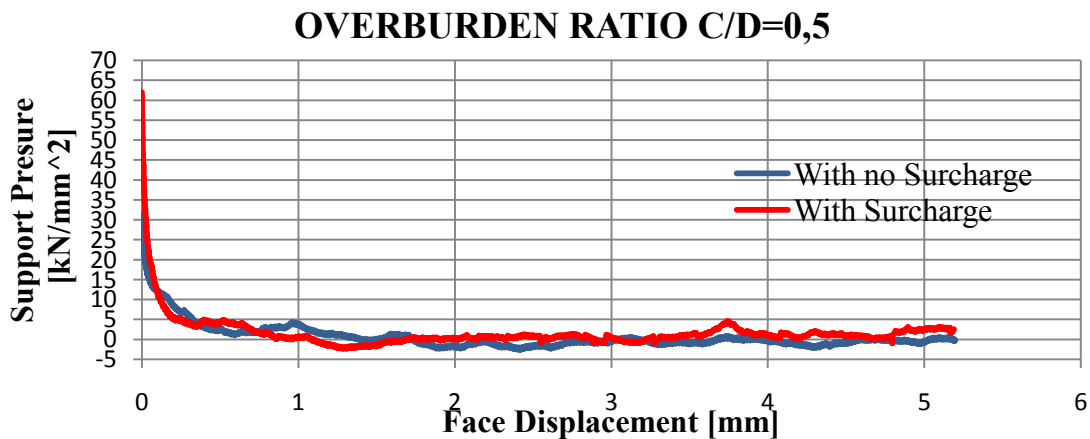


Figure 5.55: C/D=0.5 S2 loose: support pressure over face displacement; five millimetres; mean pressure after failure: a) with no surcharge $p_f=0.0\text{kN/m}^2$ b) with surcharge $p_f=0.0\text{kN/m}^2$

5.2.3 Experiment 1- Experiment 3, C/D=0.5, no surcharge

The 1st experiment is performed with S1 soil (Norman Sand), and 3rd experiment is performed with S2 soil. In this section, The effects of grain size distribution is

investigated according to changing of maximum shear strain, ground surface settlement and surface supports.(Table 5.11)

Table 5.11 : The comparing conditions of experiment 1 and experiment 3

EXPERIMENT NO	RELATIVE DENSITY(%)	MATERIAL	OVERBURDEN RATIO	SURCHARGE LOAD	TEXTILE
1	32	S1	C/D=0.5	----	----
3	25	S2	C/D=0.5	----	----

5.2.3.1 Contours of Resultant Maximum Shear Strain

a) S1 Soil

b)S2 Soil

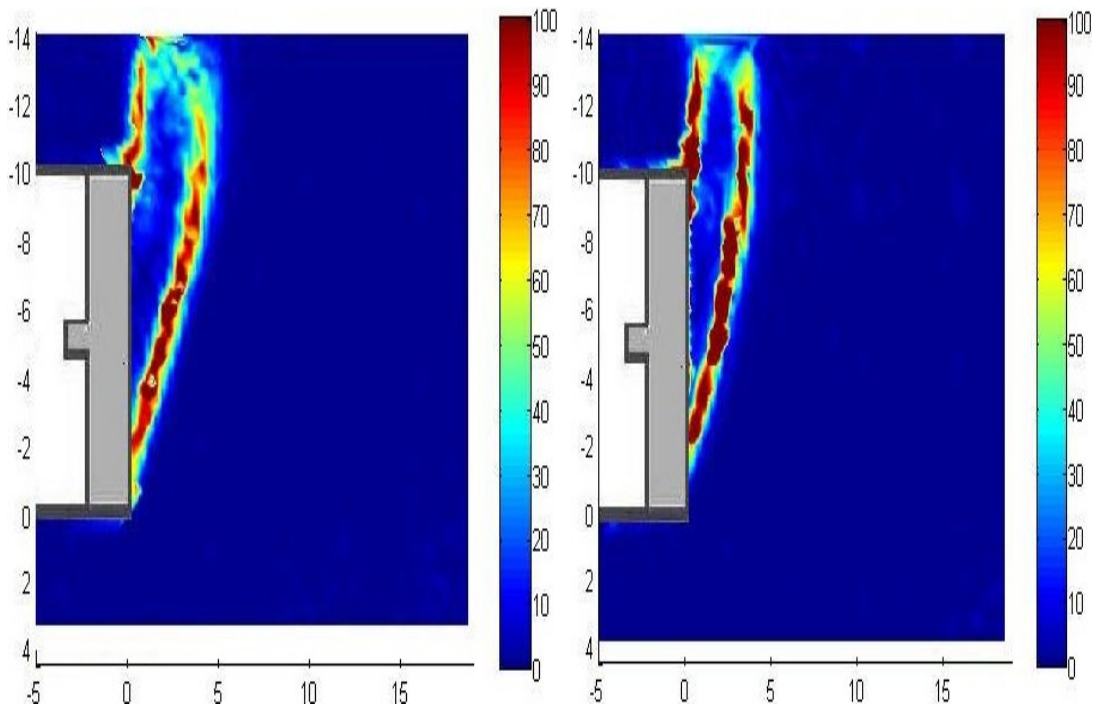


Figure 5.56 : C/D=0.5 loose contours of resultant max. shear strain after 5mm face
a)with S1 soil b)with S2 Soil

Picture on the left shows 1st experiments ‘ results, picture on the right shows 2nd experiments ‘ results. Definitely, S2 Soil’s (finer soil) contours of resultant maximum shear strain is affected more than S1 soil.

5.2.3.2 Surface Settlement

The maximum ground surface settlement increased due to the grain size distribution, the difference between the settlements is approximately 2.2 mm.

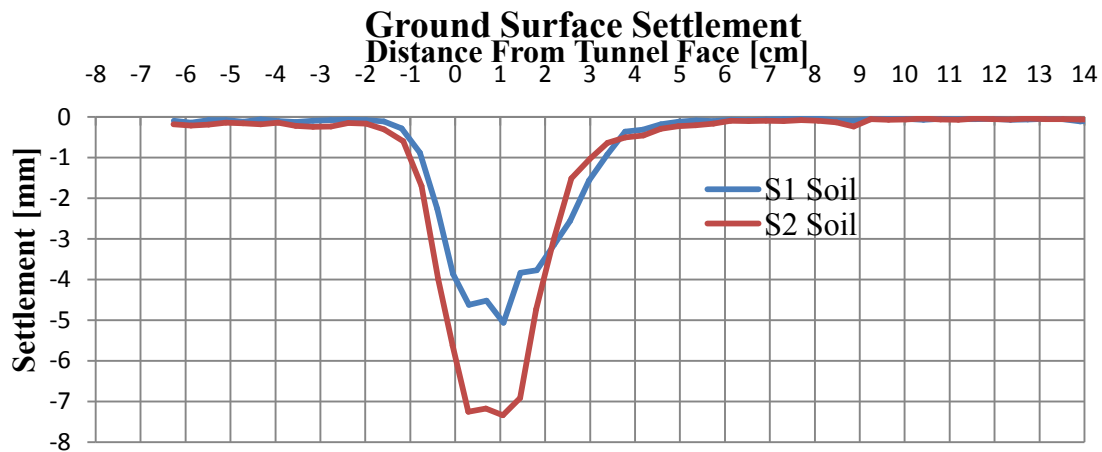


Figure 5.57 : C/D=0.5 loose: surface settlement after total face displacement $d_s=5\text{mm}$; a) with S1 Soil max. settlement: 5.0 mm b) with S2 Soil max. settlement: 7.3mm

5.2.3.3. Surface Support

In this section the effects of the grain size distribution on the support pressure investigated. When S1 soil (coarse sand) is used, the maximum value of the support pressure is equal to 32.5 kN/mm^2 , the minimum value is 10 kN/mm^2 . But S2 soil (fine sand) is used, the maximum value of the support pressure is equal to 31.5 kN/mm^2 , the minimum value is decreased till 0 kN/mm^2

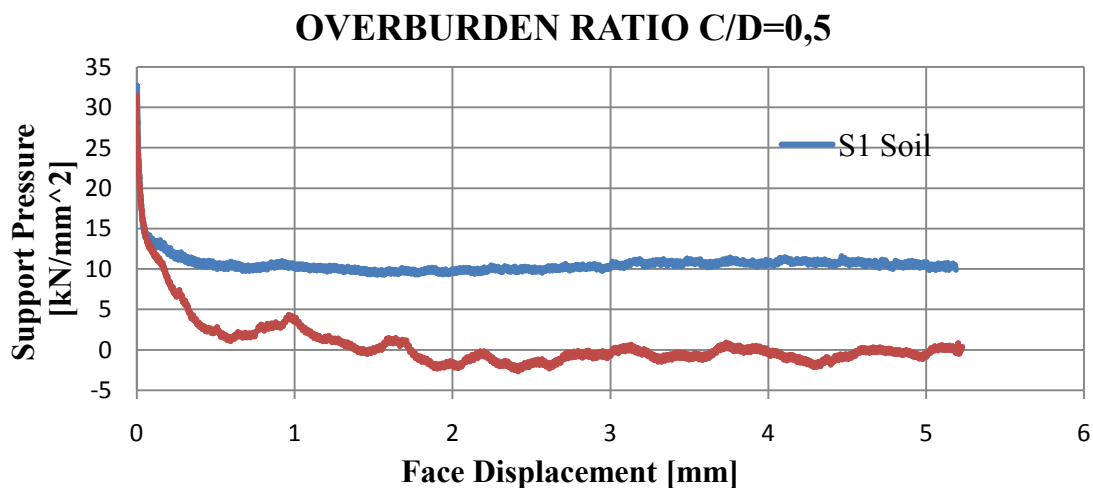


Figure 5.58 : C/D=0.5 loose: support pressure over face displacement; five millimetres; mean pressure after failure: a) with S1 soil $p_f=10.0 \text{ kN/m}^2$ b) with S2 soil $p_f=0.0 \text{ kN/m}^2$

5.2.4 Experiment 2- Experiment 4, C/D=0.5, with surcharge

The 2nd experiment is performed with S1 soil (Norman Sand), and 4th experiment is performed with S2 soil. In this section, The effects of grain size distribution under surcharge load is investigated according to changing of maximum shear strain, ground surface settlement and surface supports (Table 5.12).

Table 5.12 : The comparing conditions of experiment 2 and experiment 4

EXPERIMENT NO	RELATIVE DENSITY(%)	MATERIAL	OVERBURDEN RATIO	SURCHARGE LOAD	TEXTILE
2	32	S1	C/D=0.5	X	----
4	25	S2	C/D=0.5	X	----

5.2.4.1 Contours of Resultant Maximum Shear Strain

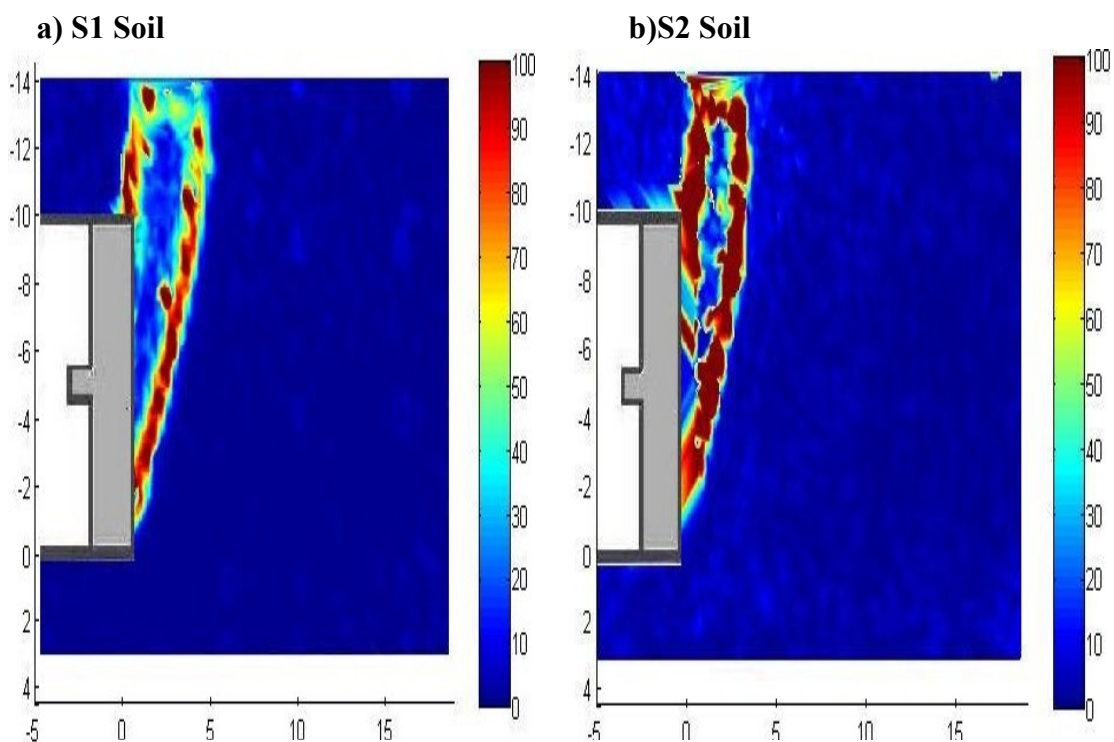


Figure 5.59 : C/D=0.5 loose (with surcharge load) contours of resultant max. shear strain after 5mm face a)with S1 soil b)with S2 Soil

Picture on the left shows 1st experiments' results, picture on the right shows 2nd experiments ' results. Definitely, S2 Soil's (finer soil) contours of resultant maximum shear strain is affected more than S1 soil.

5.2.4.2 Surface Settlement

The maximum ground surface settlement increased due to the grain size distribution, the difference between the settlements is approximately 4.7 mm.

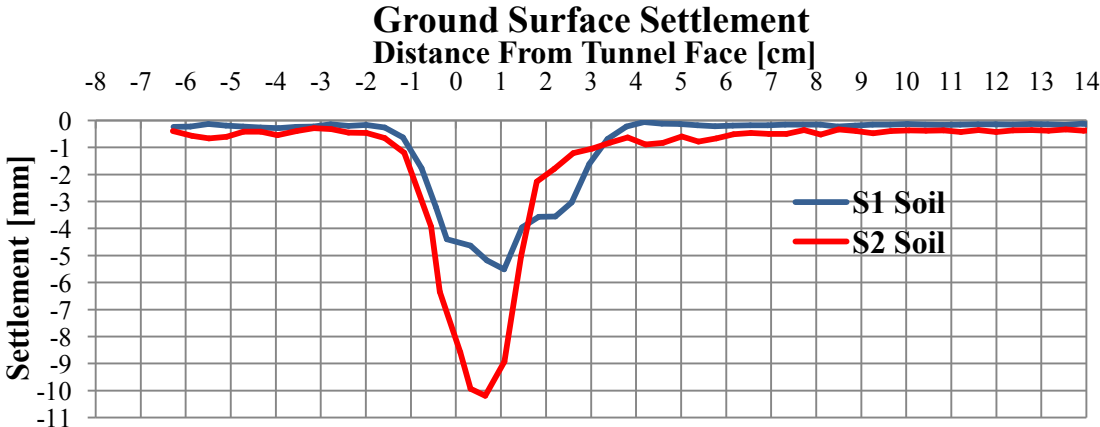


Figure 5.60 : C/D=0.5 loose: surface settlement after total face displacement $d_s=5\text{mm}$; a) with S1 Soil max. settlement: 5.5 mm b) a)with S2 Soil max. settlement: 10,2 mm

5.2.4.3 Surface Support

In this section the effects of the grain size distribution on the support pressure investigated. When S1 soil (coarse sand) is used, the maximum value of the support pressure is equal to 45.0 kN/mm^2 , the minimum value is 5 kN/mm^2 . But S2 soil (fine sand) is used, the maximum value of the support pressure is equal to 62.5 kN/mm^2 , the minimum value is decreased till 0 kN/mm^2

OVERBURDEN RATIO C/D=0,5

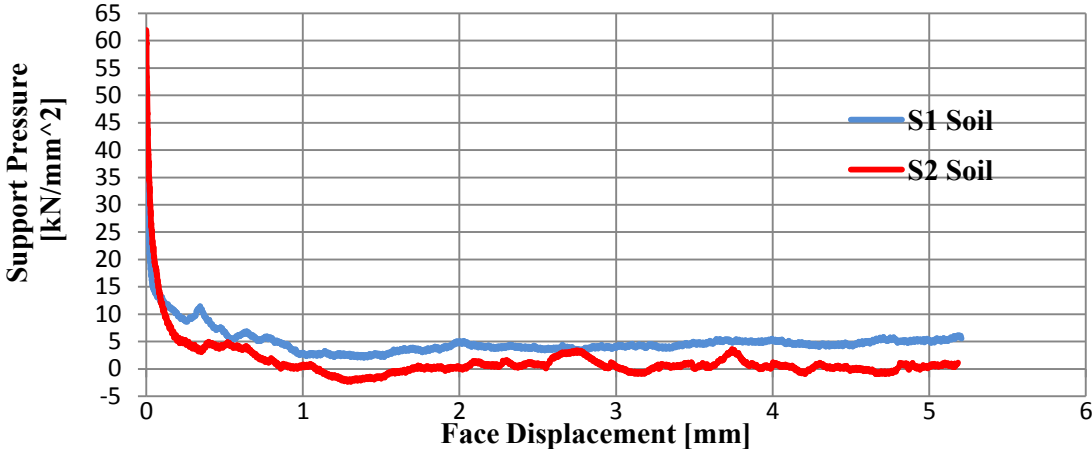


Figure 5.61 : C/D=0.5 (with surcharge) loose: support pressure over face displacement; five millimetres;mean pressure after failure:a) with S1 soil $p_f=5.0\text{kN/m}^2$ b)with S2 soil $p_f=0.0\text{kN/m}^2$

5.2.5 Experiment 1- Experiment 5, C/D=0.5, S1

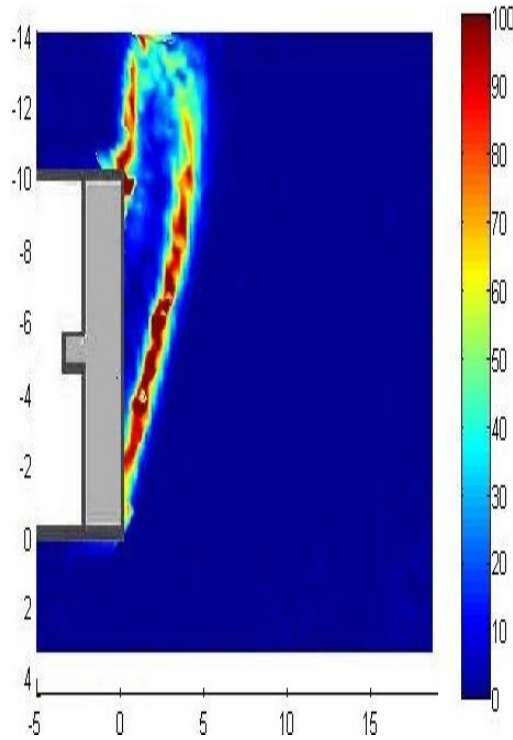
In this section, The effects of using soil improvement technique is investigated according to changing of maximum shear strain, ground surface settlement and surface supports. Both experiments are performed same conditions (Table 5.13).

Table 5.13 : The comparing conditions of experiment 1 and experiment 5

EXPERIMENT NO	RELATIVE DENSITY(%)	MATERIAL	OVERBURDERN RATIO	SURCHARGE LOAD	TEXTILE
1	32	S1	C/D=0.5	----	----
5	32	S1	C/D=0.5	----	X

5.2.5.1 Contours of Resultant Maximum Shear Strain

a) No Textile



b) With textile

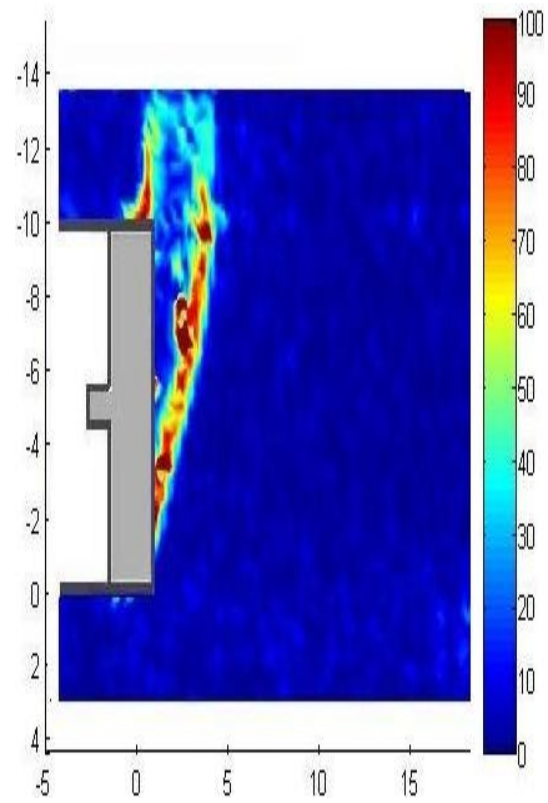


Figure 5.62 : C/D=0.5 S1 loose contours of resultant max. shear strain after 5mm face a)with no textile b)with textile

Picture on the left shows 1st experiments ' results, picture on the right shows 5th experiments ' results. Using textile decreased contours of resultant maximum shear strain.

5.2.5.2. Surface Settlement

The maximum ground surface settlement decreased due to the using textile, the difference between the settlements is approximately 0.5 mm.

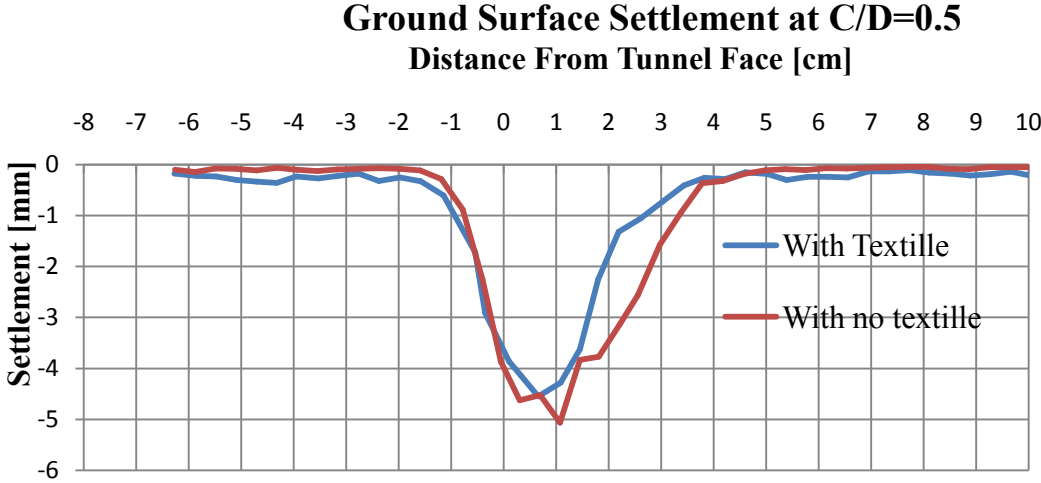


Figure 5.63 : C/D=0.5 S1 loose: surface settlement after total face displacement $d_s=5\text{mm}$; a) with no textille max. settlement: 5.0 mm b) a)with textille max. settlement: 4.5 mm

5.2.5.3 Surface Support

In this section the effects of the using textile on the support pressure investigated. At 1st experiment the maximum value of the support pressure is equal to 32.5 kN/mm^2 , the minimum value is 10 kN/mm^2 . After using the textile, the maximum value of the support pressure decreased to 27.5 kN/mm^2 , the minimum value is 0 kN/mm^2

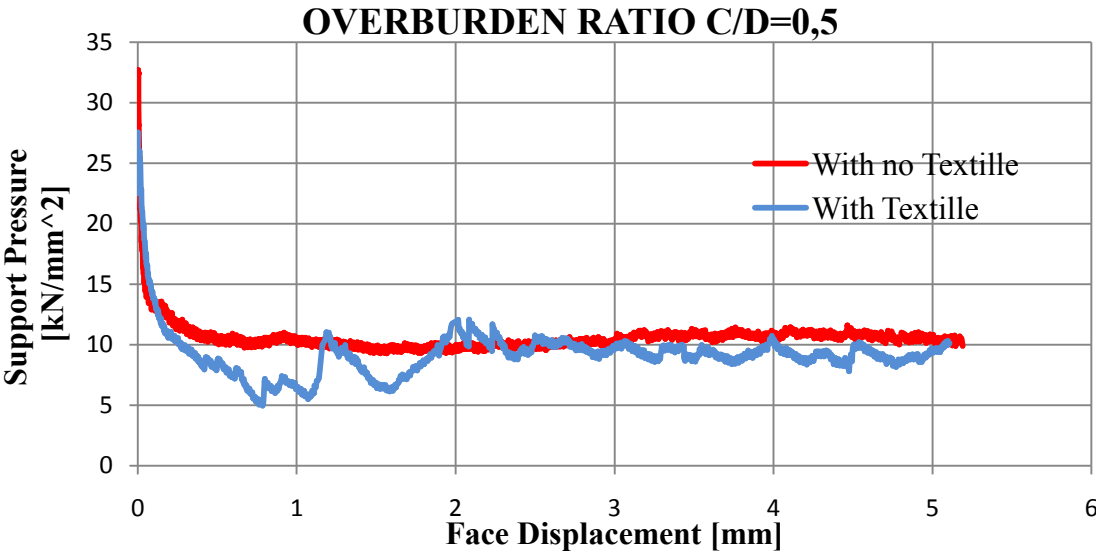


Figure 5.64 : C/D=0.5 S1 loose: support pressure over face displacement; five millimetres; mean pressure after failure: a) with no textille $p_f=10.0\text{kN/m}^2$ b) with textille $p_f= 10.0\text{kN/m}^2$

5.2.6 Experiment 6- Experiment 7, C/D=1.0, S1

In this section, the effects of using soil improvement technique is investigated according to changing of maximum shear strain, ground surface settlement and surface supports. Both experiments are performed same conditions (Table 5.14).

Table 5.14 : The comparing conditions of experiment 6 and experiment 7

EXPERIMENT NO	RELATIVE DENSITY(%)	MATERIAL	OVERBURDEN RATIO	SURCHARGE LOAD	TEXTILE
6	32	S1	C/D=1.0	----	----
7	32	S1	C/D=1.0	----	X

5.2.6.1 Contours of Resultant Maximum Shear Strain

a) No Textile

b) With textile

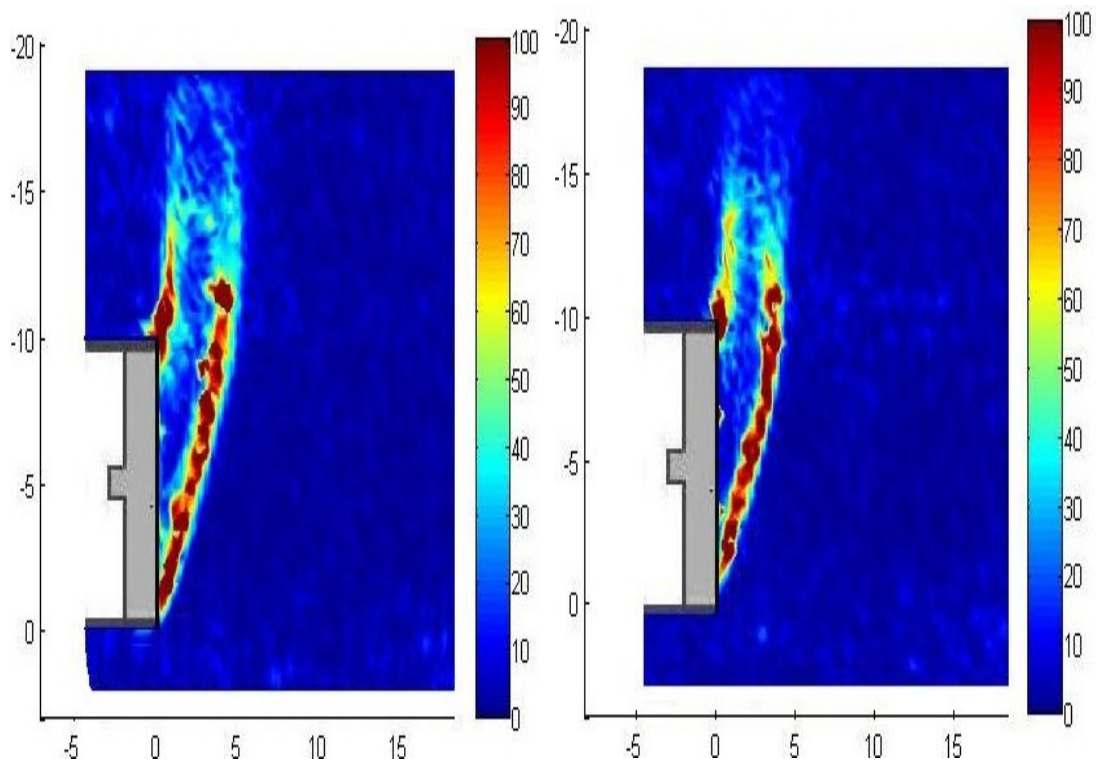


Figure 5.65 : C/D=1.0 S1 loose contours of resultant max. shear strain after 5mm face a)with no textile b)with textile

Picture on the left shows 6th experiments' results, picture on the right shows 7th experiments ' results. Using textile decreased contours of resultant maximum shear strain.

5.2.6.2 Surface Settlement

The maximum ground surface settlement decreased due to the using textile, the difference between the settlements is approximately 0.3 mm.

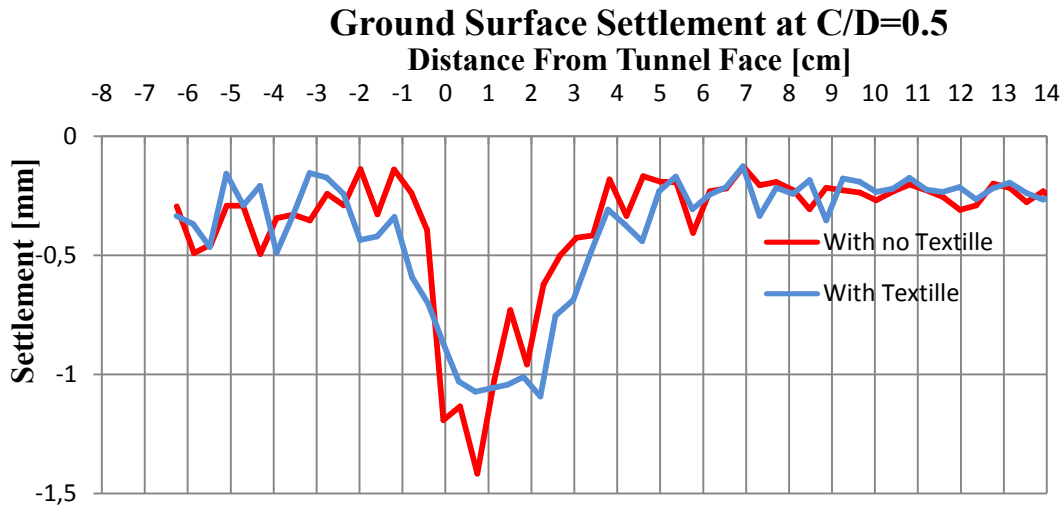


Figure 5.66 : C/D=1.0 S1 loose: surface settlement after total face displacement $d_s=5\text{mm}$; a) with no textile max. settlement: 1.4 mm b) a)with textile max. settlement: 1.1 mm

5.2.6.3 Surface Support

In this section the effects of the using textile on the support pressure investigated. At 6th experiment the maximum value of the support pressure is equal to 36.0 kN/mm^2 , the minimum value is 0 kN/mm^2 . After using the textile, the maximum value of the support pressure decreased to 30 kN/mm^2 , the minimum value is 5 kN/mm^2

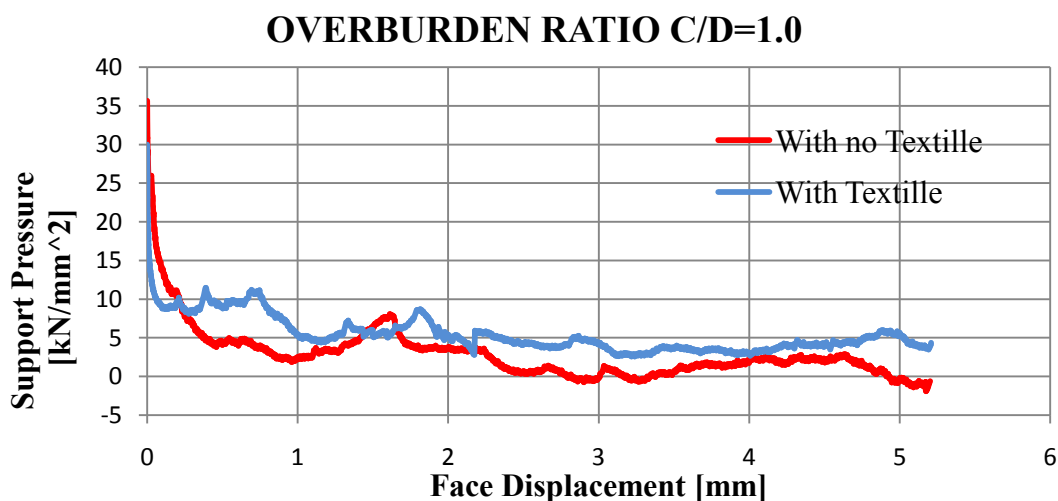


Figure 5.67 : C/D=1.0 S1 loose: support pressure over face displacement; five millimetres; mean pressure after failure: a) with no textile $p_f=0.0\text{kN/m}^2$ b) with textile $p_f= 5.0\text{kN/m}^2$

5.2.7 Experiment 1- Experiment 6, S1, no surcharge load

In this section, The effects of the layer thickness over the tunnel is investigated according to changing of maximum shear strain, ground surface settlement and surface supports. The other conditions are performed as same (Table 5.15).

Table 5.15 : The comparing conditions of experiment 1 and experiment 6

EXPERIMENT NO	RELATIVE DENSITY(%)	MATERIAL	OVERBURDEN RATIO	SURCHARGE LOAD	TEXTILE
1	32	S1	C/D=0.5	----	----
6	32	S1	C/D=1.0	----	----

5.2.7.1. Contours of Resultant Maximum Shear Strain

a) C/D=0.5

b)C/D=1

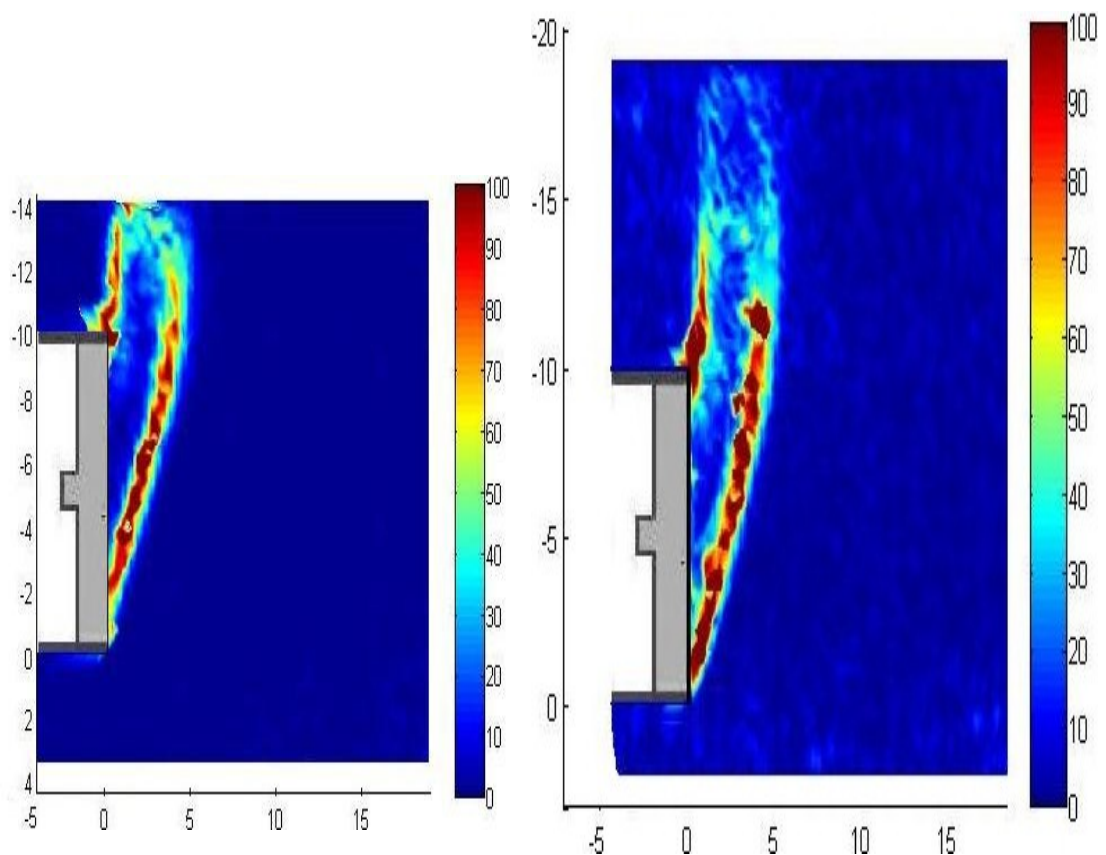


Figure 5.68 : S1 loose contours of resultant max. shear strain after 5mm face
a)C/D=0.5 b)C/D=1.0

Picture on the left shows 1th experiments' results, picture on the right shows 6th experiments ' results. When the thickness of the layer over tunnel increased, contours of the resultant maximum shear strain do not reach to the ground surface.

5.2.7.2 Surface Settlement

Because of the increment of overburden ratio (C/D), at the 6th experiment ground surface settlement value is less than 1th experiment.

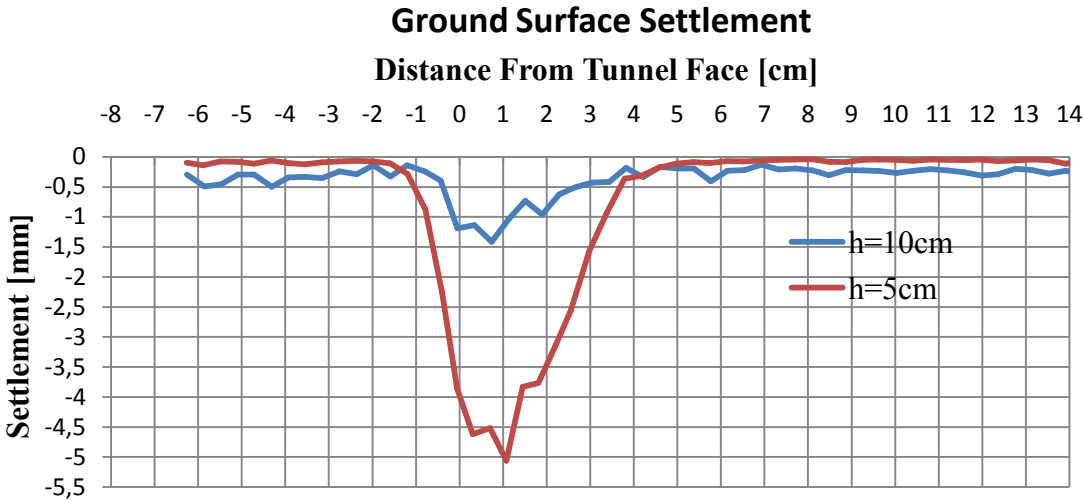


Figure 5.69 : S1 loose: surface settlement after total face displacement ds=5mm;a) C/D=0.5 max. settlement: 5.0 mm b) a)C/D=1.0 max. settlement: 1.4 mm

5.2.7.3 Surface Support

In this section the effects of the overburden ratio on the support pressure investigated. At 1th experiment the maximum value of the support pressure is equal to 32.5 kN/mm², the minimum value is 10 kN/mm². After the layer thickness increased, the maximum value of the support pressure increased to 36 kN/mm², the minimum value is 0 kN/mm²

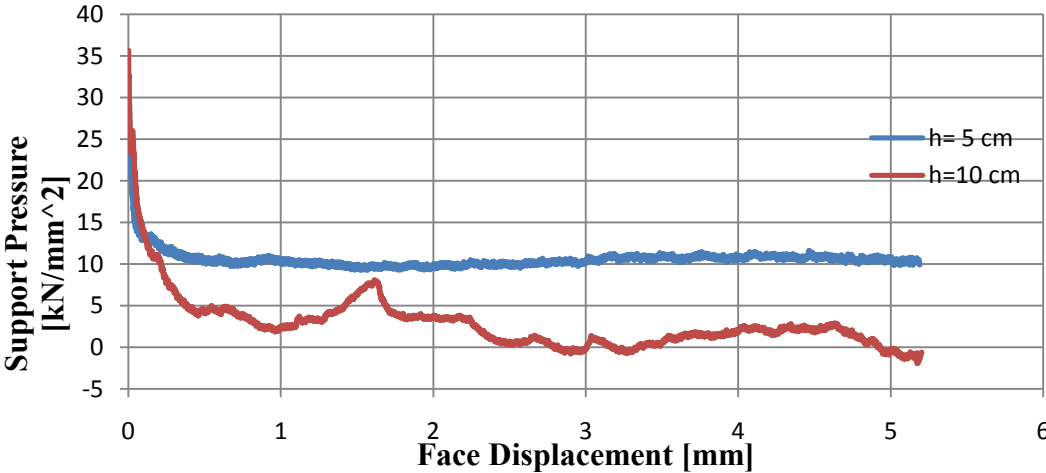


Figure 5.70 : S1 loose: support pressure over face displacement; five millimetres;mean pressure after failure:a) C/D=0.5 pf=10.0kN/m² b) C/D=1.0 pf=0.0kN/m²

6. ANALYSIS OF THE RESULTS

6.1 Interpretation Of The Results

PIV programme is used for the assessment of the surface settlements. Surface settlements are compared when C/D ratio is constant at 0.5. The reason of choosing the C/D ratio is that, as seen in the literature and in the final experiments, the surface settlements at this ratio are seen more. When this ratio increases, the surface settlements decrease even they almost do not form.

In all the experiments, the soil used is dry and loose sand.

6.1.1 Surface Settlements

Assessment of the experimental results,

In the case when Normal Sand is used without any surcharge load, the maximum surface settlement (Figure 5.6) is 5 mm. However, in a representative manner, in the second experiment where a 5-storey building is located on the ground surface, the surface settlement (Figure 5.13) has reached to 5.5. Depending on the surcharge load, it is obviously seen that the settlements have increased.

In the 3rd and 4th experiments, S2 surface with more coarse grained sand is used. In case when no surcharge load is present, the maximum surface settlement (Figure 5.20) is 7.3 mm. When the surcharge load is added, surface settlement has reached to 10.2 mm (Figure 5.27) .

The nature of the settlement is that not only does the tunnel affect the building can also alter the ground deformation induced by tunnel construction. As obviously seen from these results, the effect of the surcharge load on the settlements is considerably high and in case the surcharge loads increase, it is clear that these values will increase more. However different surfaces have a well effect on the surface settlements. Although the surfaces used are sand, despite the maximum settlement in Normal Sand (S1) is limited with 5 mm without any surcharge load, maximum settlement in the other surface (S2) has increased to 7.2 mm, an increase in the

surface where the settlements are developed is observed. With the increment of the surcharge load, the maximum settlement in Norman Sand (S1) is measured as 5.5 mm and maximum settlement in the other surface (S2) has reached 10.2 mm, also there is an increase on the surface where the settlements are formed.

In the 5th experiment (norman sand, no surcharge load), when the C/D ratio is 0.5; textile material is put on the tunnel surface. The purpose is to determine whether the increments made on the tunnel surface have an effect for the prevention of the surface settlements or not. Today similar applications are being applied by applying the Umbrella method during the tunneling process. In the 5th experiment, the maximum surface settlement(Figure 5.34) is about 4.5 mm. When we compare this result with the 1st experiment in which no textile is used under the same conditions; the decrease in the maximum settlement can be obviously seen. However, no change is seen on the width of the surface ground on which the settlements are formed.

In the 6th and 7th experiments (norman sand, no surcharge load), C/D ratio is increased to 1, in other words, the layer thickness on the tunnel surface is increased. In the 7th experiment a textile is present on the tunnel surface. In the 6th experiment, maximum surface settlement(Figure 5.41) is 1.4 mm. in the 7th experiment, as a result of using geotextile; maximum settlement(Figure 5.48) decreases up to 1.1 mm.

When an interpretation is made by observing the results; it is seen that textile usage clearly decreases the settlements. At the same time, the increase of the layer thickness on the tunnel has a lasting effect on decreasing the surface settlements (Figure 6.1).

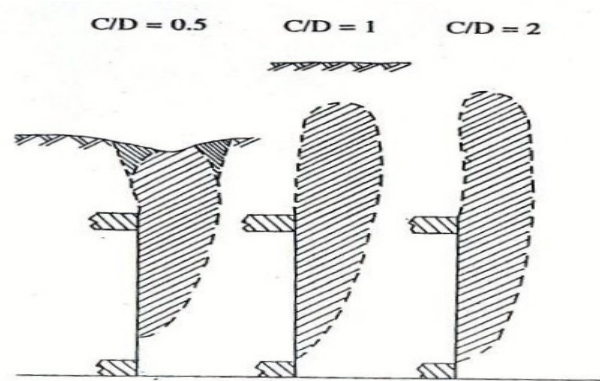


Figure 6.1 : Failure bulbs depends on overburden ratio (Chambon et al., 1991)

Table 6.1 shows the summary of experiments' results.

Table 6.1: Summary of experiment results

Experiment Number	Norman Sand (S1)	Fine Sand (S2)	H=5 (cm)	H=10 (cm)	With Surcharge	With No Surcharge	With Textile	With No Textile	Settlement (mm)	Max. Support Pressure (kN/mm²)	Min. Support Pressure (kN/mm²)
1	X		X			X		X	5.06	32.5	10
2	X		X		X			X	5.51	45	5
3		X	X			X		X	7.3	31.5	0
4		X	X		X			X	10.19	62.5	0
5	X		X			X	X		4.54	27.5	10
6	X			X		X	X		1.07	36	0
7	X			X		X		X	1.42	30	5

To obtain the in-situ values of settlement, the settlement results of the prototype has to multiply with the scale factor (for this investigation, scaling factor is 75g). It is the same linear scaling law for lengths/distances that makes the tunnel from 100cm to 7.5m.

6.1.2 Support Pressure

In the experiments the face pressure was measured behind the piston with a load cell as compressive force. This was divided by the semi-circled area of the aluminum face to gain a mean face pressure.

The under 75g arising friction of the moving piston was evaluated. Therefore a constant correction value was added to the originally measured compression data. This value was achieved from a second calibration test after accomplished experiments.

In the 1st experiment (no surcharge load, norman sand, $C/D=0.5$), maximum support pressure formed during the experiment is measured as 32.5 kN/m^2 and minimum support pressure is measured as 10 kN/m^2 (Figure 5.7). In the 2nd experiment (surcharge load present, norman sand, $C/D=0.5$); the developed maximum support pressure is measured as 45 kN/m^2 and minimum support pressure is measured as 5 kN/m^2 (Figure 5.14). With the addition of the surcharge load; an increase in the maximum support pressure and a decrease in the minimum support pressure is observed.

In the 3rd experiment (no surcharge load, fine sand, $C/D=0.5$); the maximum support pressure formed during the experiment is measured as 31.5 kN/m^2 and the minimum support pressure is measured as 0 kN/m^2 (Figure 5.21). In the 4th experiment (surcharge load is present, fine sand, $C/D=0.5$), the developed maximum support pressure is measured as 62.5 kN/m^2 and the minimum support pressure is measured as 0 kN/m^2 (Figure 5.28). With the addition of the surcharge load; an increase in the maximum support pressure occurs but no change is observed in the minimum support pressure.

In the 6th experiment (no surcharge load, norman sand, $C/D=1,0$), the developed maximum support pressure is measured as 36 kN/m^2 and the minimum support pressure is measured as 0 kN/m^2 (Figure 5.42). Based on this result, it can be said that

the increase of the layer thickness on the tunnel surface is increased the the surface support pressure.(Figure 6.2)

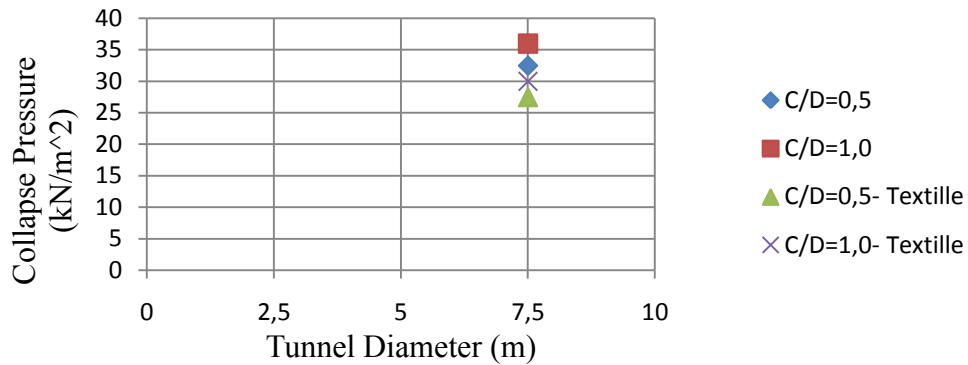


Figure 6.2 : Influence of tunnel diameter on collapse pressure

In this investigation collapse pressures take bigger values than Chambon's investigation at 1991 (Figure 1.10). On the other hand, this values are compared with the investigation of Lee et., al.(2006) , the differences between the two research is less.

Table 6.2 : The Soil Conditions of the resarch of (Lee et. al., 2006)

Sand	G_s	D_{50} , in (mm)	C_u	γ_{max}^1 (kN/m ³)	γ_{min}^1 (kN/m ³)
Quartz sand	2.65	0.18	1.58	16.6	14.1

Lee used saturated sand (Table 6.2) in his centrifuge model, and in table Pc shows the supporting pressure, p_w is pore water pressure, p_c' is effective supporting pressure at collapse. Here when C/D is equal to 1, maximum effective support pressure is 28.4 kPa (Table 6.3), in my research maximum support pressure is 36.0 kPa.

Table 6.3 : Supporting pressure p_c of the investigation of (Lee et. al., 2006)

Test No.	C/D	p_c (kPa)	p_w (kPa)	p_c' (kPa)
STEST1	1	89.1	60.7	28.4
PTEST2	1	89.5	60.7	28.8
STEST4	2	155.1	117.6	37.5
PTEST3	2	154.6	117.6	37
STEST3	3	210.1	176.4	33.7
PTEST6	3	212.8	176.4	36.4
STEST5	4	274.9	235.2	39.7

Influence of Tunnel Diameter on Collapse Pressure pf (Chambon et al., 1991)

The supporting pressure also can compare with the results of the supporting pressure of tunnelling in clayey soils are investigated by Lee et., al. (2006). The soil parameter of the resarch are given by Table 6.4. The Table 6.5 shows that when $C/D= 0.5$, the maximum support pressure (s_u) of a single tunnel takes value between 31.00 and 35.12 kPa.

Table 6.4 : Basic propertios of the soil bed (Lee et, al., 2006)

Specific gravity, G_s	2.67
Liquid limit, LL	40
Plastic limit, PL	22
Plasticity index, PI	18
Unit weight, γ (kN/m ³)	18.1
Compression index, C_c	0.28
Swell index, C_r	0.0275
Coefficient of consolidation, C_v (cm ² /s)	0.010524
Permeability, k (m/s)	4.5×10^{-9}

Table 6.5 : The supporting of the twin and single tunnels at clayey soil
(Lee et. al., 2006)

Test no. ^a	C/D	s_u (kPa)
Test11	0.5	31.00
Test12	0.5	35.12
Test5	1	36.90
Test8	1	37.90
Twin4	1	33.00
Twin5	1	39.10
Test3	2	30.25
Test9	2	35.79
Twin1	2	48.70
Twin2	2	41.00
Twin9	2	39.52
Twin12	2	35.10
Test6	3	33.30
Test7	3	34.00
Twin3	3	36.10
Twin6	3	32.90
Test10	4	32.17
Twin10	4	34.25
Twin11	4	32.83

If we examine the 5th (C/D=0,5) and 7th (C/D=1,0) experiments in which textile is used; in the 5th experiment the maximum support pressure is measured as 27.5 kN/m² and minimum support pressure is measured as 10 kN/m²(Figure 5.35), and in the 7th experiment the maximum support pressure is measured as 30 kN/m² and the minimum support pressure is measured as 5 kN/m² (Figure 5.49). The using of textill is decreased the maximum support pressure.

Accordinging to Grand and Taylor’s research horizontal distance from the tunnel centerline of inflexion on settlement trough is changing with the values of K and K is taken values between 0.25-0.35 for dry sand (Figure 1.13).

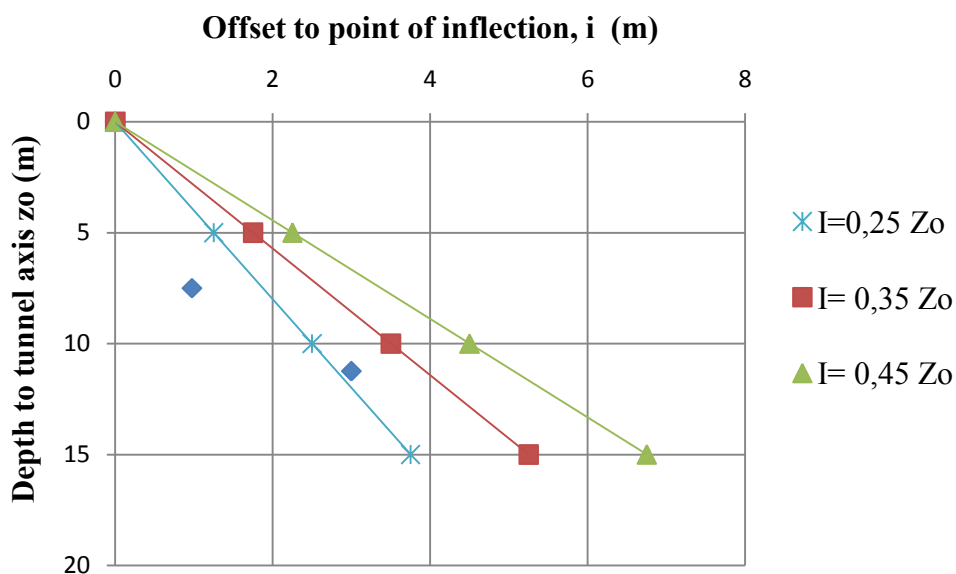


Figure 6.3 : Variation in surface settlement trough width parameter with tunnel depth for tunnels in sands and gravels

$I=K \cdot z_0$, when the C/D=0.5 , $Z_0=7.5$ m , if the K value is chosen as 0.25 , the distance is almost 1.8 m, when the C/D=1.0 , $Z_0=11.25$ m , if the K value is choosen as 0.25 , the distance is almost 2,8 m. But in this investigation, the experiments, which were performing with S1 soils, when the C/D=0.5 , $Z_0=7.5$ m, it takes 0.97 m this values is smaller than results of equiption, when the C/D=1.0 , $Z_0=11.25$ m , the value is equal to almost 3.0 m, this value is on the line (Figure 6.3) .

6.2 Conclusions

In this thesis; the surface settlements are examined about how and how long they change according to the parameters of the tunnel surface pressure. These parameters

are the loading on the ground surface (a building is present or not etc), different surface conditions, supports made during the tunnel construction and finally how the layer on the tunnel is affected by its change. The small scale centrifuge model, which is newly designed, provided dependable information about the face collapse of a shallow tunnel. A required support pressure for shield driven tunnels in soft materials, and the ground deformations along the longitudinal section of the tunnel model, can be identified by simulating a loss of tunnel face stability. When the results are interpreted depending on these parameters,

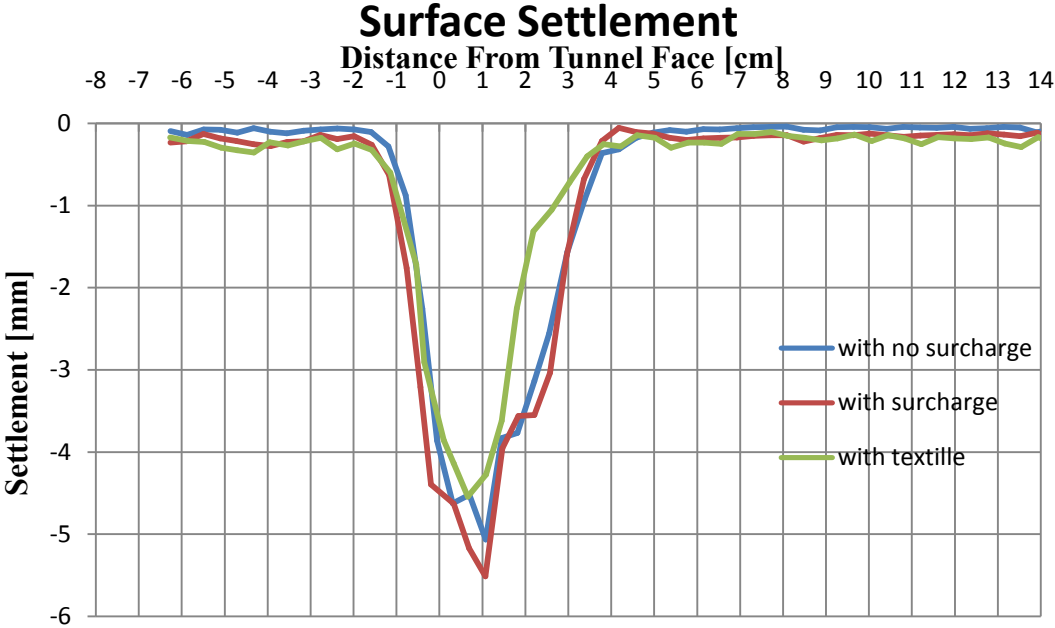


Figure 6.4 : S1 loose C/D= 0.5: surface settlement after total face displacement $d_s=5\text{mm}$; a) with no surcharge max. settlement: 5.0 mm b) With surcharge load max. settlement: 5.5 mm c) with textile max. settlement 4.5 mm

For the surface settlements; the below mentioned matters are concluded (Figure 6.4):

- 1) In case there is an extra structure on the ground surface (extra load), the settlements increase depending on the load,
- 2) In case there are different surfaces, the change in the surface settlements can get higher values than the changes formed by the surcharge loads,
- 3) The usage of tunnel supporting systems (umbrella etc) are efficient in the prevention of settlements,
- 4) By increasing the surface layer thicknesses over the tunnel surface; the settlements can be minimized.

For the tunnel support pressure; the below mentioned matters are concluded:

In all tests, same face collapse occurred. The collapse process could be investigated at three stages.

In the first stage, no movement affects the face while the internal pressure is progressively decreased from the initial value equal to the overburden pressure at the tunnel axis level. When the internal pressure gets to a rather low value (which depends on the geometry of the problem and on soil conditions), the soil starts to yield and each new decrease in pressure induces an increment of face displacement. This movement is irreversible and over a certain range of pressure there seems to be a linear relationship between the change of internal pressure and the face displacement. This behavior is not affected by time effects; when the internal pressure is maintained at a given value, the face displacement stops. In a third stage, if the internal pressure is further decreased, the face displacements increase very rapidly and allow to define failure situation. (König et al., 1991)

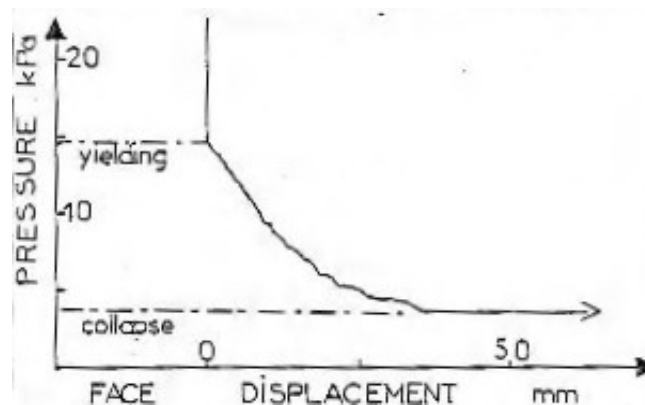


Figure 6.5 : Failure process: internal pressure versus face displacement in prototype dimensions (König, 1991)

- 1) In case there is an extra structure on the ground surface (extra load), an increase is formed in the maximum support pressure,
- 2) In case two different sand samples are used; major differences are seen between the support pressures.
- 3) The using of textill is decreased the maximum support pressure.

Support pressure increases depending on the stress over the tunnel center so depending on adding surcharge load or increment of the soil layer over the tunnel, support pressure increases. On the other hand using of textill cause to decrement of support pressure, the required support pressure, which prevent collapsing, could be decreased by using textill or soil improvement technique (Figure 6.6).

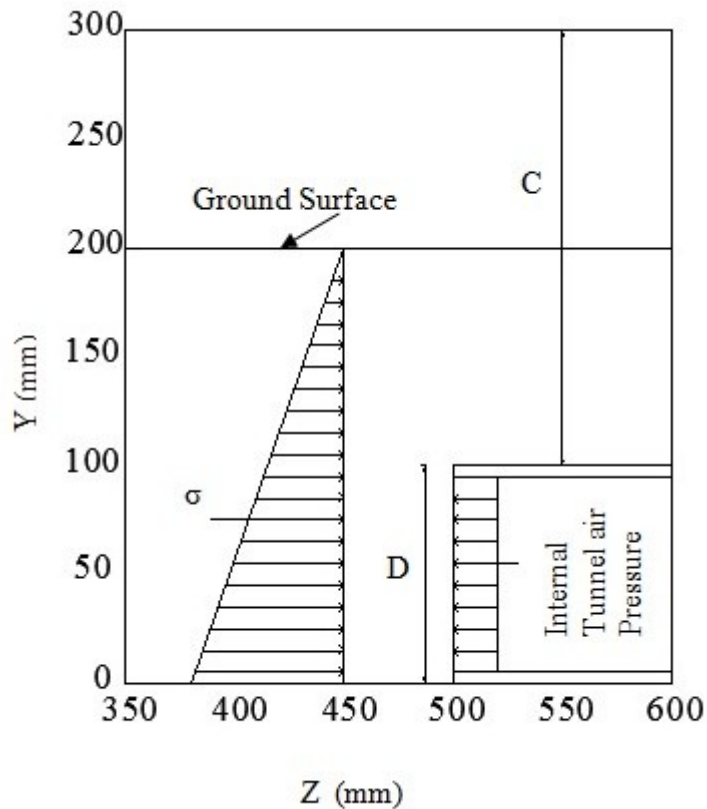


Figure 6.6: Idealised stresses acting on tunnel face (Franzius,2003)

Engineering practice in real world, however, tunneling through dry, cohesionless sand is quite uncommon. Mostly, at sites with coarse-grained soils, parts of the tunnel length can be excavated and constructed within the vadose zone above the groundwater table, where the coarse-grained soil involves sufficient moisture to generate some amount of visible cohesion. This generalisation applies especially for urban areas under which shallow tunnels are possibly to be built. But, in spite of this fact, no physical modelling data come into existence to explain the developing of ground deformations with loss of tunnel face pressure in unsaturated sands.

REFERENCES

- Anagnostou, G., Kovári, K.,** (1994), The face stability of slurry shield-driven tunnels, *Tunneling and Underground Space Technology* Vol.9, No.2, 165–174.
- Anagnostou, G., Kovári, K.,** (1996), Face Stability Conditions with Earth-Pressure-Balanced Shields, *Tunneling and Underground Space Technology* Vol.11, No.2, 165-173.
- Anitei, S.** (2008), How to Build a Tunnel, *Softpedia*
- Ashraf, O. S.,** Stability of unlined twin tunnels in undrained clay, *Tunneling and Underground Space Technology* Vol.25, 290-296
- Atkinson, J.H., Mair, R.J.,** (1981), Soil mechanics aspects of soft ground tunneling, *Ground Engineering* Vol.14, No.5, 20-38.
- Attewell, P.B., Woodman, J.P.,**(1982), Predicting the Dynamics of Ground Settlement and Its derivatives caused by tunnelling in soil. *Ground Engineering* Vol.15, 13-22
- Bucky, P.B. (1931),** Use of models for study of mining problems. *Am. Inst. Min. Met. Eng., Tech. Pub. 425, 28 pp.*
- Chambon, P., Corté, J-F.,** (1994), Shallow Tunnels in Cohesionless Soil Stability of Tunnel Face, *Journal of Geotechnical Engineering* Vol.120, No.7, 1148-1165.
- Chambon, P., Corté, J-F., Garnier, J., Konig, D.,** (1991), Face stability of shallow tunnels in granular soils, *Proceedings of the Centrifuge '91 Conference*, 13-14 June, Boulder, Colorado, 99-106.
- Cheney, J. A., Hor, O.Y.Z., Brown, R.K. , Dhat N.R.,** (1988), Foundation vibration in centrifuge models, *Proc. Conf. Centrifuge ' 88*, pp. 481-486, Balkeme, Rotterdam
- Craig, W. H.** (1989), Edouard Philips (1821-1889) and the idea of centrifuge modelling, *Geotechnique*, 39, 697-700
- Davis, E.H., Gunn, M.J., Mair, R.J., Seneviratne, H.N.,** (1980), The stability of shallow tunnels and underground openings in cohesive material, *Géotechnique* Vol.30, No.4, 397-416.
- Dimitrios, K.** Setzungen Der Oberfläche, *Geotechnik- Tunnelbau und Tunnel mechanik , VOL.32*
- Ferstl, F.,** (1998), Modellversuche zum Erddruck, *Phd Thesis, Universität für Bodenkultur, Vienna*
- Franzius, J.N.,** (2003), Behaviour of buildings due to tunnel induced subsidences, *PHD Thesis University of London, London*
- Geddes, J. D. 1991.** Discussion on: Building response to excavation-induced settlement. *Journal of Geotech. Engineering, ASCE*, 117(8), 1276-1278.
- Grant, R.J., & Taylor, R.N.** 2000. Tunnelling-induced ground movements in clay. *Proc. Instn. Civ. Engrs. Geotech. Engineering*, 143, 43-55.

- Idinger, G.**, (2010), Investigation On The Face Stability Of Shallow Tunnels In Dry Sand, *MSc Thesis, Universität für Bodenkultur, Vienna*.
- Lee, C.J., Wu, B.R., Chen, H.T., Chiang, K.H.**, 2006. Tunnel Stability and arching effects during tunneling in soft clayey soil, *Tunnelling and Underground Space Technology* Vol.21, 119-132
- Leca, E.** (2007) ITA/ AITES Report on 2006 Settlements induced by tunneling in soft Ground, *Tunnelling and Underground Space Technology* Vol.22, 119-149
- Lotysz, S.**(2010) Immersed Tunnel Technology: A Brief History of Its Development, *Civil and Environmental Engineering Reports*, No.4 97-110
- Mair. R.J., Taylor. R.N., Burland. J.B.**,(1996) Prediction of Ground Movements and Assessment of Building Damage Due to Bored Tunnelling. *In: MAIR, R.J., TAYLOR, R.N.*, International Symposium on Geotechnical Aspects of Underground Construction in Soft Ground, 659-665
- Maleki, M., Sereshteh H., Mousivand. M., Bayat M.**, (2011) An equivalent beam model for the analysis of tunnel-building interaction, *Tunnelling and Underground Space Technology* Vol.26, 524-533
- Marshall A. M., Mair. R.J.**, (2011), Tunneling beneath driven or jacked end-bearing piles in sand, *Can. Geotech. J.* Vol.48, 1757-1771
- Pantent, A., Kastner, R.,Piraud, J.**, (1993), In situ measurement and calculation of displacement field above slurry shields. *In: Options for Tunnelling, Amsterdam*, pp. 453-452
- Peck, R.B.**, (1969) Deep excavations and tunneling in soft ground, *Proc. 7th International Conference ISSMFE, Mexico State of Art Volume*, 225-290
- Pokrovskii, G. I., Fiodorov, I.S.** (1936), Studies of soil pressures and deformations by means of a centrifuge. *Proc. 1st Int. Conf. Soil Mech. Found. Eng.*, Vol.1, p.70
- Potts, D.M.**, (1997) A Structure's Influence on Tunnelling-induced Ground Movements, *In Proceedings Institution of Civil Engineers, Geotechnical Engineering*, Vol.125, April 109-125
- Rowe, R. K., Lo, K. Y., Kack, G. J.** 1983. A method of estimating surface settlement above tunnel constructed in soft ground. *Canadian Geotechnical Journal*, 20, 11-22.
- Rankin, W. J.** (1988), Ground movements resulting from urban tunnelling: predictions and effects. *Engineering geology of underground movements*.92 The Geological Society, London.
- Schofield, A. N.**, (1980), Cambridge geotechnical centrifuge operations. *Geotechnique*, 20, 227-268
- Sugiyama, T.,Hagiwara,T., Nomoto, T., Nomoto, M., Ang, Y., Mair, R. J.,Bolton, M. D., Soga, K.** , (1999) Observations of ground movements during tunnel construction by slurry shield method at the

Docklands light railway Lewisham Extension-East London, Soils and Foundations Japanese Geotechnical Society, vol.39 , No:3,99-112

- Monsees, J.E.**, (1996), Soft Ground Tunneling, Tunnel Engineering Handbook, second edition (eds. Bickel, J.O., Kuesel T.r., King, E.H.), Chapman & Hall, New York, 97-121
- Taylor, R.N.**, (1995), *Geotechnical centrifuge technology*, Blackie Academic and Professional, Glasgow.
- Taylor, R. N.**, (1995) Tunnelling in soft ground in the UK. 123 ,*Underground construction in soft ground*. Balkema, Rotterdam.
- Thusyanthan, I., White, D. J., Take, W. A., (2008)**, Deformation measurement using digital imaging and PIV (Particle Image Velocimetry) technique, Lecture Sheets, University of Cambridge, UK
- Terzaghi, K.**, (1936), Stress distribution in dry and in saturated sand above a yielding trapdoor,*Proceedings of the International Conference on Soil Mechanics* Vol.1. Harvard University, MA, 307–311.
- Thorpe , J. P.**, (2007), Ground Movement During Tunnelling in sand, *PhD. Thesis, Queen's University, Canada*.
- Trio-Tech**, (1988), *Technical proposal for a geophysical test centrifuge model 1231*, Trio-Tech International, San Francisco, CA.
- Vermer, P.A., Ruse, N., Marcher, T.**, Tunnel Heading Stability in Drained ground, *Felsbau* 20 (2002) No:6
- White, D.J., Take, W.A., Bolton, M.D.**, (2003), Soil deformation measurement using particle image velocimetry (PIV) and photogrammetry, *Géotechnique* Vol.53, No.7, 619-631.
- White, D.J., Take, W.A.**, (2002), GeoPIV: Particle Image Velocimetry (PIV) Software for use in Geotechnical Testing, *Technical Report, University of Cambridge, UK*.

APPENDICES

APPENDIX A : PIV Working Scheme

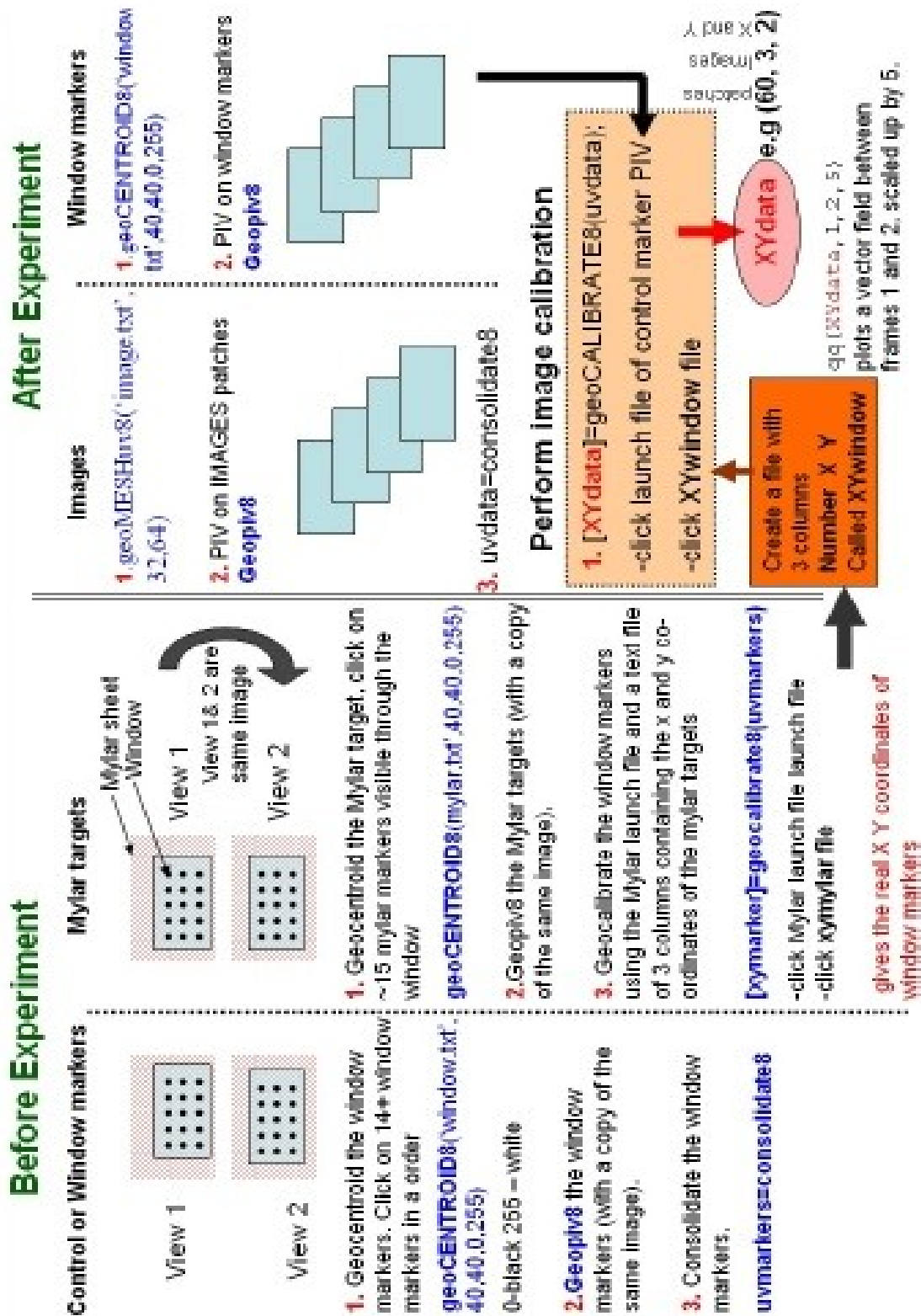


Figure A.1 : PIV working scheme (White et. al., 2002)

CURRICULUM VITAE



Name Surname: Tuğçe ERTAN

Place and Date of Birth: Istanbul, 21/06/1987

Address: Örnek Mah. Fehmi Tokay Cad. No: 5/7 Üsküdar /Istanbul, Turkey

E-Mail: tugceertan@hotmail.com

B.Sc.: Yıldız Technical University, Istanbul , Turkey

Professional Experience and Rewards:

Date: August 2010- January 2011

Company Name: Total Turkey

List of Publications and Patents:

PUBLICATIONS/PRESENTATIONS ON THE THESIS

- Ertan, T., The Investigation Of Stability Of Tunnels And Settlements With Centrifuge Modelling, *International Students' Conference of Civil Engineering, ISCCE 2012, Epoka University, Tirana, Albania*